CANDIDA ALBICANS SUPEROXIDE DISMUTASE AS PART OF AN ADAPTIVE RESPONSE TO COPPER DURING INFECTION

By
Cissy Li

A dissertation submitted to Johns Hopkins University in conformity with the requirements for the degree of Doctor of Philosophy

Baltimore, Maryland

August, 2015

Abstract

Candida albicans is a human fungal pathogen of important public health relevance. Virulence of *C. albicans* requires members of a family of antioxidant enzymes called superoxide dismutases (SODs). *C. albicans* has an unusually large collection of SODs that includes a rare pairing of a Cu/Zn-Sod1 and a Mn-Sod3 in the cytosol. The biology and regulation of these two SODs was poorly understood, and was the subject of investigation in this thesis.

First, we found that *C. albicans* Sod1 is relatively unstable compared to homologs in various other organisms (Chapter 2). We also uncovered evidence suggesting that the physical interaction between *C. albicans* Sod1 and its copper chaperone Ccs1 is unusually species-specific. These traits may reflect this yeast's adaptation to life as a pathogen.

Although others have shown that Cu/Zn-Sod1 and Mn-Sod3 were alternatively expressed at the mRNA level, nothing was known about the regulation and rationale of these seemingly redundant enzymes. We establish that these two SODs are modulated to adapt to fluctuations in copper bioavailability (Chapter 3). Utilizing both a copper-dependent and a copper-independent SOD ensures that *C. albicans* can maintain constant SOD antioxidant activity regardless of the surrounding copper environment. This alternative regulation of Cu/Zn-Sod1 and Mn-Sod3 employs the copper-sensing transcription factor Mac1, using a novel mechanism. We discovered that the host response to fungal infection includes fluctuation of kidney copper. Meanwhile, *C. albicans* expertly switches its cytosolic SODs to adapt to these changes in copper. This is the first evidence for possible copper utilization in host nutritional immunity.

Besides copper, other kidney biometals are also affected by *C. albicans* infection (Appendix I). Strikingly, sites of calcium deposits and zinc depletion overlap with immune infiltration at fungal lesions.

Finally, phagocytes are known to utilize copper toxicity to kill pathogens. We use a fluorescent probe to directly measure for the first time intracellular copper of *C. albicans* during the macrophage copper burst (Appendix II).

Altogether, this work illustrates the importance of metals at the host-pathogen interface. Specifically, we explore the host utilization of copper for microbial defense, and the adaptive capabilities of *C. albicans* using two different SODs.

Thesis advisor: Valeria Culotta

Thesis readers: Brendan Cormack, Michael Trush, Fengyi Wan

Acknowledgements

I am extremely fortunate to have had the support of many people during my years in this PhD program. I cannot possibly name everyone who has impacted me, but I can acknowledge some of these individuals here.

First, I wish to thank my advisor, Dr. Valeria Culotta, who has given me unwavering support and numerous opportunities as I worked toward this degree. She provided the environment I needed to grow and thrive as both a researcher and a professional, and she gave ample amounts of her time to ensure that my needs were met. Val is also an excellent teacher, imparting wisdom by both instruction and example. I could not have asked for a better thesis advisor and mentor.

Additionally, the members of my lab have been extremely helpful in so many ways, and fun to work with on a daily basis. I am especially grateful to Julie Gleason, who has taught me most of the experimental techniques I know, and has assisted me in troubleshooting many others. My research would have been much more difficult without Julie's support.

My thesis research committee has also been very supportive in the intellectual development of my project. Drs. Valeria Culotta, Brendan Cormack, Michael Trush, Fengyi Wan, Svetlana Lutsenko, and Susan Michaelis have all served on this committee. Drs. Culotta, Cormack, Trush, and Wan also served as my thesis readers.

I want to give a special thanks to Brendan Cormack, who has been an important collaborator on my project and has contributed intellectually to the work on our lab. He has been extremely supportive of me, serving on every single one of my school-wide committees and allowing me to complete work in his own lab.

In addition, I have had the great pleasure of working with members of Brendan's lab, especially Carlos Gomez and Liz Hwang-Wang, who taught me new techniques at pivotal moments of my project.

Other individuals have also taught me important new techniques, including Abigael Muchenditsi from Svetlana Lutsenko's lab, and Adriana Batazzi from Pierre Coulombe's lab. I also collaborated with Lydia Finney on the XRF experiments at the Advanced Photon Source, Argonne National Laboratory. All of these people enabled my research to be such a success.

Aside from research, there were many professors that also supported me during this program. Drs. Jim Yager, John Groopman, and Joe Bressler were always happy to chat with me and give helpful advice. Discussions with Dr. Mary Fox and Dr. Keeve Nachman helped me realize my post-graduation aspirations. Notably, I worked with Dr. Nachman on a raw milk literature review and policy project that has been extremely enriching and rewarding. I further thank Mary Fox and Keeve Nachman for assisting me in my professional networking, which directly led to job interviews.

During my years at this institution, I have met many wonderful people. The students in my program have been my friends and personal support group for years, they have made a true difference in my success as a PhD student. I have also had the great pleasure of befriending many students outside of my program, particularly in EHS and BMB. These friends have made my experience here infinitely more enjoyable, and I am excited to see what we are all able to achieve in the future.

There is one student that I feel very fortunate to have met. My boyfriend, Ben Davis, has been a source of constant joy. He supports me in every way, and is endlessly patient, kind, and fun. I consider myself an extremely lucky girl.

Finally, I wish to thank my family, my mom Huizhu Kong, my dad Jianwei Li, and my sister Sheri Li. All my life, their example and influence have shaped me into the person that I am. I am thankful for the innumerable life lessons that they taught me and the values that they instilled in me, all of which were instrumental in my achieving this PhD, and I'm sure will continue to be valuable to a long time to come.

Table of Contents

List of Tables

CHAPTER 3: Fungal adaptation to host copper: swapping metal co-factors for SOD enzymes during *Candida albicans* infection

List of Figures

Abbreviations and Nomenclature

°C	degrees Celsius
µg	micrograms
µM	micromolar
AAS	atomic absorption spectroscopy
AMP	adenosine monophosphate
ANOVA	analysis of variance
Asn	asparagine
BCS	bathocuproine sulphonate
BODIPY	boron dipyrromethene
bp	base pair
Ca	calcium
CCS	copper chaperone for superoxide dismutase 1
cDNA	complementary deoxyribonucleic acid
CFU	colony forming units
Cl	chlorine
CS1	coppersensor-1
Cu	copper
Cu(I)	monovalent copper
Cu(II)	divalent copper
CuRE	copper response element
$CuSO_4$	copper sulfate
Cy5	cyanine 5 dye

DAPI	4',6-diamidino-2-phenylindole
DIC	differential interference contrast
DMEM	Dulbecco's modified eagle medium
DMSO	dimethyl sulfoxide
DNA	deoxyribonucleic acid
EDTA	ethylenediaminetetraacetic acid
ETC	electron transport chain
Fe	iron
Fig.	figure
g	gram
GFP	green fluorescent protein
Gln	glutamine
GPI	glycosylphosphatidylinositol
GSH	glutathione
H^+	proton
H_2O	water
H_2O_2	hydrogen peroxide
hrs	hours
IACUC	Institutional Animal Care and Use Committee
ICP-MS	inductively coupled plasma mass spectrometry
IFNγ	interferon gamma
IHC	immunohistochemistry
IMS	intermembrane space
JHU	Johns Hopkins University

k_{cat}/K_m	specificity constant
K_d	dissociation constant
L	liter
Leu	leucine
M	molar
mA	milliamp
mg	milligram
min	minute
mL	milliliter
mM	millimolar
mm	millimeter
Mn	manganese
$MnCl_2$	manganese chloride
MOI	multiplicity of infection
M^{ox}	oxidized metal
M^{red}	reduced metal
mRNA	messenger ribonucleic acid
NADPH	reduced nicotinamide adenine dinucleotide phosphate
NBT	nitroblue tetrazolium
NET	neutrophil extracellular trap
ng	nanogram
Ni	nickel
nm	nanometer
NOX	NADPH oxidase

$O.D._{600}$	optical density at 600 nm
O_2	molecular oxygen
$O_2^{\bullet-}$	superoxide
$OH^{\bullet}$	hydroxyl radical
OPC	oropharyngeal candidiasis
P	phosphorus
P144	proline at residue 144 of *S. cerevisiae* Sod1 protein
PBS	phosphate buffered saline
PCR	polymerase chain reaction
PKA	protein kinase A
PNA-FISH	peptide nucleic acid fluorescent in situ hybridization
POR	NADPH-cytochrome P450 reductase
PVDF	polyvinylidene fluoride
qRT-PCR	quantitative real time polymerase chain reaction
RNA	ribonucleic acid
ROS	reactive oxygen species
S	sulfur
s	second
SC	synthetic complete yeast medium
Ser	serine
SOD	superoxide dismutase
V	volt
WT	wilt type
x g	times gravity

XO	xanthine oxidase
XRF	X-ray fluorescence microscopy
YPD	yeast extract, peptone, dextrose enriched yeast medium
Zn	zinc

Yeast Nomenclature

CEN	centromere, single copy plasmid
All caps, italics	wild type gene (e.g. *SOD1*)
No caps, italics	mutant gene (e.g. *sod1*)
First letter cap, no italics	protein (e.g. Sod1)
Δ	gene deletion in haploid yeast (i.e. *S. cerevisiae*)
Δ/Δ	homozygous gene deletion in diploid yeast (i.e. *C. albicans*)
Δ/+	heterozygous gene deletion in diploid yeast (i.e. *C. albicans*)

CHAPTER 1

Introduction and Background

Superoxide and Superoxide Dismutase Enzymes

Superoxide dismutases (SODs) are a family of enzymes that serve as major cellular antioxidants. They were first discovered in 1969 by McCord and Fridovich [1], and are found in all aerobic organisms from bacteria to humans. Using a metal catalytic cofactor "M", these enzymes catalyze the following disproportionation reaction to convert two superoxide radicals into molecular oxygen and hydrogen peroxide:

$$M^{ox} + O_2^{\bullet -} \rightarrow M^{red} + O_2$$

$$M^{red} + O_2^{\bullet -} + 2H^+ \rightarrow M^{ox} + H_2O_2$$

SODs are some of the fastest enzymes in existence, with the rate of reaction limited only by the rate of diffusion ($k_{cat}/K_m=2x10^9\ M^{-1}\ s^{-1}$) [2-4]. There are three classes of SODs, each using a different metal ion for catalysis: Ni-SODs, Cu/Zn-SODs, and Mn- or Fe-SODs. These classes evolved separately, but converged to perform the same function. The most ancient class of SOD was the Fe-SOD, which originated from the need to protect cells from oxidative damage in the new aerobic atmosphere. At the time, iron was abundantly bioavailable and thus Fe-SODs evolved. Later, as atmospheric oxygen levels rose and iron became less bioavailable and more toxic, Mn-SODs arose [5]. As oxygen levels continued to rise, iron and manganese continued to decline in abundance, but copper and zinc bioavailability rose greatly[6,7], leading to the evolution of Cu/Zn-SODs. This indicates that evolution of the various metal-containing SODs was driven by environmental metal bioavailability in the progressively aerobic atmosphere.

SODs and other antioxidant enzymes have evolved to deal with the production of reactive oxygen species (ROS) that are generated as a product of aerobic metabolism. The superoxide anion ($O_2^{\bullet -}$) is the result of a single electron reduction of O_2, and is

moderately reactive with other biomolecules. Superoxide is specifically damaging to iron-sulfur clusters and iron cofactors within enzymes [8,9]. Superoxide can abstract an electron from the 4Fe-4S cluster, which destabilizes the structure and results in a loss of the catalytic iron atom [10]. Fe-S clusters are found in many enzymes critical to cell metabolism, including aconitase and fumarase in the Krebs Cycle, and dehydratases in the lysine biosynthesis pathway [10-15]. Superoxide can also oxidize and release single iron cofactors from non Fe-S enzymes, which eventually leads to mismetallation of the active site with zinc and loss of enzymatic activity [8,9,16].

Disproportionation of superoxide occurs either spontaneously or orders of magnitude more rapidly via SODs, forming hydrogen peroxide (H_2O_2). Hydrogen peroxide is an important signaling molecule in the cell; by oxidizing certain thiols in proteins [17,18], it can regulate processes such as metabolic adaptation, differentiation, and proliferation [19-24]. When hydrogen peroxide levels are too high, the molecule can be further reduced to the toxic hydroxyl radical ($OH^{\bullet}$), an extremely reactive oxidant, by Fenton or Haber-Weiss reactions involving iron or copper cations [25,26]. Hydroxyl radicals are severely and irreversibly destructive to many cellular macromolecules; as one example, it can abstract hydrogen atoms from unsaturated fatty acids, setting off a chain reaction called lipid peroxidation [26,27]. To avoid the formation of hydroxyl radicals, multiple antioxidant enzymes, such as glutathione peroxidases, peroxiredoxins, and catalases, fully reduce hydrogen peroxide to non-toxic water (H_2O) [28-30]. However, eukaryotes must rely on the SOD family of enzymes to eliminate superoxide.

ROS production, while important for signaling in some cases, is largely harmful to cells. Hallmarks of oxidative stress caused by ROS include injury to many cellular

macromolecules. Proteins can be damaged by oxidation of thiols or metal cofactors, or by carbonylation of amino acid residues [8,31-34]. DNA damage is seen as single or double strand breaks, or as nucleotide modifications such as 8-hydroxyguanidine [35-37]. Cell membranes can be damaged by lipid peroxidation chain reactions [26,27]. Oxidative stress contributes to many health conditions such as aging [32,38], inflammation[39], cancer [34,40,41], and fibrosis [42,43]. To prevent these detrimental effects, organisms require antioxidant enzymes like SODs for protection.

The three classes of SODs are structurally different and exist in specific organisms and cellular compartments. The Ni-SODs are the rarest SODs, present in some gram-negative bacteria and cyanobacteria [5,44]. They function as homohexamers, each subunit coordinating one nickel ion for catalysis [5,45]. Little is known about Ni-SOD biology and evolution.

On the contrary, Cu/Zn-SODs are well understood enzymes. The sequence and structure of this SOD (Fig. 1-1A,B) is well conserved throughout evolution, from prokaryotes to eukaryotes. Cu/Zn-SODs primarily function as homodimers, where each monomer contains one catalytic copper cofactor and one zinc structural cofactor in the active site [46]. Cu/Zn-SODs are generally quite stable, but are inactivated in the presence of excess hydrogen peroxide [47]. These enzymes are localized in the periplasm of many gram-negative bacteria, and in the cytosol of most eukaryotes including plants, animals, and fungi. Cu/Zn-SODs are also found in the mitochondrial intermembrane space of fungi and animals, in the chloroplast of plants, and in extracellular space in eukaryotes [48-50].

Cu/Zn-SODs have been well studied in a variety of organisms, including the model yeast *Saccharomyces cerevisiae*. In this yeast, it was discovered that cytosolic Cu/Zn-Sod1 was activated by the copper chaperone for Sod1 (Ccs1) [51]. This activation involves a series of post-translational modifications that turns apo-Sod1 into the fully active enzyme. Ccs1 first acquires copper and then binds to an apo-Sod1 monomer. In the presence of oxygen, Ccs1 inserts the catalytic copper and facilitates formation of the intermolecular disulfide bond on Sod1 [51-53]. The mature Sod1 monomer is then released and can homodimerize to form the active enzyme [52].

In *S. cerevisiae*, Sod1 is activated solely by Ccs1; however, an alternative activation mechanism exists in other organisms. In many organisms including humans, mice, and *C. elegans*, Cu/Zn-Sod1 retains some activity in the absence of Ccs1 [54-57]. In fact, *C. elegans* does not possess a CCS-encoding gene at all [56]. The CCS-independent pathway of Sod1 activation requires glutathione to donate copper to the enzyme [55,58]. In humans, Sod1 can be activated by both the Ccs1 and glutathione pathways [59]. The Sod1 enzyme's dependence on Ccs1 for activation is fully determined by one residue, a proline at position 144 of *S. cerevisiae* Sod1 (Fig. 1-1A,B). Most other organisms contain a leucine, valine, or alanine at this position [55]. The P144 residue is located near the active site and disulfide bridge (Fig. 1-1A,B), and its presence precludes disulfide formation without CCS (Fig. 1-2) [59]. Mutating P144 in *S. cerevisiae* Sod1 allows activation of the enzyme independent of Ccs1 (e.g., P144S Sod1 as in Fig. 1-2) [57,59]. Ccs1 requires oxygen to function, thus Ccs1 activation of Sod1 is promoted in aerobic conditions in order to detoxify the high levels of ROS [57]. The P144 residue is only seen in Ascomycota fungi [55], which includes *S. cerevisiae* and

human fungal pathogen *C. albicans*. It was unknown whether *C. albicans* Sod1 activation was also dependent upon the CCS copper chaperone, but this will be addressed in Chapter 2 of this thesis.

The third class of SOD is Mn- or Fe-SODs. These SODs are structurally similar but include enzymes that can use only manganese, only iron, or either metal for catalysis. Fe-SODs are found in a wide range of prokaryotes, in protists, and in the chloroplasts of plants [60-62]. Mn-SODs are localized in the mitochondrial matrix of plants, animals, and fungi [63-66]. In rare cases, Mn-SODs replace the Cu/Zn-SODs in the cytosol of marine eukaryotes such as crustaceans and photosynthetic algae [67-69]. These organisms do not utilize a Cu/Zn-SOD so that they can spare copper for other important enzymes involved in oxygen transport or photosynthesis [67,68,70]. Thus, replacing the cytosolic Cu/Zn-SOD with Mn-SOD is an adaptation to metabolic uses of copper. While most Mn- and Fe-SODs are only catalytically active with its specific native metal, metal substitution does occur. For example, *E. coli* Mn-SOD has been observed to bind iron *in vivo* [71], and does so with an affinity equal to that of manganese [72]. In eukaryotes, the mitochondrial Mn-SOD very specifically acquires manganese, and disruption of manganese or iron homeostasis can cause iron insertion and severe detriments to the cell [73,74].

It is interesting to note that the partitioning of different types of SODs within a cell is a result of metal bioavailability, and has been conserved from prokaryotes to eukaryotes. Gram-negative bacteria have Fe-SOD and/or Mn-SODs in the cytosol, since iron and manganese are bioavailable in this compartment (Fig. 1-3A) [75-78]. Cu/Zn-SODs are limited to the periplasm because bacteria do not utilize copper inside the

cytosol, and pump all intracellular copper into the periplasmic space [79-83]. Mitochondrial SODs in eukaryotes follow this same pattern, with a Mn-SOD in the matrix and a Cu/Zn-SOD in the IMS, consistent with the endosymbiosis theory of mitochondrial evolution (Fig. 1-3A) [65]. Using the mitochondrial outer membrane pores, Cu/Zn-SODs can move in and out of the cytosol and maintain equilibrium with the IMS [50]. Many eukaryotes also express a distinct extracellular Cu/Zn-SOD to react with extracellular sources of superoxide [48,49]. Mn-SODs are generally not found in the cytosol of eukaryotes because bioavailable manganese appears insufficient [75,84,85]. However, the fungal pathogen *Candida albicans* is known to express both a Cu/Zn-SOD and a Mn-SOD in the same cytosolic compartment [86]. The rationale for this rare event was not known, and was the topic of investigation in Chapter 3 of this thesis.

Sources of Superoxide for SODs

SODs are located in cellular compartments where superoxide scavenging is necessary. For example, the Cu/Zn-SOD and Mn-SOD in the mitochondria of eukaryotes serve an essential function, because a major cellular source of superoxide is the electron transport chain (ETC) in the mitochondria. Complexes in the ETC leak electrons that reduce molecular oxygen and form superoxide radicals. Complex I and complex III are the primary sources of these free electrons, and their relative contributions depend on organism and cell type [87-90]. Complex I leaks electrons into the mitochondrial matrix, producing superoxide in that compartment. Complex III produces superoxide in both the matrix and IMS, and some of the radical may even enter the cytosol through voltage-

dependent anion channels [91]. An estimated 1-5% of oxygen consumed in aerobic respiration is reduced to superoxide [92,93]. Fortunately, superoxide in the mitochondrial IMS and cytosol can be eliminated by Cu/Zn-SOD, and the superoxide in the matrix is rapidly detoxified by Mn-SOD. Deletion of this Mn-Sod2 in *Drosophila* and mice leads to mitochondrial disease and lethality [94-98]. Thus, maintaining low levels of superoxide in the mitochondria is essential for the survival of eukaryotic organisms.

Superoxide production in the cytosol is partially the result of NADPH-cytochrome P450 reductase (POR), which is anchored to the endoplasmic reticulum membrane and extends into the cytosol [99]. This enzyme donates electrons to cytochrome P450s [100], which are a class of enzymes that metabolize many endogenous and exogenous substrates. POR is also able to reduce molecular oxygen to produce superoxide in the cytosol [101,102]. Another cytosolic source of superoxide is xanthine oxidase (XO) [103]. XO normally exists as xanthine oxidoreductase (XOR), which hydroxylates hypoxanthine to xanthine to uric acid in the purine catabolism pathway [104]. However, cysteine oxidation or proteolysis can convert the enzyme to XO, which, along with the substrate xanthine, preferentially donates electrons molecular oxygen to produce superoxide [104,105]. The superoxide produced by these sources is eliminated by the cytosolic Cu/Zn-SOD.

Another important source of cellular superoxide is NADPH oxidase (NOX) enzymes. Most multicellular organisms express NOX enzymes while prokaryotes do not have any [106,107]. NOX enzymes consist of a large transmembrane complex, with the Nox genes encoding the catalytically active subunit [108]. The naive monomer of the

protein is inactive; its binding partners are required for proper maturation and trafficking [109]. NOX enzymes are often found on the plasma membrane and produce extracellular superoxide, but mammalian Nox2 and Nox4 are located on intracellular membranes and produce superoxide in the lumen of different compartments [108,110]. Extracellular superoxide produced by mammalian cell surface NOXs may be eliminated by extracellular Cu/Zn-SODs.

While most cells in metazoans are believed to use NOX for signaling purposes [111], NOX were first described in phagocytic immune cells that use ROS to fight pathogens [112-114]; this phagocytic NOX is Nox2. Once activated, Nox2 localizes to the phagosome of phagocytic cells and generates high levels of superoxide in that compartment [14,115]. This is known as the respiratory burst, part of the phagocyte's strategy for killing microbes. Neutrophils exhibit a much higher level of NOX activity compared to macrophages [116].

Many pathogenic gram-negative bacteria are able to resist the phagocytic respiratory burst using Cu/Zn-SODs expressed in the periplasm. Examples of bacteria that use these extracellular SODs are *Salmonella typhimurium* [117-120], *Neisseria meningitides* [121], *Mycobacterium tuberculosis* [122], *Salmonella choleraesuis* [123], *Brucella abortus* [124], and *Haemophilus ducreyi* [125]. These Cu/Zn-SODs have been shown to be important for bacterial survival in macrophages and for virulence in animal models [117-125].

The Large Family of SOD Enzymes in *Candida albicans*

Compared to the wealth of information on SOD enzymes in relation to pathogenesis of bacteria, very little is understood about SODs and infection with eukaryotic pathogens, such as fungi. To this end, my thesis work has focused on the family of SOD enzymes of *Candida albicans*, an important fungal pathogen for public health. Below is an introduction to the unusually large family of SODs in *C. albicans*, followed by a discussion of *C. albicans* in infectious disease and public health.

Like the well-characterized budding yeast *S. cerevisiae*, *C. albicans* is a member of the Saccharomycetaceae family of filamentous yeasts. While yeasts such as *S. cerevisiae* are limited two SODs, a cytosolic Cu/Zn-Sod1 and a mitochondrial Mn-Sod2, *C. albicans* has these two [126,127] plus an additional four SODs: A cytosolic Mn-Sod3 [86] and three Cu/Zn-like SODs anchored to the cell surface named Sod4, Sod5, and Sod6 (Fig. 1-3B) [128]. This extensive family of SODs has been the subject of much research in the Culotta lab.

Our group recently published the crystal structure of Sod5 and characterized the enzyme as a Cu-only SOD [129]. In addition to missing the zinc binding site, Sod5 also lacks the electrostatic loop that was believed to guide superoxide to the active site. In spite of these unusual features, Sod5 is catalytically just as fast as Sod1 [129]. Sod5 is secreted from the cell and anchored to the cell wall by a glycosylphosphatidylinositol (GPI) anchor. Sod4 and Sod6 are also predicted to be GPI-anchored to the cell surface, but they have not been well analyzed. Sod5-like enzymes have been found in an extensive array of Ascomycota and Basiodomycota fungi [129] but are totally absent from the animal and plant kingdoms where the extracellular Sod is the Cu/Zn-SOD.

Studies have shown that the extracellular localization of Sod4, Sod5, and Sod6 function to protect *C. albicans* from ROS damage during the respiratory burst of phagocytes [130,131]. Others have shown Sod5 to be important for pathogenesis in a mouse model of systemic candidiasis [128]. These results demonstrate that extracellular SODs function to protect the yeast from the respiratory burst of the macrophage and neutrophil phagolysosome.

The other unusual SOD in *C. albicans* is the Mn-Sod3, because of its unique co-localization with Cu/Zn-Sod1 in the cytosol. As described above, Mn-SODs have been found in the cytosol of a few marine organisms [67,68], but only *C. albicans* and some closely related fungi have both a Cu/Zn-SOD and a Mn-SOD in this compartment. This cytosolic Sod3 and the mitochondrial Sod2 are highly homologous in sequence, differing only in that Sod3 lacks a mitochondrial targeting sequence. Sod3 was recently characterized in 2001, and studies showed that *SOD1* and *SOD3* mRNA was inversely regulated. *SOD1* mRNA was present during logarithmic growth and was replaced by *SOD3* mRNA upon entering stationary phase [86]. This curious alternative regulation of *SOD1* and *SOD3* will be extensively investigated in this thesis (Chapter 3).

The Opportunistic Pathogen *Candida albicans*

This yeast with the puzzling array of SODs is in fact a significant public health problem. *C. albicans* is a commensal inhabitant of the human microflora. It is the major fungal species that inhabits and sometimes infects humans. This yeast primarily lives on mammalian mucosal epithelial surfaces such as the intestinal lining, oral cavity, and

vagina. An estimated half of the human population is colonized by *C. albicans* [132]. Its growth is typically held in check by the host immune system and by competition with surrounding microflora such as bacteria. However, under some conditions, *C. albicans* can become pathogenic. This can occur when the epithelial surface is physically damaged, when the surrounding bacteria is depleted, such as with antibiotics, and when the host immune system is suppressed [132]. Severity of infection can vary widely, from mild infections such as vaginal or oral thrush to lethal systemic infections. By definition, candidiasis encompasses fungal infections from multiple *Candida* species. *C. albicans* is the most common cause in humans, accounting for over half of disseminated candidiasis incidents with a crude mortality rate of over 30% [133].

Risk factors for invasive candidiasis include colonization by *C. albicans*, broad spectrum antibiotics, central venous catheters, prolonged hospital stay, immunosuppression, and premature infants [132]. In spite of available antifungal treatments, incidence of lethal infections is still on the rise in the United States, especially in hospital settings [132]. Additionally, antifungal resistance is becoming problematic, and new methods of treating infections are needed. Another major clinical concern is biofilm formation on catheters. A biofilm is an organized group of cells that are embedded in an extracellular polymer matrix, and are highly resistant to drugs and mechanical removal [134]. Cells from biofilms can also disseminate through the body and lead to infection of new sites. An alarming 65-90% of patients with disseminated candidiasis had central venous catheters [132].

The virulence of *C. albicans* as a pathogen is partly due to its ability to change morphology [135]. It can reversibly switch between budding yeast, filamentous hyphal,

and pseudohyphal forms [136]. Hyphal yeast can penetrate tissue, causing significant tissue damage, and then enter the blood stream where it can disseminate through the body and invade other organs and tissues [136,137]. These morphologies are not exclusively associated with colonization or invasion in a host; most conditions involve mixed populations of budding and filamentous yeast [137].

The host immune system tolerates the presence of *C. albicans* colonizing epithelial surfaces, because the fungal load is low and the yeast is not invading and damaging epithelial cells. However, when the pathogen is actively invading the tissue, a strong immune response is activated to combat the infection [137]. As part of this immune response, tissue macrophages are present and engulf the surrounding microbes. If hyphal (invasive) *C. albicans* are detected, the macrophages will produce cytokines that activate T_H17 memory cells to recruit neutrophils to the site of invasion. Neutrophils are able to engulf and kill the invading fungus efficiently [137]. Surprisingly, macrophages are not always effective at killing *C. albicans*. *C. albicans* cells that are engulfed by macrophages can survive in the harsh conditions of the phagolysosome, and can form hyphae that ultimately pierce and kill the macrophages [138]. Neutrophils, however, can effectively kill *C. albicans* by phagocytosis, by degranulating and releasing antimicrobial proteins, and by a form of cell death that releases cellular components to trap and kill pathogens, called neutrophil extracellular traps [139].

C. albicans can colonize and infect many sites in the human body, including the intestine, vagina, oral cavity, and blood stream [132,140-142]. Systemic blood infections are the most lethal because the yeast can disseminate to many other organs, primarily the kidney but also the liver and the spleen [143]. To be able to thrive in all of these different

niches in the body, *C. albicans* must be highly adaptable to many environmental conditions such as pH, oxygen, and nutrient availability. One important class of micronutrient is metals, which the yeast must acquire from the host. Metals at the host-pathogen interface have been gaining interest among researchers, and we will investigate this further in Chapter 3 and the Appendices of this thesis.

Metals and Nutritional Immunity

An emerging concept in the innate immune response involves nutritional immunity, the process by which the host immune system withholds biologically relevant metals for microbial defense [144]. Transition metals are essential for many important biological processes, such as catalysis, respiration, and transcriptional regulation [144,145]. However, while metals are necessary for life, they are also toxic at high levels due to their high reactivity. Thus all organisms have evolved measures to tightly control their metal homeostasis, and mammalian immune systems are able to utilize these methods against microbial pathogens.

Many studies have shown that the host sequesters iron, manganese, and zinc for nutritional immunity. Iron was the first metal discovered to be withheld during microbial infection. During infection and inflammation, the level of serum transferrin-bound iron plummets, preventing many microbes from acquiring this essential metal [146,147]. Phagocytes express a divalent metal transporter on the phagosomal membrane, called natural resistance-associated macrophage protein 1 (NRAMP1), which pumps iron and manganese out of the compartment [148-150]. The S100 family of proteins is also

known to bind metals and be involved in microbial defense. One prominent example is calprotectin, which chelates Mn and Zn in tissue abscesses and neutrophil extracellular traps [139,151-153]. With these methods of nutritional immunity, the host can withhold iron, manganese, and zinc from pathogens and starve them of these essential nutrients.

Meanwhile, pathogens have evolved varied strategies for combating nutritional immunity. Bacteria and yeast, such as *C. albicans*, are able to acquire iron through three main methods: Ionic iron import, heme acquisition, and siderophore uptake [144,154]. Some pathogens express transferrin receptors which can capture transferrin for iron extraction [155,156]. Pathogens can also release siderophores, small molecules that can capture iron with extremely high affinity. The siderophores can then be imported into the cell where the iron is released [157,158]. Additionally, many pathogens have receptors for hemoglobin that can extract heme before transporting it into the cell [159,160]. Furthermore, many bacteria express cell surface metal transporters that capture manganese and zinc [161-165], which are also necessary for bacterial virulence. This complex duel for metal acquisition exemplifies the importance of these nutrients at the host-pathogen interface.

Copper is also an essential nutrient, but unlike iron, manganese, and zinc, there is no known role for copper in nutritional immunity. Instead, the host exploits the toxic properties of copper to combat pathogens. For millennia, copper has been known to have antimicrobial effects. The earliest recorded medicinal use of copper was from the Smith Papyrus of ancient Egypt, where copper was used to sterilize drinking water and wounds [80,166]. In the present day, copper is used as a biocide in disinfectants, pesticides, and hospital surfaces [80,167,168].

The innate immune systems of mammals are also adept at using copper to combat pathogens. In macrophages, copper levels increase in the phagolysosome in response to engulfed bacteria [169,170]. This effect requires macrophage upregulation of the copper importer Ctr1 to increase copper uptake, and the relocation of the Atp7A copper transporter to pump copper into the phagolysosome [171]. We call this the macrophage "copper burst." High levels of copper in the phagolysosome are toxic to microbes; in conjunction with the oxidative burst by Nox2, described previously, copper can undergo Fenton reactions to reduce hydrogen peroxide into the deadly hydroxyl radical [82,171]. Copper elevation also occurs in the blood serum during infection and inflammation [172-174]. High copper can also be observed in tissues, as has been shown during *C. neoformans* infection of the lung [172].

In spite of this, pathogens have means to defend against copper toxicity. Bacteria do not utilize copper in the cytosol, the metal is only used in a few proteins in the periplasm, so the bacteria actively export copper from the cytosol to avoid accumulation [80,82]. This is achieved by P-type ATPases that pump copper out across the plasma membrane, and some bacteria have copper transporters that further export the metal across the outer membrane [83,175,176]. Some bacteria also express cytosolic or periplasmic copper sequestration proteins, similar to eukaryotic metallothioneins, in order to limit toxic interactions of free copper [81,177]. These bacterial copper export and sequestration mechanisms are required for microbial virulence [81,83,175-178], suggesting that the pathogen response is to protect against copper toxicity, not copper starvation.

Fungal pathogens also have strategies for copper detoxification. *C. neoformans* protects itself by inducing copper-sequestration metallothioneins [172]. *C. albicans* also expresses metallothioneins Cup1 and Crd2 [179-181], and additionally has a cell surface P-type ATPase Crp1 that pumps copper out of the cell [180,181], similar to bacterial ATPases. Both copper efflux by Crp1 and copper detoxification by Cup1 are needed for *C. albicans* survival during the macrophage copper burst [182].

Regulation of Copper Homeostasis in *C. albicans*

All cells must maintain strict control of internal copper levels, keeping enough for cellular functions but not too much to cause toxicity. Thus a complex network of proteins has evolved to acquire, distribute, and store copper within the cell. The cellular level of unbound copper is sustained at an exceedingly low concentration, around 10^{-19} M [183]. The following mechanisms of copper homeostasis were first elucidated in *S. cerevisiae*, and most are conserved in *C. albicans* [184,185].

Prior to uptake of extracellular copper, the metal is first reduced from Cu(II) to Cu(I) by cell surface reductases such as Fre7 [186-189], then imported into the cell largely by high affinity copper transporter Ctr1 (Fig. 1-4) [190-192]. Once inside the cell, copper is mobilized by copper chaperones along discrete pathways. Atx1 delivers copper to the P-type ATPase Ccc2, located on secretory membranes [193-195]. A different chaperone Cox17 is required to deliver Cu to the mitochondria for cytochrome c oxidase (Fig. 1-4) [196-202]. The last chaperone is Ccs1, discussed previously, which transfers a copper ion and disulfide bond to activate Cu/Zn-Sod1 [51-53]. Ccs1 has been

extensively characterized in *S. cerevisiae*; in Chapter 2 we demonstrate how this protein functions in *C. albicans* compared to CCS molecules of other organisms.

These and many other copper homeostasis proteins are regulated at the transcriptional level by a pair of copper-sensing transcriptional activators, Cup2 and Mac1 (Fig. 1-4) [203-206]. Cup2 is activated by high copper levels and chelates four copper ions to change conformation and gain activity [207]. Active Cup2 can bind to specific sequences in the promoters of target genes, including the aforementioned metallothioneins and the copper-exporting ATPase Crp1, to facilitate copper detoxification [181,205,206,208].

In *C. albicans* as well as other fungi including *S. cerevisiae* and *P. anserina*, Mac1 is a transcription factor that functions during copper deficiency to activate copper uptake genes. It has been best characterized in *S. cerevisiae* where it contains a nuclear localization sequence, a zinc-containing DNA binding domain, and a copper-binding trans-activation domain that binds eight copper ions within two cysteine-rich repeats [209-211]. This holds the DNA-binding domain in a stable but inactive conformation [210]. When cellular copper is depleted, Mac1 loses the copper ions in at least one cysteine-rich repeat, and the resulting conformational change leaves the DNA-binding domain exposed and ready to interact with DNA [210,211]. Mac1 binds to DNA at sites called copper response elements (CuREs), with the consensus sequence 5'-TTTGC(T/G)C(A/G)-3' [189,212]. This sequence is largely conserved in *C. albicans* and *P. anserina*, with the introduction of some flexibility at the first position [213,214]. Although Mac1 function is conserved from *S. cerevisiae* to *C. albicans* [214,215], sequence comparison of the polypeptides reveal only 18% identity, with the DNA-

binding domain containing the most homology. In *S. cerevisiae*, homodimerization of Mac1 is required for transcriptional activation [211], whereas *C. albicans* Mac1 functions as a monomer [215]. In spite of the differences, *C. albicans* Mac1 is still activated by low copper and upregulates transcription of copper uptake genes like *CTR1* and *FRE7* using the CuRE consensus sequence [215]. Mac1 regulation in *C. albicans* will be investigated further in Chapter 3 of this thesis.

Additionally, copper regulation in *C. albicans* involves Gpa2, a G-protein α subunit that can modulate copper uptake genes such as *CTR1*, *FRE7*. Gpa2 is thought to work by connecting Mac1 through the cyclic-AMP protein kinase A (PKA) pathway [205].

Overview of Thesis Research

The work described in this thesis is aimed at understanding the biology of the intracellular SODs, Cu/Zn-Sod1 and Mn-Sod3, in the opportunistic fungal pathogen *C. albicans*. Chapter 2 focuses on Cu/Zn-Sod1 and its activation. We found that *C. albicans* Sod1 and Ccs1 cross-react poorly with the corresponding SOD and copper chaperone of *S. cerevisiae*, suggesting structural differences that may impact physical interactions, copper insertion, or disulfide formation. We also found that *C. albicans* Sod1 is relatively unstable, which may be driven by this pathogen's unusual need for Sod1 turnover in some environmental conditions, described below. Chapter 3 provides a thorough investigation of the function and regulation of the co-localized Cu/Zn-Sod1 and Mn-Sod3. A previous study determined that *SOD1* mRNA was present in log phase

growth and *SOD3* mRNA replaced it during stationary phase [86]. We now demonstrate that this switch in SODs is a function of changing copper levels. *C. albicans* has evolved with a pair of cytosolic SODs with different metal co-factors to ensure that cytosolic SOD activity remains constant over a wide range of intracellular copper levels. This occurs via the copper-responsive transcription factor Mac1. We identified and confirmed the CuRE sequences required for Mac1 binding, and uncovered a novel method by which Mac1, known to be a trans-activator, can in fact repress gene transcription. We further demonstrated that the switch between Sod1 and Sod3 in response to copper occurs in the kidneys of mice during disseminated candidiasis. This evidence of copper limitation during late stage systemic infection could be an example of copper nutritional immunity. In Appendix I, we further explore changes in localization of copper and other metals during disseminated kidney infection. We find that copper levels decline uniformly across the kidney, but other metals such as calcium and zinc are altered as a result of immune infiltration at fungal lesions. In Appendix II, we provide direct evidence for the first time of yeast cells hyperaccumulating copper during macrophage infection by using a copper-sensing fluorescent probe to monitor copper levels within *C. albicans* cells when subjected to macrophage engulfment. Together, these studies underscore the importance of copper and SODs at the host-pathogen interface during fungal infection.

Figure 1-1: Sequence and structure of *S. cerevisiae* Cu/Zn-Sod1.

The crystal structure (A) and amino acid sequence (B) of Cu/Zn-Sod1 from *S. cerevisiae* is shown as an example of eukaryotic Cu/Zn-SODs. **(A)** The electrostatic loop (ESL), copper and zinc cofactors, intramolecular disulfide bridge (DS), and proline 144 are indicated. **(B)** The residues that coordinate copper are notated with C, residues binding zinc are notated with Z, the disulfide cysteines are notated with DS, and the residues forming the electrostatic loop are underlined. Proline 144 is very close to the electrostatic loop and disulfide cysteine, as indicated.

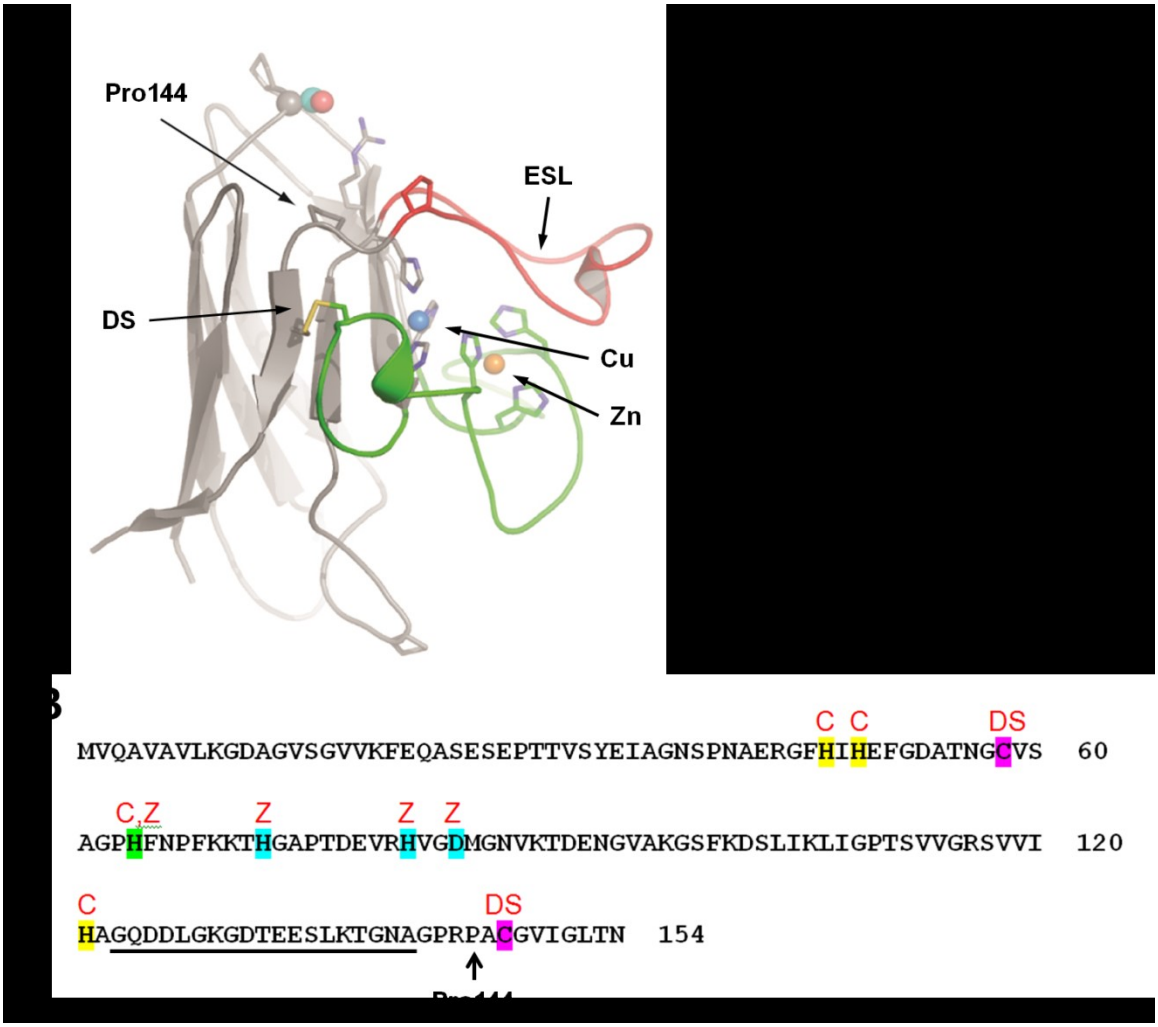

Figure 1-2: Proline 144 on *S. cerevisiae* Sod1 controls the Ccs1-dependence of Sod1 activation.

S. cerevisiae Sod1 contains a proline at position 144, rendering the Sod1 molecule dependent upon Ccs1 for activation (top) [59]. In the presence of oxygen, Ccs1 inserts the catalytic copper and reduces the disulfide bond to confer enzymatic activity to Sod1 [52,53]. Mutation of P144 to another residue such as serine (bottom left) liberates Sod1 from requiring Ccs1, allowing it be activated with the help of glutathione (GSH). The role of GSH in CCS-independent activation is still unclear but may involve GSH binding to copper and/or effects on the Sod1 thiols [55]. *C. elegans* Sod1 does not contain P144, and it is solely activated by the CCS-independent pathway (bottom right) [59].

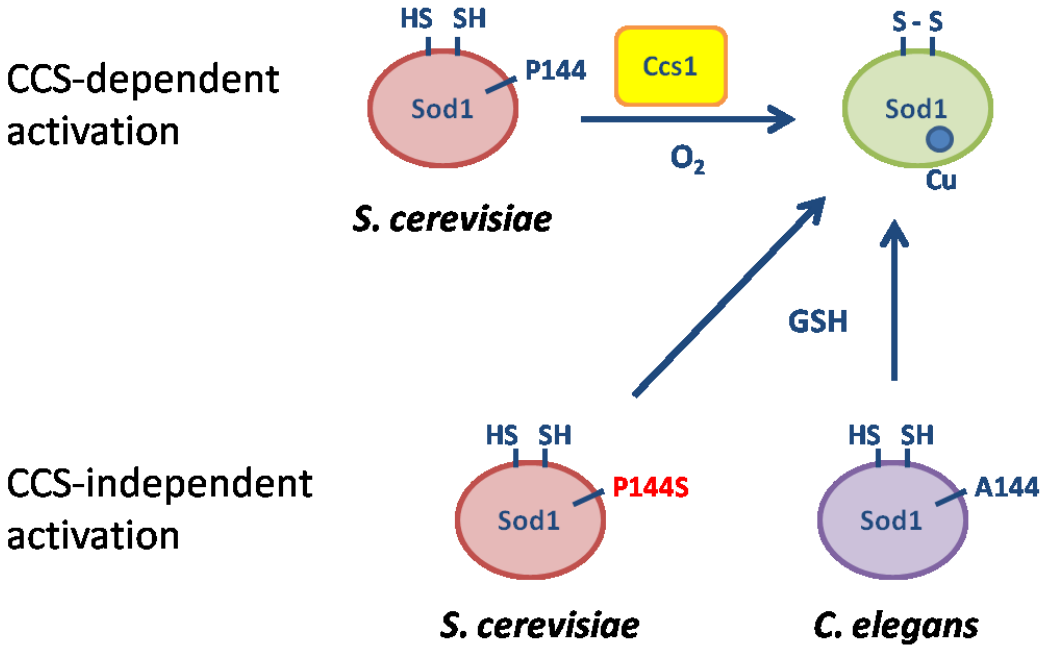

Figure 1-3: Cellular localization and metal content of SODs in various organisms. **(A)** Gram-negative bacteria contain a Mn- or Fe-SOD in the cytosol [61,216] and a Cu/Zn-SOD in the periplasm [217]. This is analogous to the localization of SODs in eukaryotic mitochondria, with Mn-SOD in the matrix [65] and the Cu/Zn-SOD in the IMS [50]. This same Cu/Zn-SOD is also present in the eukaryotic cytosol [50], while a separate Cu/Zn-SOD is sometimes present in the extracellular space [49]. **(B)** *S. cerevisiae* and *C. albicans* both express a mitochondrial Mn-Sod2 [127,218] and a Cu/Zn-Sod1 in the cytosol and IMS [66,126]. However, *C. albicans* has an additional four SODs, including three extracellular Cu-only SODs that are anchored to the cell wall [129], and a rare cytosolic Mn-Sod3[86].

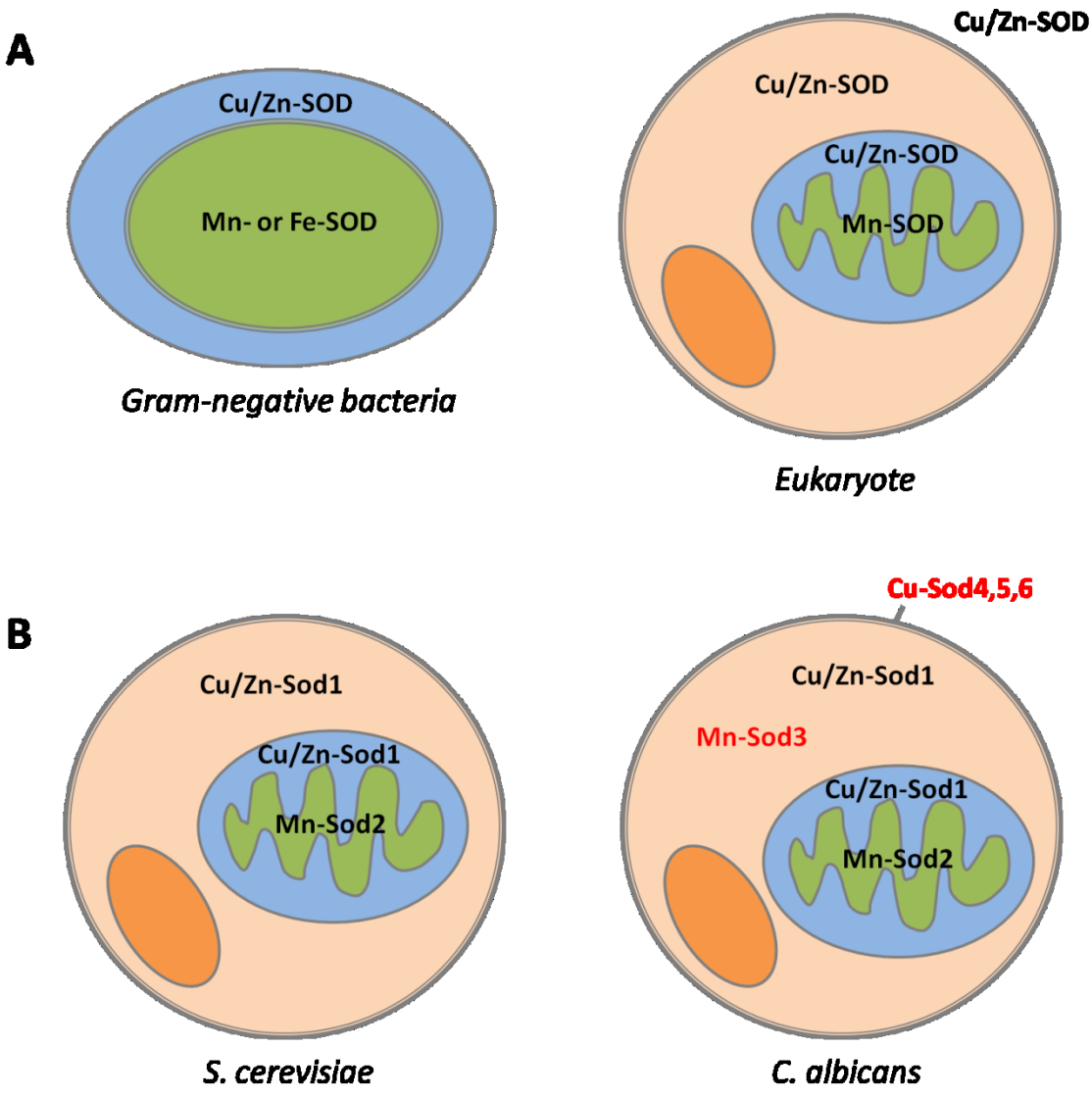
A
Cu/Zn-SOD
Mn- or Fe-SOD
Gram-negative bacteria
Cu/Zn-SOD
Cu/Zn-SOD
Cu/Zn-SOD
Mn-SOD
Eukaryote
B
Cu/Zn-Sod1
Cu/Zn-Sod1
Mn-Sod2
S. cerevisiae
Cu-Sod4,5,6
Cu/Zn-Sod1
Mn-Sod3
Cu/Zn-Sod1
Mn-Sod2
C. albicans

Figure 1-4: Regulation of copper homeostasis in *C. albicans*.

(A) A summary of the *C. albicans* proteins involved in sensing, acquisition, distribution, and mobilization of copper is shown. Each protein and its function are discussed in the main text. **(B)** The function of the Mac1 transcription factor during cellular copper depletion is depicted. Details are discussed in the main text.

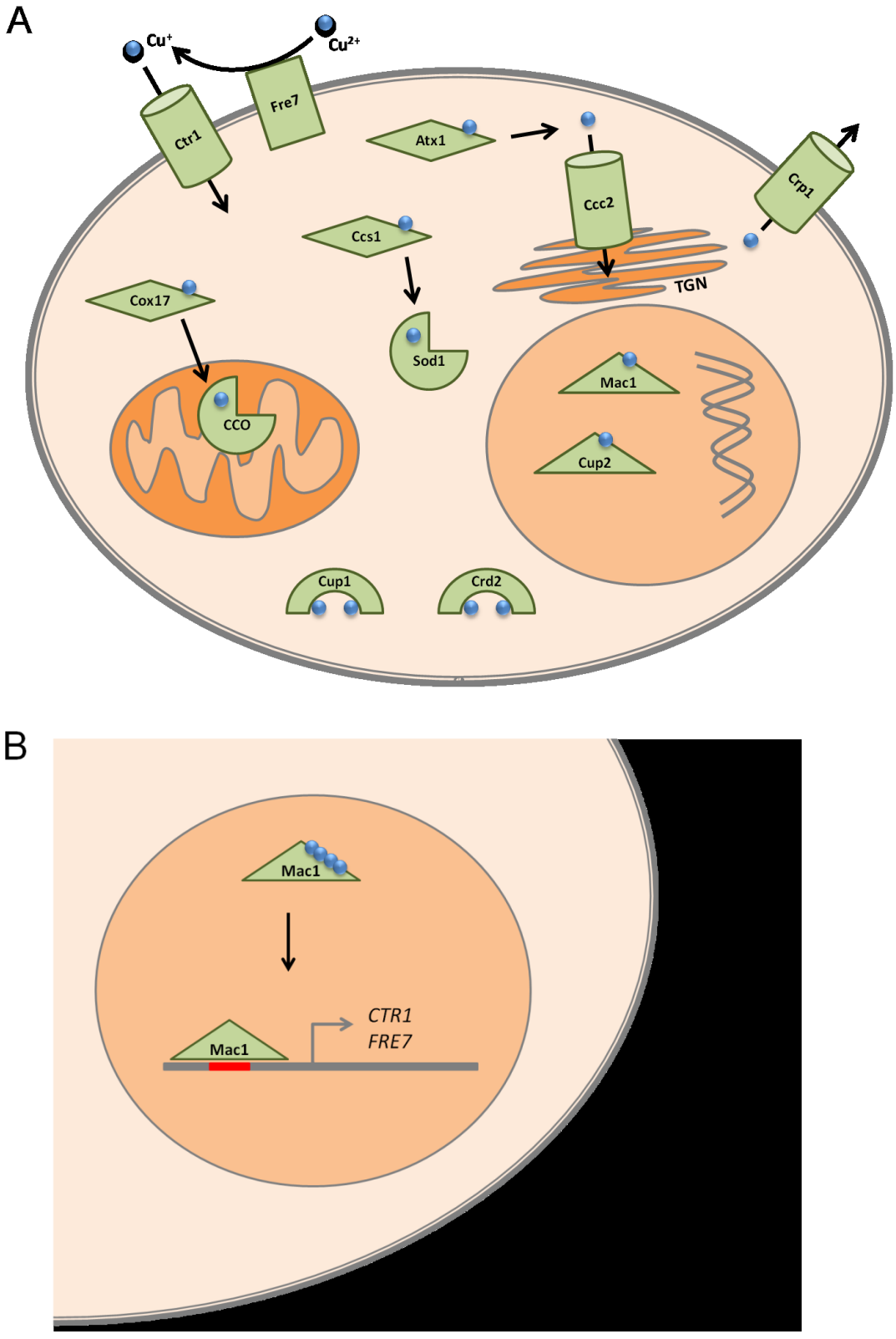
A
Cu+
Cu2+
Fre7
Ctr1
Atx1
Ccc2
Crp1
Ccs1
TGN
Cox17
Sod1
CCO
Mac1
Cup2
Cup1
Crd2
B
Mac1
CTR1
FRE7
Mac1

CHAPTER 2

Species-specific activation of Cu/Zn-SOD by its CCS copper chaperone in the pathogenic yeast *Candida albicans*

The figures and text appearing in this chapter were published in **J. Biol. Inorg. Chem., vol. 19, pp.595-603, 2014** and have been reproduced here by the permission of Springer.

Contributions

This project was initiated by Julie Gleason, currently a research associate in our lab. She identified the *CCS1* gene in *C. albicans* and made the gene deletion to demonstrate its requirement for Sod1 activity (Fig. 2-4). Julie also engineered the P144 and H139 mutants of *C. albicans* Sod1 that are stably expressed in *S. cerevisiae* (Fig. 2-3, 2-7).

I took on this project when I joined the lab in the summer of 2011. At the time, we had no evidence that *C. albicans* Sod1 was enzymatically active, in spite of copious protein production. We could not detect Sod1 activity on the native gel assays that work well for all other Sod1 enzymes that we have studied, including those from *S. cerevisiae*, *C. elegans*, and humans. Various experiments failed to identify the cause for this apparent lack of activity, but ultimately I found that *C. albicans* Sod1 is unstable during the prolonged electrophoresis typically used in our native gel assays, and I optimized the electrophoresis conditions that stabilize *C. albicans* Sod1 activity. I also designed a primary antibody specifically against *C. albicans* Mn-Sod3, one that would not cross-react with the highly similar mitochondrial Mn-Sod2. These tools were instrumental in completing all the work described here in Chapter 2 and in Chapter 3.

For my specific contributions in this Chapter, I developed the assay to simultaneously monitor activity of all three intracellular SODs of *C. albicans* (Fig. 2-1) and elucidated the species-specific nature of *C. albicans* Sod1 interactions with its CCS copper chaperone (Fig. 2-2, 2-5, 2-6A). In total, I completed half the experiments, former rotation student Hana Odeh contributed Fig. 2-6B, and the remainder was done by Julie Gleason.

Introduction

From *E. coli* to humans, the copper and zinc-containing superoxide dismutase (Cu/Zn-SOD or Sod1) enzyme participates in reactive oxygen metabolism by disproportionating superoxide anion to hydrogen peroxide and oxygen [1,217]. The chemistry is carried out by a copper ion at the active site while the zinc co-factor provides more of a structural role. In addition to metal co-factors, an intramolecular disulfide in each Cu/Zn-SOD monomer stabilizes the quaternary structure [219]. The maturation process for Cu/Zn-SOD in which the apo-reduced polypeptide is converted to an active metallated enzyme has been thoroughly investigated. In eukaryotes, this maturation requires a helper protein known as CCS for the copper chaperone for SOD that acts to insert copper and oxidize the disulfide. The zinc is acquired through an unknown mechanism. CCS was originally identified in the baker's yeast *Saccharomyces cerevisiae* as Ccs1 [51], and is now known to span nearly all eukaryotic phyla, however it is absent in bacteria [59]. A peculiar exception is the nematode *C. elegans* which has evolved with no CCS accessory factor for its Cu/Zn-SOD [56].

The CCS copper chaperone harbors three distinct domains that work in concert to capture copper, to dock with Cu/Zn-SOD and to transfer the metal and oxidize the disulfide [220,221]. The N-terminal domain I is similar to the Atx1-family of soluble copper chaperones which includes a CXXC copper binding site that participates in copper capture from an upstream source and insertion of copper into Cu/Zn-SOD [220,222,223]. A central domain II exhibits homology to the Cu/Zn-SOD target and serves to physically dock CCS to apo-SOD1 [224-227]. The C-terminal domain III harbors a CXC motif that plays a critical role in oxidation of the Cu/Zn-SOD disulfide and may also bind copper

[52,220,222,228-230]. This structural paradigm of CCS has been well-conserved with minor exceptions. For example, certain insect CCS molecules (e.g., Ccs from *Drosophila melanogaster*) lack the N-terminal CXXC copper site [231], and the fission yeast *Schizosaccharomyces pombe* CCS carries a fourth cysteine-rich domain at the C-terminus that is used in copper buffering [232]. In spite of these differences, CCS-SOD1 interactions are well-conserved across diverse species. When expressed in the baker's yeast *S. cerevisiae*, Cu/Zn-SOD molecules from *Drosophila*, the *Arabidopsis* plant and humans can all be activated by the yeast Ccs1 copper chaperone [55,231,233,234]. The converse is also true: *S. cerevisiae* Sod1 is well-activated by expression of plant, mammalian and *S. pombe* CCS molecules [51,232,235], and partially by *Drosophila* Ccs lacking the N-terminal CXXC copper site [231].

CCS is not the sole means for activating Cu/Zn-SOD, and in most eukaryotes the SOD can also acquire copper and oxidize the disulfide through a CCS-independent method (reviewed in [57]). The dependence on CCS can be dictated by a single residue in the Cu/Zn-SOD polypeptide, namely the position corresponding to proline 144 in *S. cerevisiae* Sod1. In studies with baker's yeast, P144 strongly inhibits activation of Sod1 *in vivo* without the Ccs1 copper chaperone [55,57,59,236]. P144 appears to restrict Sod1 disulfide oxidation and dimer formation without the aid of Ccs1 [57,59,237]. However, substitution with a non-proline residue at position 144 (e.g., Ser, Leu, Gln) enables some disulfide oxidation in the absence of Ccs1, and the Sod1 can be activated without Ccs1 [55,57,59,236]. Thus far, P144 has only been noted in Cu/Zn-SOD molecules of certain Ascomycota fungi; all plant and animal Sod1 molecules contain non-proline residues at the equivalent position, and these Cu/Zn-SODs can be activated with or without a copper

chaperone [57]. Yet even in these higher organisms, the CCS copper chaperone pathway is the preferred mechanism for Cu/Zn-SOD activation [57].

The pathogenic fungus *Candida albicans* represents an interesting model system to study Cu/Zn-SOD activation. Unlike all other eukaryotes studied to date, this pathogen has uniquely evolved with two cytosolic SODs: a Cu/Zn-containing Sod1 and a highly irregular manganese-containing Sod3 [4,86,238]. In Chapter 3 of this thesis, I describe how these dual SODs have evolved to accommodate the changing copper environment of the animal host. The *C. albicans* pathogen requires Sod1 for virulence [239], but little is known about the biochemistry and cell biology of this important enzyme for pathogenesis. As with other Ascomycota fungi, *C. albicans* Sod1 contains P144 and is therefore predicted to require a copper chaperone, but a CCS molecule has not been described for *C. albicans*.

In this study, we examine the expression of *C. albicans* Sod1 in the native *C. albicans* host as well as the heterologous *S. cerevisiae* expression system. We find that in spite of its close homology to *S. cerevisiae* Sod1, *C. albicans* Sod1 is not capable of activation by the baker's yeast Ccs1. We identified a single CCS-encoding gene in *C. albicans* that is necessary to activate *C. albicans* Sod1 in both the native *C. albicans* host and the heterologous *S. cerevisiae* system. Through our comparative studies of CCS molecules from insects, humans and fungi, we describe a specie-specific barrier to CCS activation of Sod1 in the *C. albicans* pathogen.

Experimental Procedures

Yeast strains and growth conditions

C. albicans yeast strains were cultured at 30ºC either in an enriched YPD (yeast extract, peptone, 2% dextrose) or minimal (SC) synthetic complete medium [240], and *S. cerevisiae* strains were grown in selecting SC medium to maintain episomal plasmids. *S. cerevisiae sod1*Δ mutants were maintained in anaerobic culture jars (BBL GasPak) in medium containing 15 mg/L ergosterol and 0.5% Tween 80 to support anaerobic growth. For tests of *S. cerevisiae* aerobic lysine auxotrophy, 10^5, 10^4, 10^3 and 10^2 cells were spotted onto SC medium containing or lacking lysine and allowed to grow for 2-3 days either in air or in anaerobic culture jars.

The *S. cerevisiae sod1*Δ*::KanMX4* and *ccs1*Δ*::KanMX4* strains are commercially available derivatives of BY4741, *MATa his3*Δ*1 leu2*Δ*0 met15*Δ*0 ura3*Δ*0* (Open Biosystems). The JG100 *sod1*Δ*::URA3 ccs1*Δ*::KanMX4* strain was created by deleting *SOD1* in the *ccs1*Δ*::KanMX4 S. cerevisiae* mutant using the *sod1*Δ*:URA3* disruption plasmid pAR010b.

The *C. albicans* CA-IF100 (*arg4*Δ*/arg4*Δ*, leu2*Δ*/leu2*Δ*::cmLEU2, his1*Δ*/his1*Δ*::cdHIS1, URA3/ura3*Δ) and isogenic *sod1*Δ*/*Δ CA-IF003*, sod2*Δ*/*Δ CA-IF007, and *sod3*Δ*/*Δ CA-IF011 strains were kind gifts of K. Kuchler [131]. The *CCS1/ccs1*Δ heterozygous (JG101) and the *ccs1*Δ*/*Δ homozygous (JG103) *C. albicans* mutants, as well as the *CCS1* complemented strain, were constructed by Julie Gleason from parent SN78 using disruption marker cassettes and fusion PCR [241], as described in detail in our publication [242].

Plasmids

Plasmid pLS108 is a CEN *LEU2* vector that expresses *S. cerevisiae SOD1* [50]. The pJG100 plasmid for expressing *C. albicans SOD1* in *S. cerevisiae* was derived from pLS108 by replacing the *S. cerevisiae SOD1* coding region with that of *C. albicans SOD1*. Vectors for expressing the P144A (pJG101), P144L (pJG102), P144Q (pJG103) and H139N (pJG104) derivatives of *C. albicans SOD1* were created from pJG100. The CEN *HIS3* pJG110 vector for expressing *C. albicans CCS1* in *S. cerevisiae* was derived from pLJ366 [231], replacing the *S. cerevisiae CCS1* coding region with that of *C. albicans CCS1*. The pLS113, pLJ375, and pPS015 CEN *HIS3* vectors for expressing *S. cerevisiae*, *D. melanogaster*, and human CCS molecules, respectively, in *S. cerevisiae* have been described [50,231,243]. Additional information on the construction of these plasmids, as well as the *C. albicans CCS1* rescue plasmid, are described in our publication [242].

Biochemical analysis

Whole cell lysates from *S. cerevisiae* or *C. albicans* were prepared by glass bead homogenization as described [244]. For native gel electrophoresis, 30 µg lysate protein was subjected to electrophoresis (50 mA) on pre-cast 10% Tris-glycine gels (Novex). We noted that *C. albicans* WT Sod1 looses activity with prolonged electrophoresis on native gels; hence all studies with this SOD were carried with 90 min electrophoresis at 4ºC. Prolonged electrophoresis conditions were carried out over 150 min at 4ºC. SOD activity in native gels was monitored by Nitroblue tetrazolium (NBT) staining [245]. To eliminate Cu/Zn-SOD activity, gels were soaked in 5 mM H_2O_2 prior to NBT staining as

described [75]. Immunoblot analysis was conducted with 15-30 µg whole cell lysate protein run on precast NuPage 4-12% Bis-Tris gels (Novex) at 200 V, followed by transfer onto PVDF membranes using iBlot (Novex). A universal anti-Cu/Zn-SOD antibody (originally directed against *C. elegans* Sod-1 [56]) was used at 1:10,000 dilution. An antibody directed against *C. albicans* Sod3 was generated using the synthetic peptide EKISLPKIDWALDALEPY and a 90 day Rabbit Protocol (Pierce Antibodies). When both Sod1 and Sod3 are analyzed, anti-Sod3 antibody (1:10,000 dilution) was added first, followed by washing and incubation with anti-Sod1, then subsequent reaction with anti-rabbit secondary antibody. Immunoblots were visualized by the Odyssey infrared imaging system (Licor Biosciences).

Results and Discussion

SOD activity from the *C. albicans* pathogen can be monitored using a native gel assay. In Fig. 2-1, soluble lysates from *C. albicans* grown to early stationary stage exhibit three soluble SOD enzymes that easily resolve by native gel electrophoresis. These include the mitochondrial Mn-Sod2, cytosolic Mn-Sod3 and the cytosolic Cu/Zn-Sod1. Verification of the three soluble SODs was obtained using strains with individual mutations in the corresponding genes (Fig. 2-1 top). Additionally, the copper- and manganese-containing SODs can be distinguished based on in-gel peroxide sensitivity [75], and as seen in Fig. 2-1 middle, Cu/Zn-Sod1 activity was lost with hydrogen peroxide treatment whereas both Mn-SODs were resistant.

To study *C. albicans* Sod1 further, we employed the baker's yeast expression system that has proven fruitful for examining maturation of Cu/Zn-SOD from invertebrates, plants and humans [55,56,231,234]. Given the 70% identity between *C. albicans* and *S. cerevisiae* Sod1 molecules (Fig. 2-2A), we anticipated faithful activation of *C. albicans* Sod1 in baker's yeast. The coding region for *C. albicans SOD1* was placed under control of the *S. cerevisiae SOD1* promoter and was expressed in a *S. cerevisiae sod1*Δ strain; lysates were analyzed by the gel assay. On native gels, Sod1 easily resolves from the Mn-Sod2 of *C. albicans* (Fig. 2-2B top lane 4) but not from *S. cerevisiae* Mn-Sod2 (lane 2). The prolonged electrophoresis needed to resolve *S. cerevisiae* Sod2 and Sod1 is detrimental to WT *C. albicans* Sod1 activity as described in more detail below (see Fig. 2-7); thus our analysis of *C. albicans* Sod1 typically involves shorter durations of electrophoresis (as in Fig. 2-1 and Fig. 2-2B top). Under these conditions, the endogenous *C. albicans* Sod1 and Sod2 are easily discernible (Fig. 2-2B, lane 4) and in baker's yeast, Sod1 is detected as peroxide-inhibitable activity over Sod2, as seen with endogenous *S. cerevisiae* Sod1 (Fig. 2-2B lane 2). However, no activity over background could be detected with *C. albicans* Sod1 expressed in baker's yeast (Fig. 2-2B top, lane 3), even though the Sod1 polypeptide was produced (Fig. 2-2B bottom, lane 3). As a more sensitive and reliable assay for Sod1 activity *in vivo* we employed a growth test. Specifically, *S. cerevisiae* cells devoid of Sod1 activity cannot grow in air without lysine due to superoxide damage to lysine biosynthetic enzymes [15,246]. Aerobic growth without lysine requires as little as 2% of normal Sod1 activity [233] and is therefore a highly sensitive indicator of *in vivo* Sod1 activity. As seen in Fig. 2-1C, *sod1*Δ cells expressing *C. albicans* Sod1 failed to grow aerobically on medium

lacking lysine. There are no signs of enzyme activity with *C. albicans* Sod1 expressed in *S. cerevisiae.*

The inactivity of *C. albicans* Sod1 in baker's yeast was surprising given the fact that Cu/Zn-SOD molecules from more distant species (e.g., *Drosophilia*, *C. elegans,* plants and mammals) are all abundantly active in this heterologous system [55,56,231,234]. As one possibility, *C. albicans* Sod1 might be incapable of interacting with the *S. cerevisiae* Ccs1 copper chaperone. To release *C. albicans* Sod1 from any CCS requirement, we mutated P144 needed for CCS-dependence (Fig. 2-2A). As seen in Fig. 2-3A, P144A, P144L and P144Q alleles of *C. albicans* Sod1 were abundantly active when expressed in *sod1*Δ strains of baker's yeast, and activity was stable even during prolonged electrophoresis on native gels. Moreover, this activity was independent of CCS because activity was identical in *CCS1*+ versus *ccs1*Δ strains (Fig. 2-3B, lanes 1 and 3; Fig. 2-3C). The gain of function with P144 mutant alleles indicates that *C. albicans* Sod1 cannot be activated *in vivo* by the *S. cerevisiae* Ccs1 copper chaperone.

To date, a CCS copper chaperone has not been described for *C. albicans*. However, by inspection of the Candida Genome Database, we identified a single potential CCS encoding loci in *C. albicans* (hypothetical protein CaO19.11929) that shares 43% identity and 61% similarity with Ccs1 of *S. cerevisiae* (Fig. 2-4A). Conserved features include the MXCXXC copper binding site at the N-terminus and the CXC site at the C-terminus (Fig. 2-4A). To determine whether the putative *C. albicans* CCS functions as a copper chaperone, homozygous and heterozygous gene deletions were introduced at the CaO19.11929 locus in *C. albicans*. As seen in Fig. 2-4B lane 3, the homozygous null strain for CaO19.11929 exhibits a dramatic loss in Sod1 activity.

Polypeptide levels of *C. albicans* Sod1 were also somewhat lowered as has been reported with CCS gene deletions in other organisms [231,247]. These changes in Sod1 were reversed upon integration of the cDNA for CaO19.11929 (Fig. 2-4B, lane 4). Based on these findings and others described below, we have denoted *C. albicans* CaO19.11929 as *CCS1* (Genbank accession number KF040455).

We tested whether *C. albicans* Ccs1 could restore activity to *C. albicans* Sod1 expressed in *S. cerevisiae*. The coding region for *C. albicans CCS1* was placed under control of the *S. cerevisiae CCS1* promoter and was co-expressed with *C. albicans SOD1* in a *ccs1*Δ *sod1*Δ null strain of baker's yeast. Results were compared to strains co-expressing *C. albicans SOD1* with CCS molecules from *S. cerevisiae* (44% identity to *C. albicans* Ccs1), human (32% identity), and *Drosophilia* (28% identity). Activity of *C. albicans* Sod1 was monitored by both the sensitive lysine dependency test (Fig. 3-5A) and by the native gel assay (Fig. 2-5B). Although *C. albicans* Sod1 is inactive when co-expressed with *S. cerevisiae* Ccs1, expression of its partner *C. albicans* Ccs1 bestowed activity to this Sod1 by both the aerobic lysine auxotrophy test and the native gel assay (Fig. 2-5A and 2-5B). *C. albicans* Ccs1 is clearly functioning as a copper chaperone, as it activates WT *C. albicans* Sod1 (Fig. 2-5), but has no effect on the CCS-independent P144L Sod1 mutant (Fig. 2-3B lane 2). It is noteworthy that in addition to *C. albicans* Ccs1, the copper chaperone from humans was also capable of activating WT *C. albicans* Sod1 (Fig. 2-5). *Drosophila* Ccs was poorly re-active with *C. albicans* Sod1 (Fig. 2-5A). Thus, *C. albicans* Sod1 is best activated by its native Ccs1 partner and by human hCCS, but not at all by the closely related Ccs1 from baker's yeast.

We also conducted the converse experiment and tested whether *C. albicans* Ccs1 can activate expression of baker's yeast Sod1. As seen in Fig. 2-6A, *C. albicans* Ccs1 was capable of conferring some activity to *S. cerevisiae* Sod1, but the actual level of activity seems poor compared to that obtained with *S. cerevisiae* Ccs1 (Fig. 2-6B). Although there is no antibody available to monitor levels of the *C. albicans* Ccs1 polypeptide, this copper chaperone is certainly expressed in baker's yeast as it activates *C. albicans* Sod1 in the same expression system (Fig. 2-5).

The lack of apparent reactivity between baker's yeast Ccs1 and *C. albicans* Sod1 (Fig. 2-5) was quite unexpected, particularly since baker's yeast Ccs1 reacts well with Cu/Zn-SOD molecules from far distant species including plants, insects and humans [55,231,234]. There must be some unique attribute to *C. albicans* Sod1 that dictates this barrier in spite of 80% similarity between *S. cerevisiae* and *C. albicans* Sod1 molecules. To begin to address this, we searched for residues that are unique to *C. albicans* Sod1, but conserved among other eukaryotic Cu/Zn-SOD molecules. Attention was drawn to H139 in *C. albicans* Sod1, which is a highly conserved Asn in other organisms (Fig. 2-7A). In studies that have been conducted with human SOD1, N139 helps form solvent-exposed hydrogen bonds to residues in the electrostatic loop, and N139K and N139D are documented SOD1 mutations in familial amyotrophic lateral sclerosis [248,249]. In addition, position 139 in fungal Sod1 shares close proximity to P144 and C146 that control CCS-dependence and the Sod1 disulfide (Fig. 2-7A). A H139N substitution was introduced in *C. albicans* Sod1 and the enzyme was co-expressed with Ccs1 from either *S. cerevisiae* or *C. albicans*. As seen in Fig. 2-7B top, H139N *C. albicans* Sod1 exhibits precisely the same Ccs1 preference as is seen with WT *C. albicans* Sod1: activity was

obtained with co-expression of *C. albicans* Ccs1 (lane 5) but not *S. cerevisiae* Ccs1 (lane 6). Although Ccs1 selectivity was unchanged, the H139N mutation may affect Sod1 stability. As seen in Fig. 2-7B middle, H139N *C. albicans* Sod1 activity was resistant to prolonged periods of native gel electrophoresis, precisely as is seen with WT Cu/Zn-SOD from baker's yeast, humans, *Drosophilia* and nematodes, all of which naturally contain N139 [55,56,231]. The apparent stability gained with H139N *C. albicans* Sod1 could reflect alterations in the aforementioned hydrogen-bonding network.

Together these studies support an unanticipated species-specificity in the activation of *C. albicans* Sod1. Up until now, there has been great flexibility reported for CCS interactions with Cu/Zn-SOD. *S. cerevisiae* Sod1 reacts well with CCS molecules from humans, plants and the Ascomycota fungus *S. pombe* [51,232,235]. The converse is also true: Cu/Zn-SOD molecules from humans, plants and insects are all strongly activated by baker's yeast Ccs1 [231,233,234]. The barrier between *C. albicans* Sod1 and *S. cerevisiae* Ccs1 is not understood, but could involve blockages in CCS-SOD physical interactions, in copper insertion or in disulfide oxidation.

Although *C. albicans* Sod1 cannot react with baker's yeast Ccs1, it appears compatible with human hCCS (Fig. 2-5). This is not readily explained by sequence divergence because human hCCS and *C. albicans* Ccs1 share only 32% identity versus the 44% identity between the two fungal Ccs1 molecules. Since *C. albicans* naturally co-exists with human cells, there is a distant possibility that at some point during the life cycle, *C. albicans* Sod1 encounters the copper chaperone of its human host.

Cu/Zn-SOD are notoriously stable molecules with relatively long half lives *in vivo*, and activity that remains stable *in vitro* over a range of conditions including

prolonged electrophoresis on native gels. We observe a peculiar instability with *C. albicans* Sod1 not seen with other WT Cu/Zn-SODs, namely a progressive loss in activity during native gel electrophoresis. This instability results in part from sequences at the C-terminus, including P144 and an unusual H139 that is a highly conserved Asn in other Cu/Zn-SODs. Unlike other eukaryotes, *C. albicans* expresses two cytosolic SODs: the Cu/Zn-Sod1 and a distinct Mn-requiring Sod3 enzyme. In Chapter 3 of this thesis, we demonstrate that when copper availability is low, *C. albicans* will switch from expressing Sod1 to the Mn-Sod3 enzyme. It is possible that the instability of *C. albicans* Sod1 described here is important to the turnover of Sod1 as the cell makes the switch to Sod3.

Future Directions

In future studies we will investigate the nature of the peculiar instability of *C. albicans* Sod1. As one possibility, *C. albicans* Sod1 may lose its catalytic copper more easily than Sod1 molecules from other organisms. To test this we can use extensive dialysis against metal chelators, as is routinely done to monitor copper binding stability of SODs [1,250], in order to compare the copper binding capacities of Sod1 from *C. albicans* and *S. cerevisiae*. If *C. albicans* Sod1 more readily loses its copper, one consequence may be increased protein turnover. We can test the turnover rate of *C. albicans* Sod1 compared to *S. cerevisiae* Sod1 with cycloheximide treatment of cultured cells to stop protein synthesis. Samples will be collected over several hours and analyzed by immunoblot to detect Sod1 protein stability. We expect *C. albicans* Sod1 to exhibit rapid turnover as it is not the only cytosolic SOD that this yeast can use (Chapter 3).

Figure 2-1: Active Sod1 enzyme from the *C. albicans* native host.

The WT *C. albicans* strain CA-IF100 or the indicated homozygous SOD deletion mutants [131] were grown to early stationary phase in YPD, conditions where both cytosolic Sod1 and Sod3 are active. Cell lysates were prepared and analyzed by (top and middle) native gel electrophoresis and NBT staining for SOD activity, and (bottom) denaturing gel electrophoresis and immunoblotting using anti-Sod1 and anti-Sod3 antibodies as described in *Experimental Procedures*. Electrophoresis of native gels proceeded for 90 minutes. "+H_2O_2": Prior to NBT staining, gel was treated with 5 mM H_2O_2 to eliminate Cu/Zn-SOD activity [75]. The positions of active Sod1, Sod2 and Sod3 enzyme on the native gels are shown, as well as the positions of Sod1 and Sod3 polypeptide on the immunoblot.

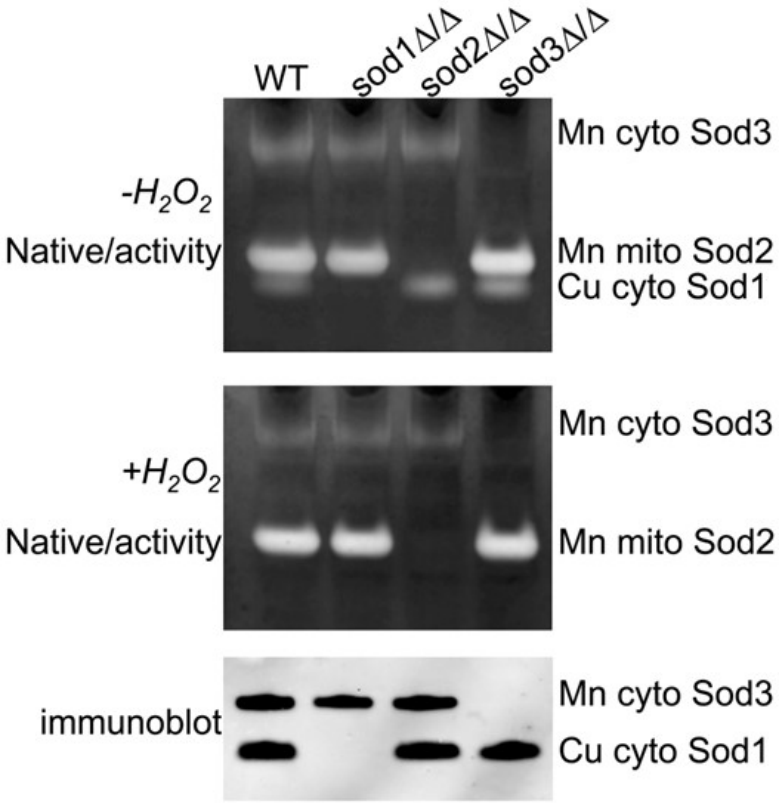

Figure 2-2: *C. albicans SOD1* expressed in the baker's yeast *S. cerevisiae.*

(A) Sequence alignment of Sod1 molecules from *C. albicans* and *S. cerevisiae* as determined by Clustal Omega. Asterisks and dots indicate amino acid identity and similarity, respectively. Copper binding residues are marked by C and yellow highlights; zinc binding by Z and aqua; the shared zinc and copper binding histidine is marked in green; disulfide cysteines by DS in fuchsia. Arrow points to P144 that dictates CCS-dependence. **(B)** Whole cell lysates were prepared from either WT *C. albicans* (lane 4) or from a *S. cerevisiae sod1*Δ strain expressing Sod1 from either *S. cerevisiae* (Sc) or *C. albicans* (Ca) or not expressing Sod1 (-). Lysates were subject to SOD activity analysis (top and middle) and immunoblotting for Sod1 (bottom) as in Fig. 2-1. Native gels were treated with H_2O_2 where indicated as in Fig. 2-1. The positions of the various SOD enzymes from *C. albicans* or *S. cerevisiae* on the native gels are marked accordingly. The > symbol indicates co-migration of *S. cerevisiae* Sod2 and Sod1 under these electrophoresis conditions (see main text). **(C)** Serial dilutions of the *S. cerevisiae* strains described in *b* were spotted onto SC medium containing or lacking lysine and grown either aerobically ($+O_2$) or in anaerobic culture jars ($-O_2$) as described in *Experimental Procedures*.

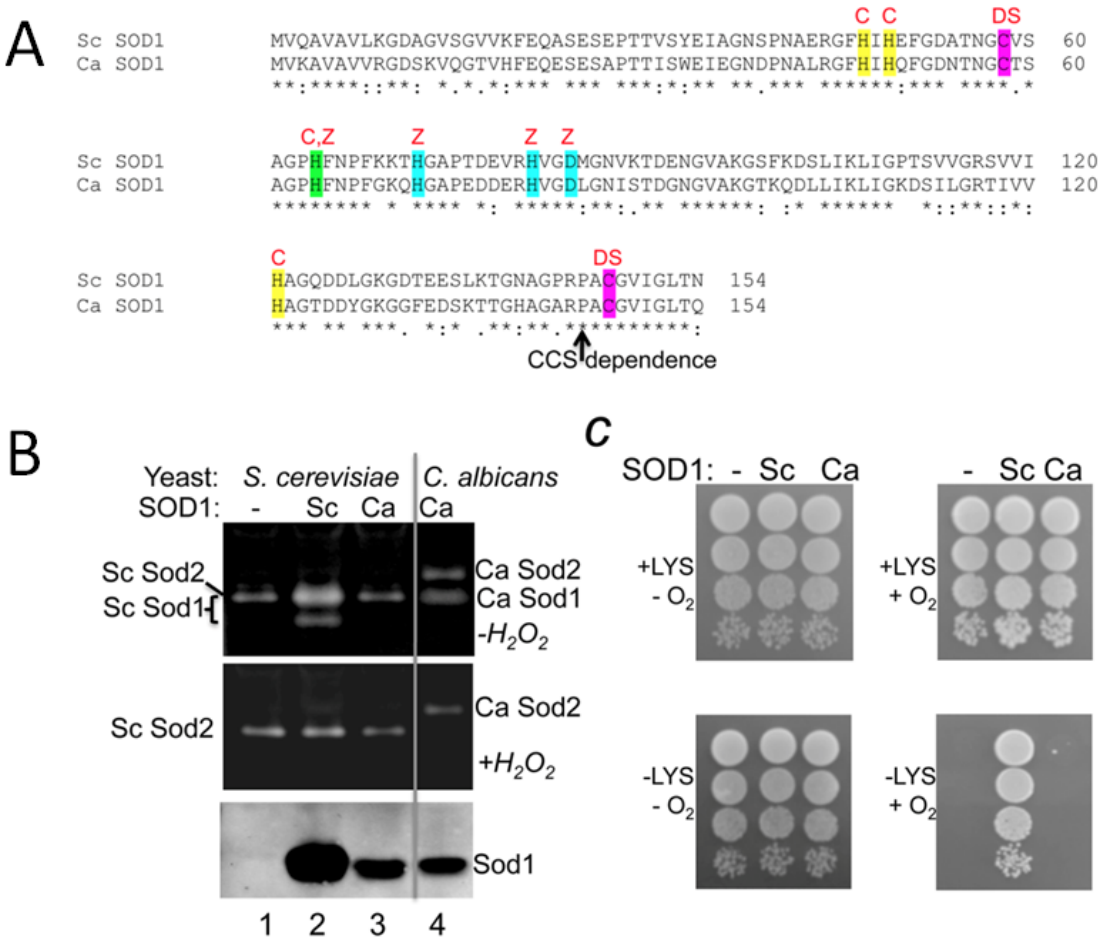
A
C C DS
Sc SOD1 MVQAVAVLKGDAGVSGVVKFEQASESEPTTVSYEIAGNSPNAERGFHIHEFGDATNGCVS 60
Ca SOD1 MVKAVAVVRGDSKVQGTVHFEQESESAPTTISWEIEGNDPNALRGFHIHQFGDNTNGCTS 60
C,Z Z Z Z
Sc SOD1 AGPHFNPFKKTHGAPTDEVRHVGDMGNVKTDENGVAKGSFKDSLIKLIGPTSVVGRSVVI 120
Ca SOD1 AGPHFNPFGKQHGAPEDDERHVGDLGNISTDGNGVAKGTKQDLLIKLIGKDSILGRTIVV 120
C DS
Sc SOD1 HAGQDDLGKGDTEESLKTGNAGPRPACGVIGLTN 154
Ca SOD1 HAGTDDYGKGGFEDSKTTGHAGARPACGVIGLTQ 154
CCS dependence
B
Yeast: S. cerevisiae C. albicans
SOD1: - Sc Ca Ca
Sc Sod2
Sc Sod1
Ca Sod2
Ca Sod1
-H2O2
Sc Sod2
Ca Sod2
+H2O2
Sod1
1 2 3 4
C
SOD1: - Sc Ca - Sc Ca
+LYS - O2
+LYS + O2
-LYS - O2
-LYS + O2

Figure 2-3: Gain of *C. albicans* activity in *S. cerevisiae* with mutations in P144.

The *S. cerevisiae sod1*Δ single mutant **(A)** or *sod1*Δ *ccs1*Δ double mutant **(B,C)** were transformed with vectors for expressing either WT *C. albicans* Sod1 or the indicated P144 mutant alleles of *C. albicans* Sod1. **(B,C)** Cells also expressed Ccs1 from either *S. cerevisiae* (Sc) or *C. albicans* (Ca) or no CCS (-). Cell lysates where analyzed for SOD activity by the native gel assay (A and B,C top) and for Sod1 protein by immunoblot (B,C bottom) as in Fig. 2-1 except native gels were subjected to prolonged electrophoresis (150 minutes) to resolve the active P144 Sod1 mutants from *S. cerevisiae* Sod2 (see main text).

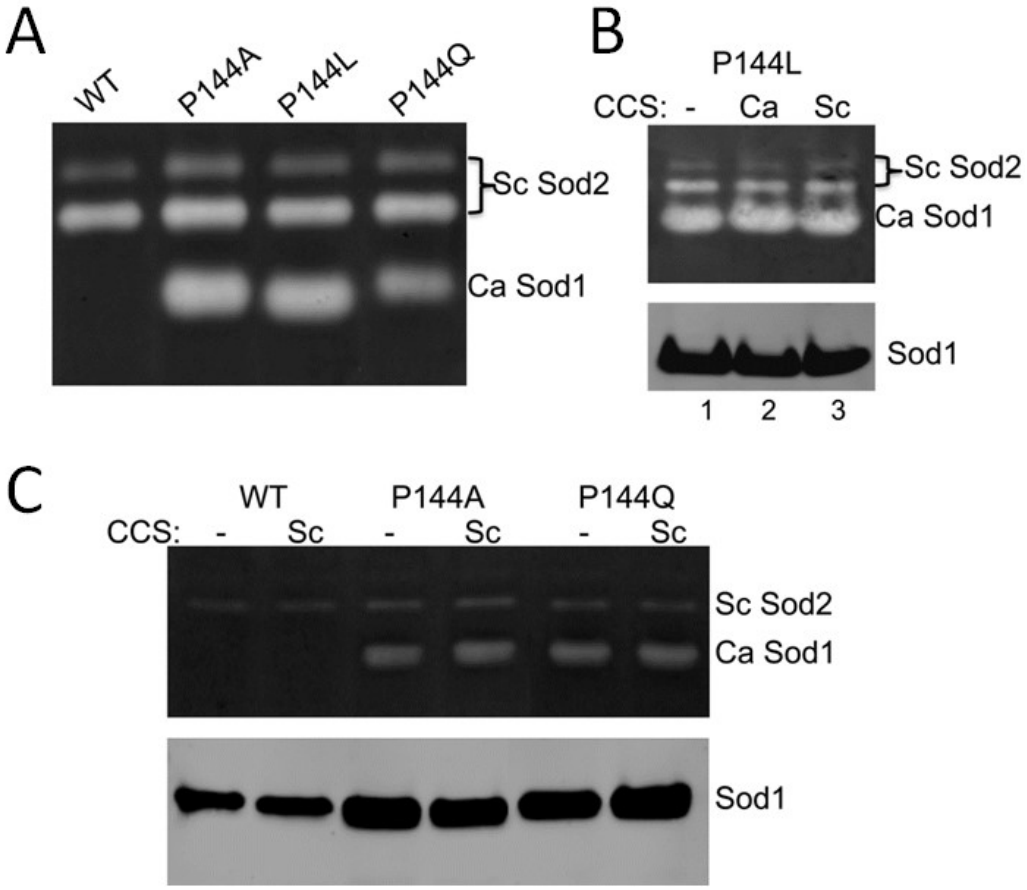

Figure 2-4: A single CCS-encoding gene in *C. albicans.*

(A) Sequence alignment of Ccs1 molecules from *C. albicans* and *S. cerevisiae* fungi as determined by Clustal Omega. Asterisks and dots indicate amino acid identity and similarity, respectively; shaded areas demark conserved copper binding cysteines in the N- and C-terminus of CCS molecules. **(B)** The indicated strains of *C. albicans* were grown to mid log in low methionine SC medium as described in *Experimental Procedures*, and cell lysates were subjected to SOD activity (top) and Sod1 protein (bottom) analyses as in Fig. 2-1. Strains utilized are the SN78 WT for *Ccs1* (+/+); the heterozygous JG101 (+/Δ) and homozygous JG103 (Δ/Δ) *ccs1* deletion strains; Δ/Δ:CCS1 represents JG103 with *CCS1* integrated at the RP10 locus as described in *Experimental Procedures*.

A

```
C. albicans     -----MTN--TFEIVFAVPMECDSCVDSIASVLKGLDGVEKFNINLKDNLVSTEGSLPPSEISKA  58
S. cerevisiae   -----MTTNDTYEATYAIPMHCENCVNDIKACLKNVPGINSLNFDIEQQIMSVESSVAPSTIINT  60
H. sapiens      MASDSGNQGTLCTLEFAVQMTCQSCVDAVRKSLQGVAGVQDVEVHLEDQMVLVHTTLPSQEVQAL  65
                      .        :*: * *:.**: :   *:.: *::..:..::::: : .. ::... :

C. albicans     IQSTGKDAIIRGTGKPDSAAVCILESFDPNDIQHP----VKGLARLVEVSPNDLFVDLTVNGLPK 119
S. cerevisiae   LRNCGKDAIIRGAGKPNSSAVAILETFQKYTIDQKKDTAVRGLARIVQVGENKTLFDITVNGVPE 125
H. sapiens      LEGTGRQAVLKGMGSGQ------LQNLGAAVAILGGPGTVQGVVRFLQLTPERCLIEGTIDGLEP 124
                   :.. *::*:::* *. :      *:.:         *:*:.*::::  :  :.: *::*:

C. albicans     G-VYYPSIRVSGNLSQGALSTGPSFYELN-PIEVKTPVNAETTISSRGAKLEEDSTLYAGQAFLH 180
S. cerevisiae   AGNYHASIHEKGDVSKGVESTGKVWHKFDEPIECFN----ESDLG---------KNLYSGKTFLS 177
H. sapiens      G-LHGLHVHQYGDLTNNCNSCGNHFNPDGASHGGPQ---DSDRHRGDLGNVRADADGRAIFRMED 185
                .      ::  *::::.  * *  :   . .         .                  :   :

C. albicans     AKLNINQLIGRSIILSKIKDQ--------------VAPDSLCGVIARSAGVWENDKQVCSCSGKT 233
S. cerevisiae   APLPTWQLIGRSFVISKSLNHP-------ENEPSSVKDYSFLGVIARSAGVWENNKQVCACTGKT 235
H. sapiens      EQLKVWDVIGRSLIIDEGEDDLGRGGHPLSKITGNSGERLACGIIARSAGLFQNPKQICSCDGLT 250
                   *  ::*****:::.:  :.                     *:*******:::* **:*:* * *

C. albicans       VWQERIDARVKGVHV--------- 248
S. cerevisiae     VWEERKDALANNIK---------- 249
H. sapiens        IWEERGRPIAGKGRKESAQPPAHL 274
                  :*:**  . .   :
```

B

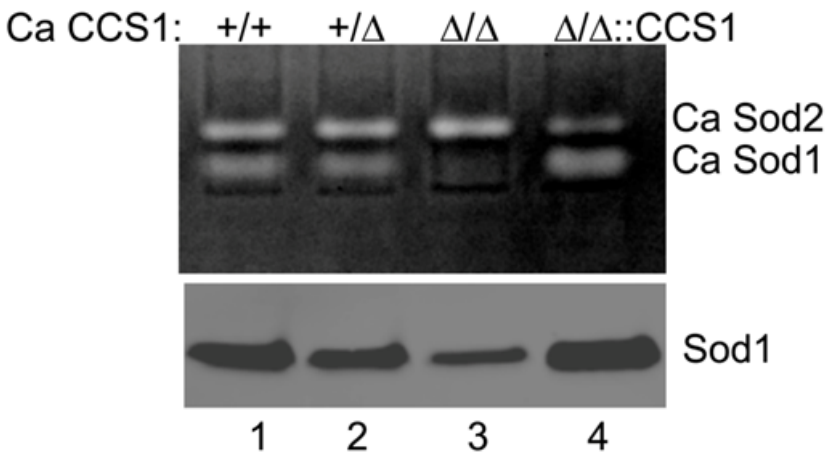

Figure 2-5: *C. albicans* Sod1 is activated by its partner *C. albicans* Ccs1.

The *sod1*Δ *ccs*Δ*1* double mutant of *S. cerevisiae* expressing WT *C. albicans* Sod1 and co-expressing CCS molecules from *C. albicans* (Ca), *S. cerevisiae* (Sc), *D. melanogaster* (Dm) and humans (Hs) or no CCS (-) were tested for (A) lysine independent growth in air as in Fig. 2-2C; and (B) for SOD activity and Sod1 protein levels as in Fig. 2-2B.

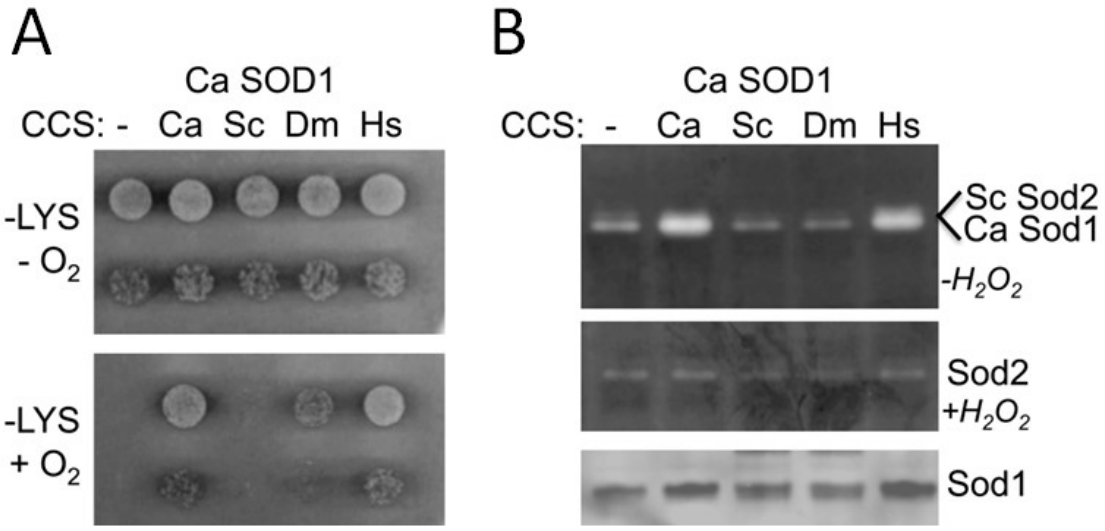

Figure 2-6: Activation of *S. cerevisiae* Sod1 by *C. albicans* Ccs1.

The *sod1*Δ *ccs1*Δ strain expressing *S. cerevisiae* Sod1 and co-expressing Ccs1 molecules from *C. albicans* (Ca) or *S. cerevisiae* (Sc) no CCS (-) were tested for (A) lysine independent growth in air as in Fig. 2-2C; and (B) for SOD activity and Sod1 protein levels as in Fig. 2-3.

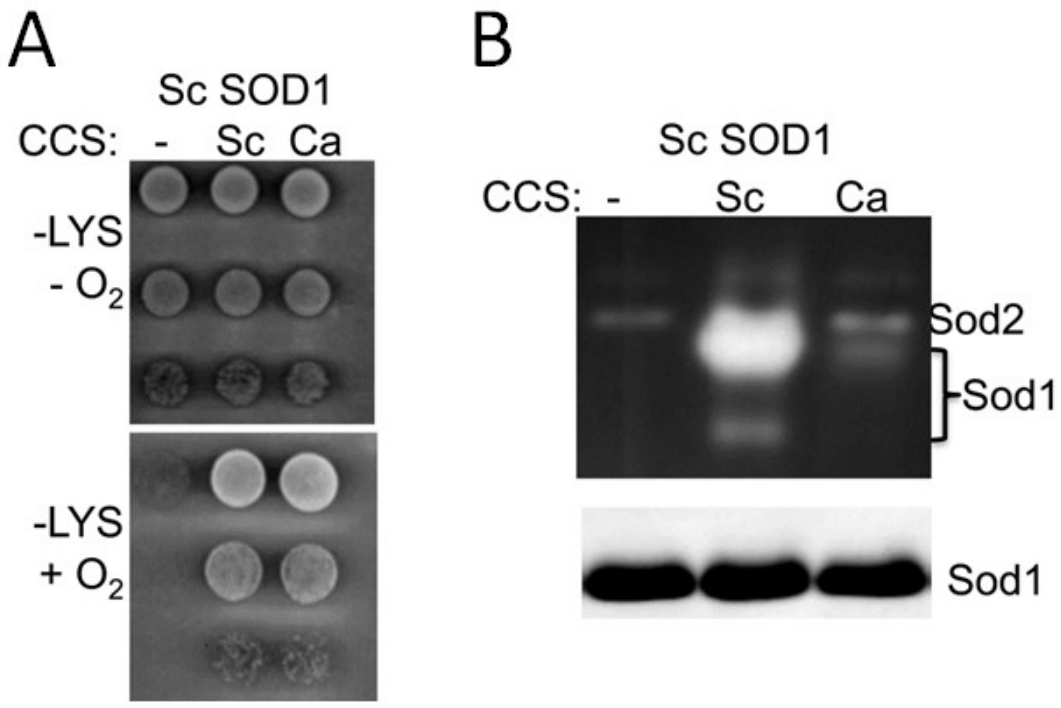

Figure 2-7: The unique H139 of *C. albicans* Sod1.

(A) Shown is an alignment of the C-terminal region of Cu/Zn-SOD molecules from *C. albicans* (Ca), *S. cerevisiae* (Sc), humans (Hs) and *D. melanogaster* (Dm). Yellow marks the conserved N139 in diverse Sod1 molecules that is a histidine in the case of *C. albicans* Sod1. Red and blue shading mark P144 for CCS-dependence and the C146 disulfide cysteine, respectively. **(B)** The *sod1*Δ *ccs1*Δ *S. cerevisiae* strain expressing WT or H139 mutant *C. albicans* Sod1 and co-expressing *C. albicans* (Ca) or *S. cerevisiae* (Sc) Ccs1, or no CCS (-) were subjected to the native gel assay for SOD activity (top and middle) and immunoblot for Sod1 (bottom). "Short" (90 min) and "prolonged" (150 min) indicates duration of native gel electrophoresis as in Fig. 2-2B and 2-3, respectively.

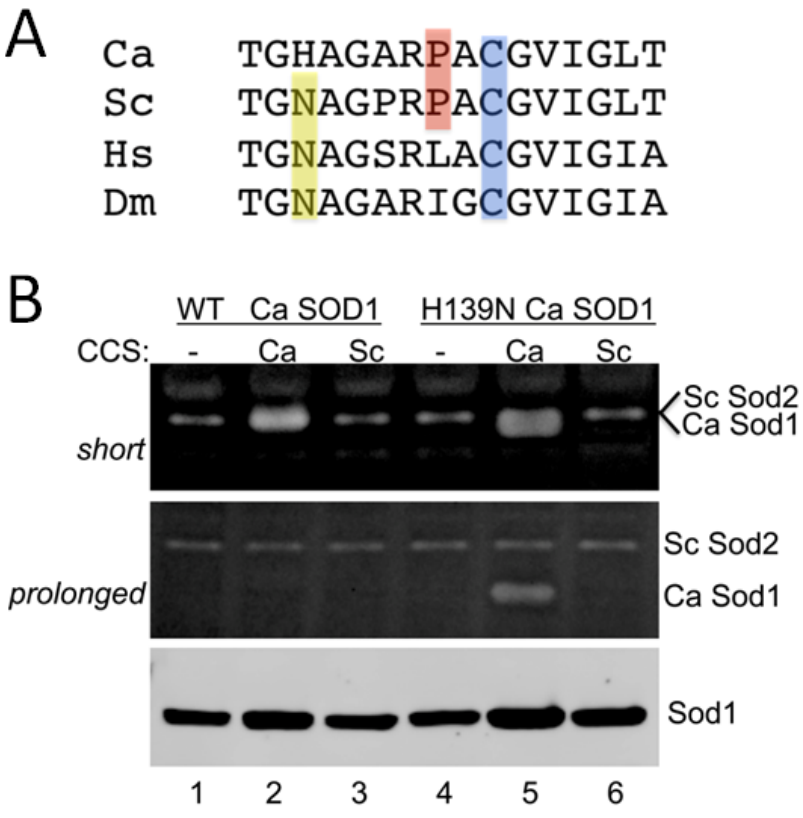

CHAPTER 3

Fungal adaptation to host copper: swapping metal co-factors for SOD enzymes during *Candida albicans* infection

Introduction

Candida albicans is the most prevalent of human fungal pathogens. The organism usually exists as a harmless commensal, but has the potential to become invasive, infectious, and even fatal by targeting numerous organ systems [132,251]. As other pathogens, *C. albicans* relies on its host for micronutrients such as metals, and the bioavailability of metals can greatly vary at the host-pathogen interface. As part of the innate immune response, the host deliberately withholds metals such as iron, zinc, and manganese from invading microbes in a process known as "nutritional immunity" [159,252,253]. Like other infectious agents, *C. albicans* is equipped to handle restrictions placed on these micronutrients by activating diverse pathways for scavenging host sources of iron and zinc [154,254-257].

Unlike iron, zinc, and manganese, there is no known nutritional immunity response for copper. Instead studies with *M. tuberculosis, Salmonella*, *E. coli* and *C. neoformans* have inferred the opposite, where the host elevates this metal to attack pathogens with copper toxicity [170-172,258]. Copper is an effective antimicrobial agent [79,259,260], and during infection, host elevations in copper can occur at the level of macrophages [170,171] and in certain tissues, e.g. the lung during pulmonary invasion by *C. neoformans* [172]. However, not all tissues may exhibit a heightened copper response as has been reported for the brain during *C. neoformas* invasion [261,262]. In the case of *C. albicans,* the copper response of the host is poorly understood. The only studies to date include macrophage based *in vitro* systems where *C. albicans* is clearly subject to macrophage-imposed copper toxicity [181,182]. It is not known whether the host

response to *C. albicans in vivo* is to elevate or restrict availability of copper, which serves as both potential toxin and essential nutrient for this fungal pathogen.

As a micronutrient, copper is co-factor for *C. albicans* enzymes involved in respiration, metal uptake, and anti-oxidant defense involving superoxide dismutase enzymes (SOD) [129,239,263,264]. SODs are highly conserved metalloenzymes that use a copper, manganese, iron, or nickel co-factor to catalyze the conversion of superoxide anion to oxygen and hydrogen peroxide [265]. Through this redox chemistry, SODs play important roles in anti-oxidant protection and in cell signaling processes involving reactive oxygen species [21,266,267]. Curiously, *C. albicans* has evolved with an unusually large family of SODs. While most eukaryotes express only two or three SODs, *C. albicans* has six [86,128,239,268]. Unique to *C. albicans* and related fungi are a family of extracellular copper -only SODs (Sod4, Sod5, Sod6) [128-131] as well as an irregular pair of cytosolic SODs that use either copper (Cu/Zn-Sod1) or manganese (Sod3) as catalytic co-factor [86]. The vast majority of eukaryotes have only a Cu/Zn-SOD in the cytosol, and a few rare organisms (crustaceans and photosynthetic microbes) contain a cytosolic Mn-SOD, but not Cu/Zn-SOD [67,68]. *C. albicans* and related fungi are the only organisms known to have both. The rationale for this apparent redundancy in SODs with different metal co-factors was not known.

In the current study, we investigated the basis for overlapping SODs in the *C. albicans* cytosol and have uncovered a new adaptation to copper deficiency in this yeast. We observe that rapidly growing cultures of *C. albicans* with abundant copper exclusively express Cu/Zn-Sod1. But when copper is depleted, cells will switch to expressing Mn-Sod3 through a mechanism involving the copper-sensing transcription

factor Mac1 [214,215]. Notably, this swapping of metallo-SOD enzymes becomes prevalent during *C. albicans* invasion of the kidney in a mouse model for disseminated candidiasis. During fungal infection, the host responds with marked variations in copper availability and *C. albicans* adapts by modulating copper transport genes and co-factor selection for SODs.

Experimental Procedures

Yeast strains and culture conditions

All the *C. albicans* laboratory strains used in this study are derivatives of SC5314 and include: KC2 (*ura3*Δ*::imm434/ura3*Δ*::imm434*), a gift from D. Kornitzer [269]; CA-IF100, *sod1*Δ/Δ, and *sod3*Δ/Δ, described in Chapter 2, and the additional isogenic strains *sod1*Δ/+ CA-IF001, *sod3*Δ/+ CA-IF009, obtained from K. Kuchler [131]; SN152 (*his1*Δ*/his1*Δ*, leu2*Δ*/leu2*Δ*, arg4*Δ*/arg4*Δ*, URA3/ura3*Δ*::imm434, IRO1/iro1*Δ*::imm434)* and two independent isogenic *mac1*Δ/Δ isolates, TF065-X and TF065-Y (Fungal Genetics Stock Center [270,271]).

The three clinical isolates were random blind samples obtained from Dr. Sean Zhang at the repository of the Johns Hopkins Hospital Clinical Microbiology Laboratory. Samples were isolated from either the blood or respiratory tract of patients and one of the isolates was resistant to fluconazole, as determined by the YeastOne YO-9 panel (TREK diagnostic systems, Oakwood Village, OH, USA). *C. albicans* speciation was determined by Dr. Sean Zhang including positive germ tube testing, colorimetric growth on Chromagar plates, and microscopic examination. It was also differentiated

from *C. dubliniensis* by a PNA-FISH test (AdvanDx Inc., Woburn, MA) and BD Phoenix panel (Becton Dickinson, Franklin Lakes, NJ).

To engineer strains expressing *SOD1* and *SOD3* with mutant Mac1 consensus sequences, an ends-in recombination method [272] was employed using gene replacement plasmids constructed as follows. Primers are listed in Table 3-1. *SOD1* sequences -1000 to +506 were amplified using primers that introduced terminal Not1 and Apa1 sites at the upstream and downstream positions. The Apa1 site was preceded by a triple stop codon that would terminate Sod1 translation at residue 87. *SOD3* sequences -1000 to +351 were similarly amplified with stop codons engineered after amino acid position 97. PCR products were digested with NotI and Apa1 and inserted into these same sites of pSN52 [241], containing the *C. dubliniensis (Cd) HIS1* marker. By Q5 site directed mutagenesis (NEB), a BplI restriction site was introduced at positions +358 and +200 in *SOD1* and *SOD3* respectively, to ultimately allow direct integration at the corresponding genomic loci. The resultant pCL13 (SOD1) and pCL14 (SOD3) plasmids were subjected to a second round of mutagenesis to alter the Mac1 consensus sequence to contain an AflII restriction site: TTTGCTCA to TCTTAAGA at +148 to +155 in *SOD1* (generating pCL15), and ATTGCTCA to ACTTAAGA at -147 to -154 in *SOD3* (pCL16). Plasmids pCL13-16 were linearized with BplI and used to transform either the *sod1*Δ/+ heterozygote strain CA-IF001 (pCL13 and pCL15) or the CA-IF009 *sod3*Δ/+ strain (pCL14 and pCL15). Faithful integration of the plasmids resulted in a tandem duplication of *SOD1* or *SOD3* sequences, including a truncated non-functional protein and a full length protein associated with either mutated or unaltered Mac1 consensus

sequences. Plasmid sequences and accurate chromosomal integration were verified by PCR amplification, restriction digestion, and gene sequencing.

For laboratory growth of *C. albicans* strains, budding cells were typically cultured at 30°C in enriched media (YPD, BD Difco) containing yeast extract, peptone, and 2% dextrose. Cell growth was monitored by absorption at 600 nm as described in Chapter 2. For log phase cultures, *C. albicans* were grown 12-16 hours to an $O.D._{600}$ between 1-4. Stationary phase cultures were obtained by 24-48 hours of growth following a starting $O.D._{600}$ of 0.1. To obtain hyphal yeast, a log phase culture of budding *C. albicans* was starved in water at a concentration of $O.D._{600}$=3 for 1 hour at 30°C, then diluted in YPD medium with 10% fetal bovine serum (Sigma), at $O.D._{600}$=0.1 and grown for 6 hours at 37°C. Light microscopy of budding and hyphal cells was carried out at 40x using an Eclipse 80i upright microscope (Nikon) equipped with a dry dark field condenser (Nikon).

The murine infection model for disseminated candidiasis

The mouse studies were carried out in accordance with the National Institutes of Health guidelines for the ethical treatment of animals. This protocol was approved by the Institutional Animal Care and Use Committee (IACUC) of the Johns Hopkins University medical institutions, protocol number MO13M264. Studies involved both males and females with no difference noted with sex under any parameter tested. 6-8 week old Balb/C mice were infected by lateral tail vein injection with $5x10^5$ yeast cells of *C. albicans* SC5314. After 24, 48, and 72 hours of infection, 5-13 mice per time point were sacrificed, along with 5 control uninfected mice. Blood was collected, allowed to

congeal on ice for 30 minutes, and then centrifuged at 1000 x g for 10 min to isolate serum. Prior to harvesting, tissues were perfused by injecting 10 mL sterile PBS into the left ventricle of the heart and by draining from an incision in the right atrium. With each mouse, one kidney was placed in 1 mL RNA-later (Sigma) and stored at -80^{o}C. The second kidney was bisected sagittally, one half was homogenized, serially diluted, and plated onto YPD plates with 1% penicillin-streptomycin to determine colony forming units (CFUs). The other half was dissected into cortex and medulla and dissolved in 1 mL of 20% Ultrex II Ultrapure nitric acid (J.T. Baker) overnight at 90°C in preparation for metal analysis by atomic absorption spectroscopy (AAS, see below). Liver and spleen were also harvested and prepped for determination of CFUs and of copper content as described above for kidney. Just prior to sacrificing, urine was collected from live mice placed on Parafilm, and was centrifuged at 13,000 x g to remove debris.

Biochemical analysis

SOD protein and enzyme activity were analyzed using the native gel assay and immunoblot as described in Chapter 2.

Metal analysis of *C. albicans* cells in culture and of infected mouse tissues by AAS was performed on a PerkinElmer Life Sciences AAnalyst 600 graphite furnace atomic absorption spectrometer. With *C. albicans* cultures, 10 O.D.$_{600}$ units of cells were isolated and washed twice with TE buffer (10 mM Tris, 1 mM EDTA, pH 8) and twice in MilliQ deionized water (Millipore) and resuspended in 1 mL of deionized water prior to analysis of copper and manganese by AAS. Mouse tissue samples (typically 20-200 mg wet weight/mL 20% nitric acid) were diluted 1:50 in MilliQ deionized water, while

serum and urine samples were similarly diluted 1:20 or 1:50 prior to copper analysis by AAS. Statistical analysis was performed using one-way ANOVA with Tukey's post hoc test.

RNA analysis of *C. albicans* in laboratory cultures and in infected kidneys was carried out by qRT-PCR. For laboratory cultures, RNA was isolated from 30 $O.D._{600}$ cell units by acid phenol extraction and ethanol precipitation, followed by cDNA synthesis as described [273]. Real-time PCR was essentially as described [273] with the following modifications. Standard curves for each primer were generated using 50-fold serial dilutions of genomic DNA from *C. albicans* strain SN152. cDNAs were diluted 20-fold before PCR amplification with EvaGreen (Biotium), and values were normalized to *TUB2* transcripts in each sample. Amplicons of approximately 150 bp were obtained using the PCR primers (IDT) described in Table 3-1. The thermal cycling conditions (Bio-Rad CFX96 real-time system) included denaturation at 95°C for 3 min, followed by 39 cycles of 95°C for 10 s, 55°C for 30 s, 72°C for 30 s, and finally a melt curve from 65°C to 95°C.

For infected kidneys, samples were removed from RNA-later, finely chopped with a razor blade, and then added to 1 mL of TriPure Isolation Reagent (Roche). Samples were homogenized using a Polytron 1200e tissue homogenizer (Kinematica), followed by vortexing with 0.5 mm zirconia beads for 30 min at 4°C. Samples were subjected to organic RNA extraction according to the TriPure Isolation Reagent instructions with these modifications: Homogenate was clarified by centrifugation at 12,000 x g at 4°C for 10 min and incubated at room temperature for 30 min before continuing with the phase separation step. The isolated RNA was purified by DNAse

treatment and spin column extraction using the NucleoSpin RNA kit clean-up protocol (Machery-Nagel). cDNA was synthesized using oligo-dT primers and the SuperScript III reverse transcriptase (Life Technologies). PCR amplification using the 2x iQ SYBR Green Supermix (Bio-Rad) was performed using the thermocycling conditions described above for yeast cultures, except that 50 cycles were completed.

Results

Alternating Cu/Zn- and Mn-SOD enzymes in C. albicans

To study the dual cytosolic SODs of *C. albicans* in culture, we employed a native gel assay that readily discerns intracellular Sod1, Sod2 and Sod3 enzymes, as described in Chapter 2 [242]. Consistent with previous studies on SOD mRNA [86], log phase cells are seen with abundant Sod1, but not Sod3 enzymatic activity (Fig. 3-1A top, lane 1). As cultures age over 48 hours, cells shift towards active Mn-Sod3 (Fig. 3-1A top, lanes 4-5) and activity parallels SOD protein as determined by immunoblot (Fig. 3-1A middle). Although Sod1 and Sod3 alternate with growth state, activity of the mitochondrial matrix Mn-Sod2 remained relatively constant (Fig. 3-1A top). The switch from Sod1 to Sod3 is readily reversible. When aged cultures were allowed to resume growth by diluting back into fresh growth medium, cells reverted to expressing Sod1 (Fig. 3-1B).

We explored the metabolic condition(s) that trigger the switch between Sod1 and Sod3. Glucose is rapidly consumed in cultures of *C. albicans* and is almost non-detectable within 24 hrs [274], however, glucose depletion cannot account for the

reciprocal control of Sod1 and Sod3. As seen in Fig. 3-2A, aged cultures still exhibited the switch from Sod3 to Sod1 when cells were allowed to resume growth in low (0.5%) glucose. An alternative possibility is that stationary cultures may be relatively hypoxic, and that low oxygen availability may be driving the switch from Sod1 to Sod3. However, growing cells in hypoxic conditions (5% O_2) did not prevent the switch from Sod1 to Sod3 (Fig. 3-2B). Thus we ruled out glucose and oxygen availability as regulators of the Sod1/Sod3 switch in *C. albicans*.

Another possible regulatory signal is metal availability. Manganese SOD enzymes are highly susceptible to changes in the bioavailability of manganese relative to competing metals such as iron [71,73,74,238,275,276]. However, raising intracellular manganese by orders of magnitude through manganese supplements had no impact on the switch of SOD enzymes. Sod3 was still lost in the presence of high manganese when aged cultures were diluted and resumed logarithmic growth (Fig. 3-2C).

We next tested whether copper drives the switch to Mn-Sod3. Intracellular copper typically decreases during stationary phase (Fig. 3-3A) to levels that induce the *CTR1* copper transporter gene (Fig. 3-3B), a hallmark of copper deficiency in *C. albicans* [214,215]. As seen in Fig. 3-3C and 3-4A, the switch to Mn-Sod3 with stationary phase was totally abolished by supplementing cultures with copper salts. The converse was also true, where copper starvation favored Sod3; rapidly dividing cells exhibited a premature shift from Sod1 to Sod3 when cells were starved for copper by treatments with the Cu(I)-specific chelator bathocuproine sulphonate (BCS) (Fig. 3-4B, lanes 7-9). High copper favors Sod1, and low copper induces Sod3. This toggling of the SODs in response to copper is not an all-or-nothing event. By calibrating intracellular copper

through copper salts and BCS treatments, a clear reciprocal dose response is observed with Sod1 and Sod3 (Fig. 3-4A,B). *C. albicans* can adapt to a wide range in intracellular copper levels by fine-tuning levels of Cu/Zn-Sod1 versus Mn-Sod3. This adaptation to copper is seen with both budding cultures of *C. albicans* (Fig. 3-4) and filamentous/hyphal forms of the yeast (Fig. 3-5A) that are particularly important for tissue invasion [135-137]. Moreover, this phenomenon is an inherent property of infectious *C. albicans* and was seen in three independent clinical isolates, including one from a patient's blood and two from the respiratory tract, one of which shows resistance to the antifungal drug fluconazole (Fig. 3-5B).

Copper-starved cells have low Sod1 enzymatic activity in part due to loss of the catalytic cofactor for this SOD (Fig. 3-4B) and we tested whether such losses in Sod1 activity trigger the switch to Mn-Sod3. As seen in Fig. 3-6A, the complete absence of Cu/Zn-Sod1 in a *sod1*Δ/Δ strain was not sufficient to induce Mn-Sod3 (lane 2); only copper starvation was effective (lane 5). Conversely, absence of Sod3 in the *sod3*Δ/Δ strain did not impact Sod1 regulation by copper (lanes 3 and 6). Therefore, it is changes in intracellular copper and not SOD enzymatic activity that dictates expression of Cu/Zn-Sod1 versus Mn-Sod3.

Mac1 as the trans-regulator for SOD1 and SOD3

Copper-regulation of *C. albicans* SODs occurs at the mRNA level. As seen in Fig. 3-6B, *SOD1* and *SOD3* mRNA are reciprocally expressed in response to copper depletion induced by either BCS or by growth in stationary phase. As an attractive candidate for this regulation, we examined Mac1, the copper-sensing transcription factor

that induces *CTR1* copper uptake in response to low copper [205,214,215]. We find that Mac1 is essential for copper regulation of *SOD1* and *SOD3,* as *mac1*Δ/Δ null cells failed to switch to *SOD3* upon copper depletion either through BCS treatment or during stationary phase growth (Fig. 3-6B,C). Mutations in *mac1*Δ/Δ seemed to mimic high copper with regard to constitutively expressing Cu/Zn-Sod1 (as in Figs. 3-3C and 3-4B). However, copper was not elevated in *mac1*Δ/Δ cells, if anything copper was low (Fig. 3-6C bottom), presumably reflecting loss of Ctr1 copper transport. Copper starvation therefore works through Mac1 to induce *SOD3* and repress *SOD1*.

Across *S. cerevisiae*, *P. anseria*, and *C. albicans* fungi, Mac1-like regulators recognize the 8-mer TTTGCTCA in the promoter region of target genes, with some flexibility in the T at the first position [189,213,215,277]. By this definition, we identified a single Mac1 consensus site at *SOD3* position -146 (Fig. 3-7A), consistent with its induction by Mac1 during copper starvation. No such sequences were noted in the *SOD1* promoter, but a match was identified at intronic position +148 (Fig. 3-7A). To test if these sequences are responsible for *SOD1* and *SOD3* regulation, we engineered *C. albicans* strains to express genomic copies of *SOD1* or *SOD3* containing substitutions in the aforementioned Mac1 consensus sequences. As seen in Fig. 3-7B, loss of the putative Mac1 site in the *SOD3* promoter totally abolished Mn-Sod3 induction by copper starvation, while Cu/Zn-Sod1 was still repressed (lane 6). Conversely, mutating the downstream Mac1 consensus site in the *SOD1* intron rendered cells unable to repress Cu/Zn-Sod1 while Mn-Sod3 induction was preserved (Fig. 3-7C lane 6). These studies demonstrate that *SOD1* and *SOD3* are regulated independent of one another by copper and that this regulation requires Mac1 consensus sequences in the *SOD3* promoter and

SOD1 intron. Mac1 is well known for its role as a transcriptional activator [186,189,211,213-215,277,278] but our studies with *C. albicans SOD1* provide strong evidence that Mac1 can also act in gene repression using downstream consensus sites.

Sod1 and Sod3 in an infection model for disseminated candidiasis

The natural habitat of *C. albicans* is the animal host and it was therefore critical to assess whether the organism alternates between Sod1 and Sod3 *in vivo*. Based on studies with other pathogens, host copper is predicted to rise during infection [82,170-172,279,280], calling into question the significance of a copper starvation response in *C. albicans*. To investigate this, we used a murine model of disseminated candidiasis where kidney is the primary target organ of infection [143]. In this model, kidney abscesses appear as early as 24-48 hrs of infection and the animal typically succumbs to lethal candidiasis within a week [143]. As seen in Fig. 3-8A, serum copper levels significantly increased during 72 hrs of candidiasis ($p<0.001$ for control vs. 72 hrs), consistent with the notion of elevated host copper during infection and inflammation [79,82,170-174,260,279,280]. However, kidney copper did not follow suit. There was a brief rise in kidney copper at early stages of infection, but later stages were associated with reductions in total kidney copper and levels consistently decreased ~2 fold between 24 and 72 hours post-infection ($p<0.001$ for 24 hrs vs. 72 hrs) (Fig. 3-8B). This pattern was identical in isolated medulla and cortex sections of the kidney, indicative of tissue-wide changes in copper ($p<0.001$ for 24 hrs vs. 72 hrs in medulla and cortex) (Fig. 3-8C,D). We also examined copper in the spleen and liver where the fungal burden is 3-4 orders of magnitude lower than that of kidney based on CFUs (Fig. 3-8D). Trends in splenic

copper were similar to that of kidney, i.e., an initial rise, followed by decreases at later stages ($p<0.01$ for 24 hrs vs. 72 hrs) (Fig. 3-8E), while copper in the liver remained relatively constant ($p>0.05$ for all groups) (Fig. 3-8F). Overall, the progressive elevation in serum copper during infection (Fig. 3-8A) is not mirrored in these tissues.

To examine the impact of such changes in host copper on *C. albicans,* we conducted qRT-PCR analysis of fungal *SOD1* and *SOD3* in kidneys, where fungal burden was the highest (Fig. 3-9D). As seen in Fig. 3-9A,B, early stages of infection were associated with abundant *SOD1* and relatively low *SOD3* mRNA, indicative of abundant copper availability for the invading fungus. However, as infection proceeded, *SOD1* was repressed and *SOD3* was induced. Expression of the *C. albicans CTR1* target of Mac1 was also elevated during later stages of infection (Fig. 3-9C). This response in *C. albicans* strongly indicates that the yeast is sensing the drop in kidney copper.

So why is the kidney losing copper during prolonged infection? One possibility is increased copper excretion in the urine. However, when samples of urine were collected, urine copper levels seem to follow kidney copper and decline ~2 fold from 24 to 72 hrs of infection ($p<0.005$ for 24 hrs vs. 72 hrs) (Fig. 3-10). This indicates that kidney copper is not excreted; it is likely redistributed elsewhere in the body instead.

Discussion

C. albicans has evolved with an elaborate system for adjusting to copper deficiency. In addition to inducing copper uptake systems, the organism will substitute its copper-requiring Sod1 enzyme with cytosolic Mn-Sod3. In this manner, the cell can

maintain oxidative stress protection in the cytosol over a wide range of environmental copper conditions. One other instance of such swapping of SODs with different metal co-factors has been reported for plants where in chloroplasts, an iron-containing SOD will replace Cu/Zn-SODs during plant copper deprivation [281]. In the case of *C. albicans*, this ability to exchange Cu- and Mn-containing SODs serves to accommodate changes in copper at the host-pathogen interface.

The switch in *C. albicans* SODs during copper starvation is mediated through the copper-sensing regulator Mac1 that is well known for its role as a transcriptional activator of copper uptake genes in *S. cerevisiae* and *C. albicans* [214,215,278]. *C. albicans SOD3* can now be added to the list of transcriptional activation targets for Mac1 involving consensus sequences in the gene promoter. However, the puzzling downstream placement of the Mac1 consensus site in the *SOD1* intron is unprecedented. Our studies demonstrate that this downstream site is essential for repression of *SOD1* with low copper. It is possible that Mac1 binding at this intronic site blocks progression of the transcriptional machinery or interacts with factors upstream for transcriptional initiation to down-regulate *SOD1*. In any case, this situation may not be unique to *SOD1*. In studies by Cashmore and colleagues, expression of the *C. albicans SFU1* regulator of iron homeostasis was elevated in *mac1*Δ/Δ strains [215], suggesting possible repression by Mac1, and we noted a possible Mac1 consensus sequence at downstream *SFU1* position +141. Thus *C. albicans* Mac1 may serve an expansive function in copper-regulated gene control to both activate and repress gene expression depending on positioning of its consensus binding sequence.

A well-accepted concept in innate immunity is host-imposed copper toxicity where elevated copper serves as an effective biocide against microbial pathogens [79,82,170-172,260,279,280]. Our studies reveal two faces of host copper during infection with *C. albicans*: While serum copper elevates, copper can become limiting at the major site of infection in the kidney. As one possibility, the host may intentionally restrict copper as part of an innate nutritional immunity response, similar to host withholding of iron, manganese, and zinc for invading microbes [154,159,252-257]. Recent studies by Brown have shown that during *C. albicans* infection of the kidney, iron moves away from sites of fungal lesions in the cortex to the medulla as an apparent mechanism for iron withholding [256]. However we observe no similar movement of copper towards the medulla, rather the drop in copper is uniform kidney-wide. Furthermore, this is not due to increased urinary output as urine levels of copper seem to decline just like kidney copper. If the kidney is not losing copper by excretion, the metal should be reabsorbed into circulation, perhaps contributing to the continual rise in serum copper. It is noteworthy that the majority of serum copper is in the form of the acute phase cuproprotein ceruloplasmin, largely produced by the liver [279,282,283]. We find that liver does not follow the same late stage decline in copper seen with kidney and spleen, raising the intriguing possibility that copper may be mobilized from non-liver tissues to meet the demands for elevating serum copper and cupro-ceruloplasmin production by the liver. Regardless of the mechanism, these studies demonstrate that the host response to infection is not simply to attack pathogens with toxic copper, but that copper can become limiting during infection as well. *C. albicans* is well equipped to

withstand restrictions in host copper by adjusting copper uptake and the utilization of copper as an enzymatic co-factor for SOD enzymes.

Future Directions

The mechanism by which copper is depleted from the kidney during infection remains unknown. If copper from the kidney is reabsorbed into the blood, we expect it to occur with the help of the mammalian copper pump Atp7a. Atp7a is known to translocate from the trans-Golgi network to the basolateral membrane during copper elevation to pump copper out of renal cells and into the blood [284]. We can examine if this occurs in our infection model by measuring *ATP7a* transcript levels in infected kidney using qRT-PCR. We expect to see an induction of *ATP7a* mRNA at late stages of infection corresponding with the decline of kidney copper levels. Even if mRNA levels are not affected, we anticipate the relocalization of Atp7a protein from intracellular sites to the basolateral membrane of kidney epithelial cells. This can be detected using immunohistochemistry (IHC) on sectioned kidney tissue with an anti-Atp7a antibody, which will be provided by our collaborator Dr. Svetlana Lutsenko here at JHU. Alternatively, copper might be excluded from kidney tissue due to lack of copper uptake, rather than increased copper export. This can be examined using the methods just described to detect mRNA and protein levels of the copper permease Ctr1.

In our model of disseminated candidiasis, we also noted the strong increase of serum copper during infection, which we hypothesize is due to increased ceruloplasmin production. In future studies, this can be tested by immunoblot analysis of serum ceruloplasmin, where we expect ceruloplasmin levels to increase in parallel to previously

detected serum copper (Figs. 3-8A, 3-10). We can also distinguish between holo- and apo-ceruloplamsin levels using native gel electrophoresis followed by immunoblotting. Furthermore, we can perform *C. albicans* infection experiments using ceruloplasmin knock-out mice [285] from our collaborator Dr. Mick Petris at University of Missouri, in which we do not expect to see the same rise in serum copper and drop of kidney copper.

We currently do not know if the potential nutritional immunity effects of copper are limited to kidneys during disseminated infection. We may broaden our focus and use qRT-PCR to identify whether fungal copper response genes like *SOD1*, *SOD3*, and *CTR1* are impacted in secondary infection sites such as liver and spleen. We can even try different infection models. For example, our collaborator at University of Maryland, Dr. Mary Ann Jabra-Rizk, uses an oropharyngeal candidiasis (OPC) model [286] that will enable us to analyze copper levels and gene expression in infected tongue tissue.

Other investigators have shown that Sod1 is a virulence factor; deletion of SOD1 results in attenuated virulence during disseminated infection [239]. Based on our work detailing the complimentary functions of Sod1 and Sod3, we expect that Sod3 is also a virulence factor. Because these SODs are regulated by Mac1, this transcription factor may also be important for virulence. To test these ideas, we can generate homozygous gene deletions in *C. albicans* using the SAT-FLP method, creating *sod3Δ/Δ*, *sod1Δ/Δ sod3Δ/Δ*, and *mac1Δ/Δ* strains, then use these strains to infect mice and monitor mouse survival over time. All experiments using mouse models of systemic candidiasis will be performed with continuing collaboration with Dr. Brendan Cormack at JHU.

Figure 3-1: *C. albicans* will reversibly switch from Cu/Zn-Sod1 to Mn-Sod3 enzyme during prolonged growth or stationary phase.

A log phase culture ($O.D._{600} \approx 1.0$) of *C. albicans* strain KC2 was diluted back to an $O.D._{600} = 0.1$ and incubated for the indicated time points at 30°C (A). A 48 hour culture of *C. albicans* strain CA-IF100 was diluted back to an $O.D._{600} = 0.1$ in fresh YPD medium and cultured at 30°C for the indicated time points (B). Cells were analyzed for SOD activity by the native gel assay (A top) and for Sod1 and Sod3 protein levels by immunoblot (A middle, B top). Bottom graphs indicate cell growth monitored at $O.D._{600}$. The positions of Sod1, Sod2, and Sod3 migration on the native gel and of Sod1 and Sod3 on the denaturing gel are indicated.

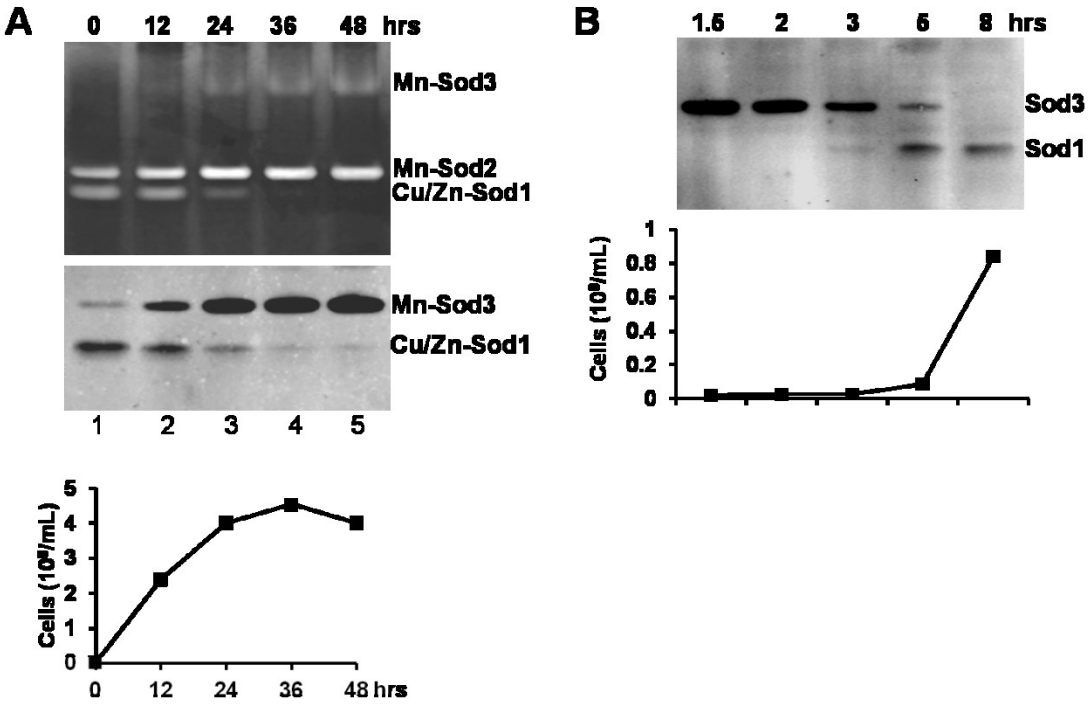

Figure 3-2: Aged cultures of *C. albicans* will revert to expressing Sod1 when logarithmic growth resumes.

A 48 hour culture of *C. albicans* strain CA-IF100 was diluted back to an $O.D._{600}$ = 0.1 in fresh YPD medium that was supplemented where indicated with 0.5% glucose rather than the standard 2% (A) or with 1 mM $MnCl_2$ (C). CA-IF100 cells were grown as in Fig. 3-1A in the presence of either air or 5% oxygen (B). Cells were cultured for the indicated time points in hours; Sod1 and Sod3 levels were monitored by immunoblotting. Total intracellular manganese (C bottom) was measured by atomic absorption spectroscopy. Results represent the averages of technical duplicates; error bar is standard deviation.

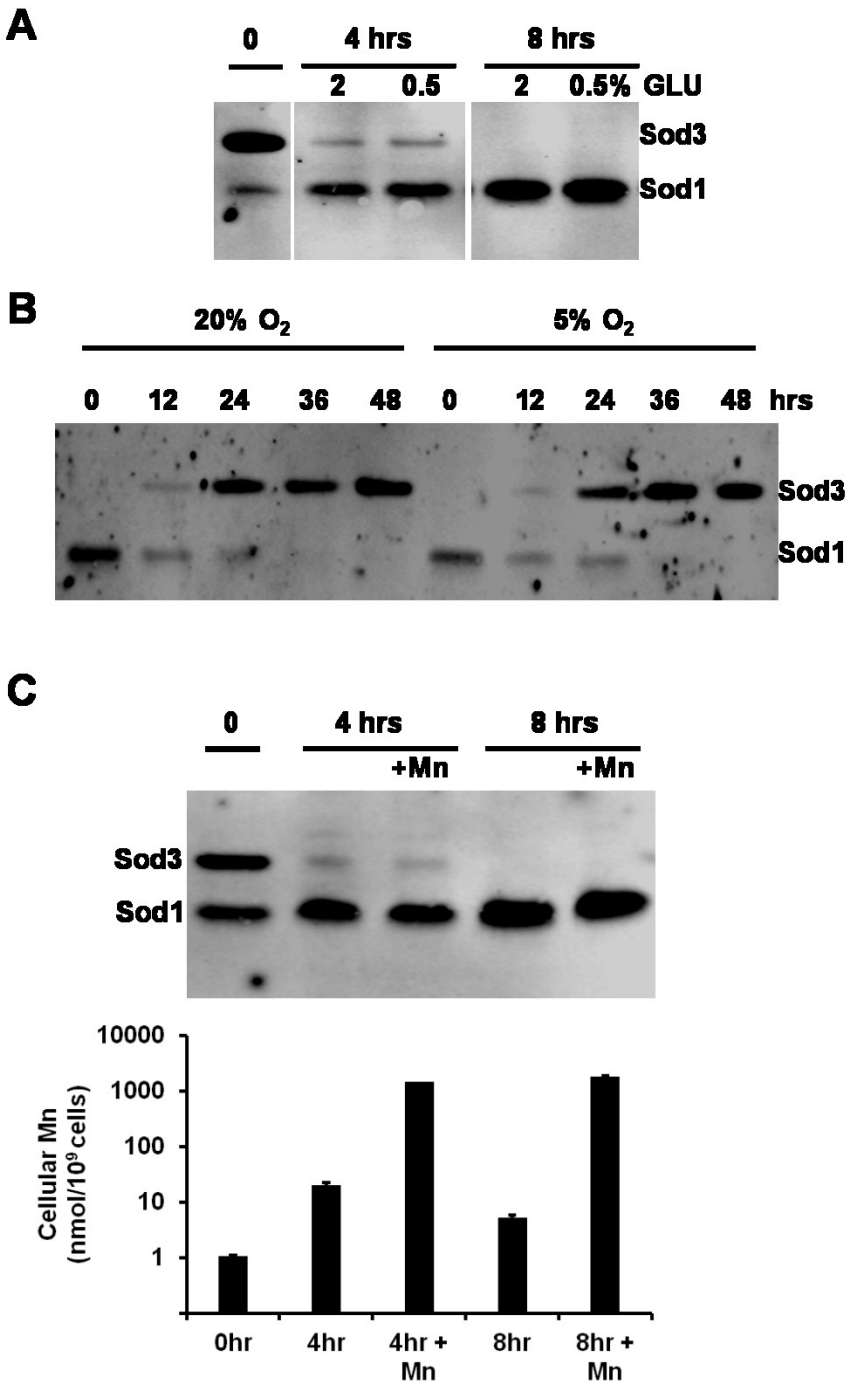
A
0
4 hrs
8 hrs
2
0.5
2
0.5% GLU
Sod3
Sod1
B
20% O2
5% O2
0 12 24 36 48 0 12 24 36 48 hrs
Sod3
Sod1
C
0
4 hrs
+Mn
8 hrs
+Mn
Sod3
Sod1
Cellular Mn (nmol/10^9 cells)
10000
1000
100
10
1
0hr
4hr
4hr + Mn
8hr
8hr + Mn

Figure 3-3: Induction of Sod3 during stationary phase growth is due to diminishing copper.

(A,B) CA-IF100 cells were grown for either 12 (log) or 48 hrs (stationary). **(A)** Cells were analyzed for total copper by AAS where results represent the averages of two independent experiments and error bars are standard deviation. **(B)** *CTR1* expression by qRT-PCR compared to *TUB2* mRNA as described in *Experimental Procedures.* Results represent three independent experimental trials where error bars are standard error. **(C)** Immunoblot analysis of Sod1 and Sod3 was carried out on log phase cells ("0") that where indicated, were grown for an additional 24 or 48 hrs with or without 8 mM $CuSO_4$.

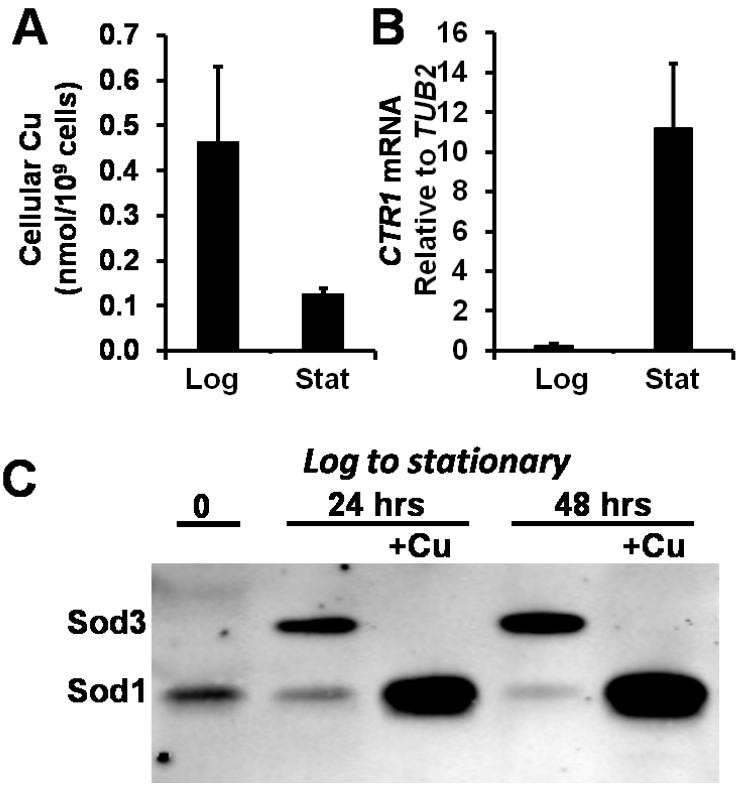

Figure 3-4: *C. albicans* will switch from Cu/Zn-Sod1 to Mn-Sod3 enzyme in response to copper starvation.

(A) Cells were grown to stationary phase for 48 hours in medium supplemented with the various concentrations of $CuSO_4$. Top shows dose dependent increase in intracellular copper as measured by AAS. Immunoblot at bottom shows reciprocal control of Sod1 versus Sod3 as a function of intracellular copper. **(B)** A log phase culture of *C. albicans* strain CA-IF100 was grown for 12 hours in the presence of increasing concentrations of the Cu(I) chelator BCS. Intracellular copper levels were monitored by AAS (top), Sod1 and Sod3 protein levels by immunoblot (middle), and SOD activity by the native gel assay (bottom). Sod2 is the manganese-containing SOD of the mitochondrial matrix that is highly homologous to cytosolic Sod3 [86] but remains constant with varied copper. High copper favors Sod1 and low copper favors Sod3 while both SODs are present at intermediate copper levels.

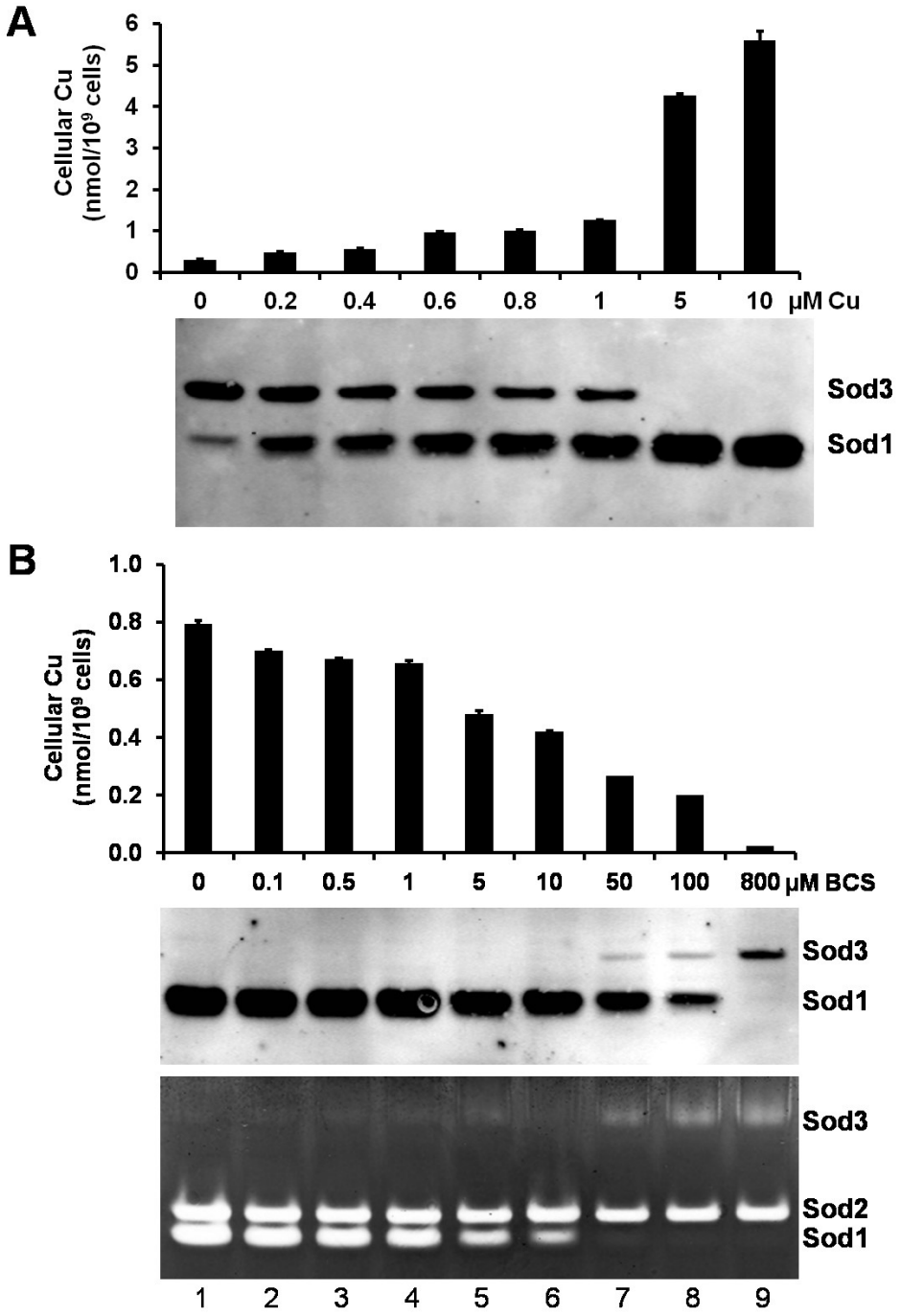
A
Cellular Cu
(nmol/10⁹ cells)
0
1
2
3
4
5
6
0
0.2
0.4
0.6
0.8
1
5
10
μM Cu
Sod3
Sod1
B
Cellular Cu
(nmol/10⁹ cells)
0.0
0.2
0.4
0.6
0.8
1.0
0
0.1
0.5
1
5
10
50
100
800 μM BCS
Sod3
Sod1
Sod3
Sod2
Sod1
1
2
3
4
5
6
7
8
9

Figure 3-5: Alternating SOD enzymes in hyphal yeast and in clinical isolates of *C. albicans*.

(A) A log phase culture of CA-IF100 at 30°C ("budding") was incubated in water for 60 minutes at 30°C ("starved"), and then induced to form hyphae by incubating in YPD medium + serum at 37°C for 6 hrs ("hyphal"). Where indicated ("hyphal +BCS") 800 μM BCS was added during hyphal formation. Sod1 and Sod3 expression was analyzed by immunoblot (top) and yeast cell morphology by light microscopy (bottom). **(B)** Three clinical isolates of *C. albicans* isolated from human blood, the respiratory tract, and a fluconazole-resistant ($Fluc^R$) isolate from the respiratory tract were grown as in Fig. 3-4A with cells treated where indicated with 800 μM BCS; the laboratory strain CA-IF100 served as control. Sod1 and Sod3 expression was determined by immunoblot.

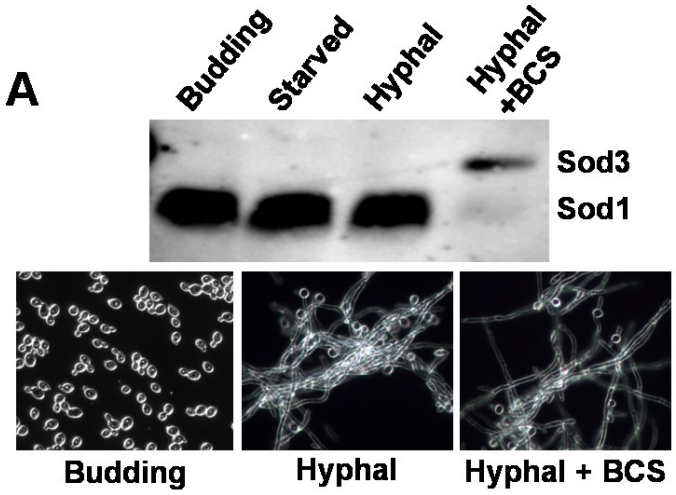
A
Budding
Starved
Hyphal
Hyphal +BCS
Sod3
Sod1
Budding
Hyphal
Hyphal + BCS

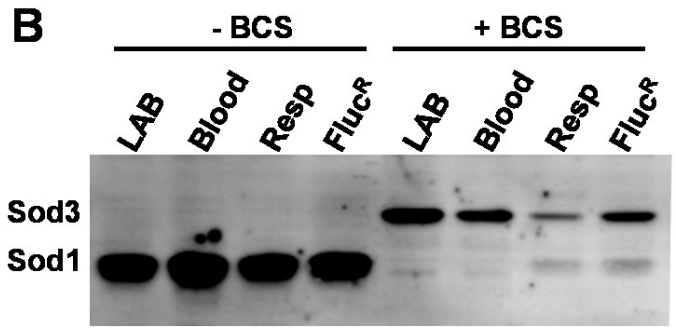
B
- BCS
+ BCS
LAB
Blood
Resp
FlucR
LAB
Blood
Resp
FlucR
Sod3
Sod1

Figure 3-6: Role of Mac1 in regulating *SOD1* and *SOD3* mRNA by copper.

(A,C top) Immunoblot analysis of Sod1 and Sod3 with the indicated strains grown to log phase and supplemented where indicated with 800 μM BCS. **(B)** *SOD1* and *SOD3* mRNA were quantified by qRT-PCR in the indicated strains grown to log or stationary (48 hrs) phase in cultures supplemented with either 800 μM BCS or 8 mM $CuSO_4$ where indicated. Results are shown as a comparison to *TUB2* mRNA and represent the averages of three independent experimental trials where error bars are standard error. **(C bottom)** Cells from C top were analyzed for intracellular copper by AAS. Strains used: (A) WT CA-IF100 and *sod1*Δ/Δ strain CA-IF003 and *sod3*Δ/Δ strain CA-IF011; (B,C) WT SN152 and isogenic *mac1*Δ/Δ TF065-X. The same trends in Sod1 and Sod3 expression were obtained with an independent *mac1*Δ/Δ isolate TF065-Y (not shown).

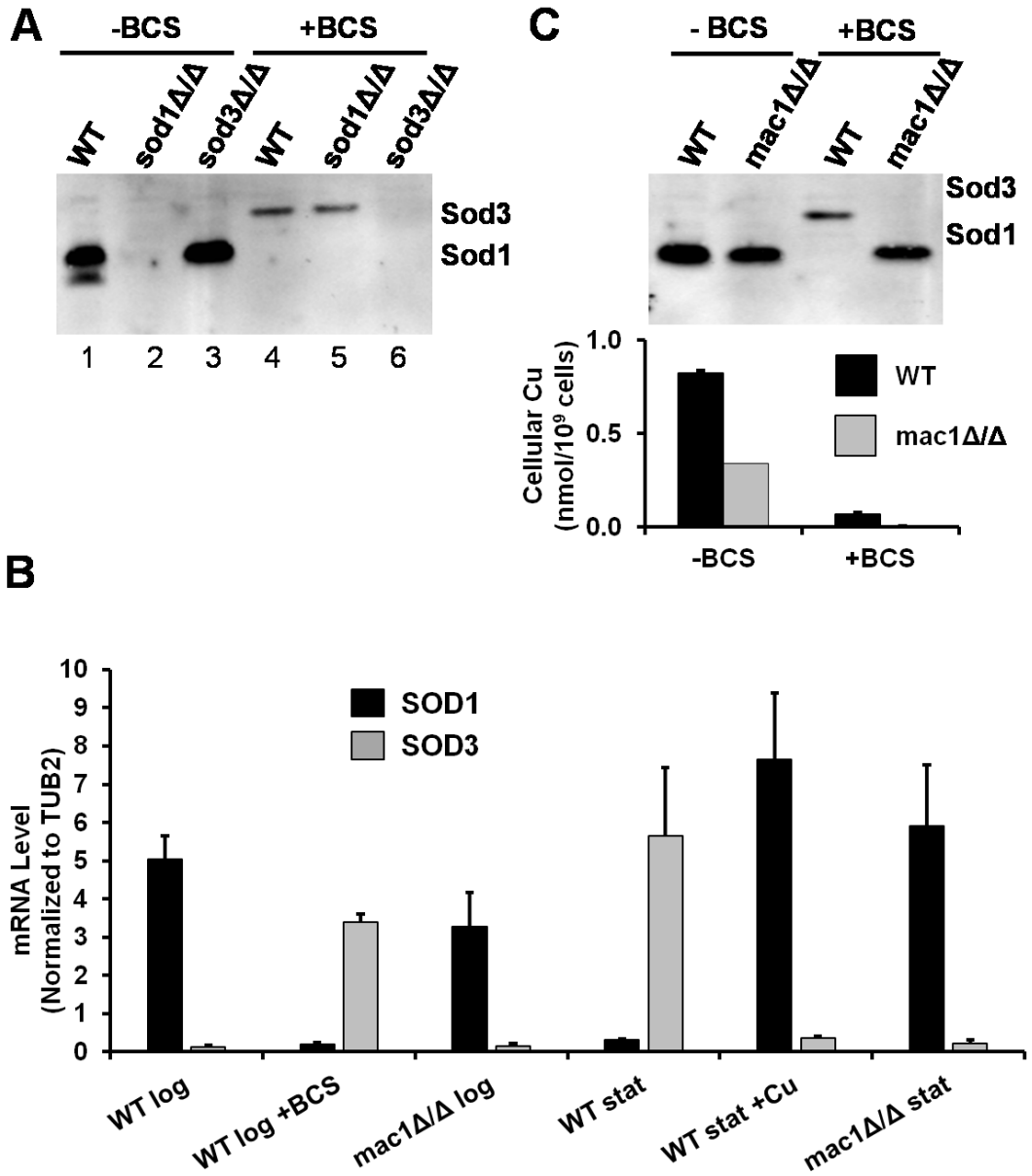
A
-BCS
+BCS
WT
sod1Δ/Δ
sod3Δ/Δ
WT
sod1Δ/Δ
sod3Δ/Δ
Sod3
Sod1
1 2 3 4 5 6
C
- BCS
+BCS
WT
mac1Δ/Δ
WT
mac1Δ/Δ
Sod3
Sod1
Cellular Cu (nmol/10^9 cells)
1.0
0.5
0.0
WT
mac1Δ/Δ
-BCS
+BCS
B
mRNA Level (Normalized to TUB2)
SOD1
SOD3
10
9
8
7
6
5
4
3
2
1
0
WT log
WT log +BCS
mac1Δ/Δ log
WT stat
WT stat +Cu
mac1Δ/Δ stat

Figure 3-7: Mac1 consensus sequences needed for regulation of *SOD1* and *SOD3* by copper.

(A) Mac1 consensus sequences in the *SOD3* promoter and *SOD1* intron are aligned against the published Mac1 binding site [189,213,215,277]. There appears to be some flexibility in the first position, as the 5' T is substituted with a G in certain *P. anseria* target genes [213] and appears as A in *SOD3*. **(B)** A *C. albicans sod3*Δ/+ strain was engineered to express recombinant *SOD3* that contained either the native Mac1 site at -154 or an ATTGCTCA to AcTtaagA substitution at this site. The parental and recombinant *SOD3* derivatives were grown to log phase in the presence of 800 μM BCS where indicated and SOD expression analyzed by immunoblot. **(C)** The predicted Mac1 site in the *SOD1* intron was analyzed similarly to that of *SOD3* in part B except the starting strain was a *sod3*Δ/+heterozygote engineered to express *SOD1* with either native (TTTGCTCA) or the substituted (TcttaagA) Mac1 site at +148.

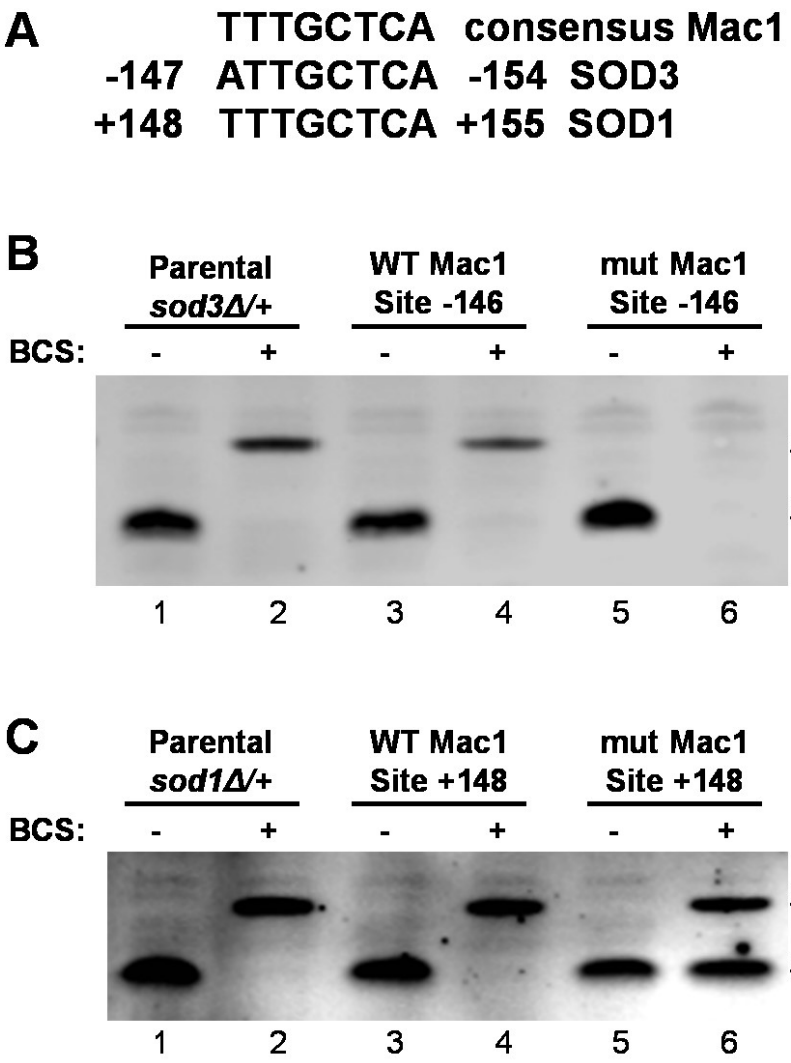
A
TTTGCTCA consensus Mac1
-147 ATTGCTCA -154 SOD3
+148 TTTGCTCA +155 SOD1
B
Parental
sod3Δ/+
WT Mac1
Site -146
mut Mac1
Site -146
BCS:
- + - + - +
Sod3
Sod1
1 2 3 4 5 6
C
Parental
sod1Δ/+
WT Mac1
Site +148
mut Mac1
Site +148
BCS:
- + - + - +
Sod3
Sod1
1 2 3 4 5 6

Figure 3-8: Copper responses during a murine model of disseminated candidiasis. Mice were infected with *C. albicans* by lateral tail vein injection as described in *Experimental Procedures.* At the specified time points, serum (A), whole kidney (B), kidney medulla (C), kidney cortex (D), spleen (E), and liver (F) were analyzed for copper by AAS. Tissues were analyzed as a function of wet weight. Copper analysis shows individual values from 5-13 mice at each time point; bar represents average. Kidney copper represents ng Cu/mg wet weight of whole tissue (cortex and medulla combined) (B).

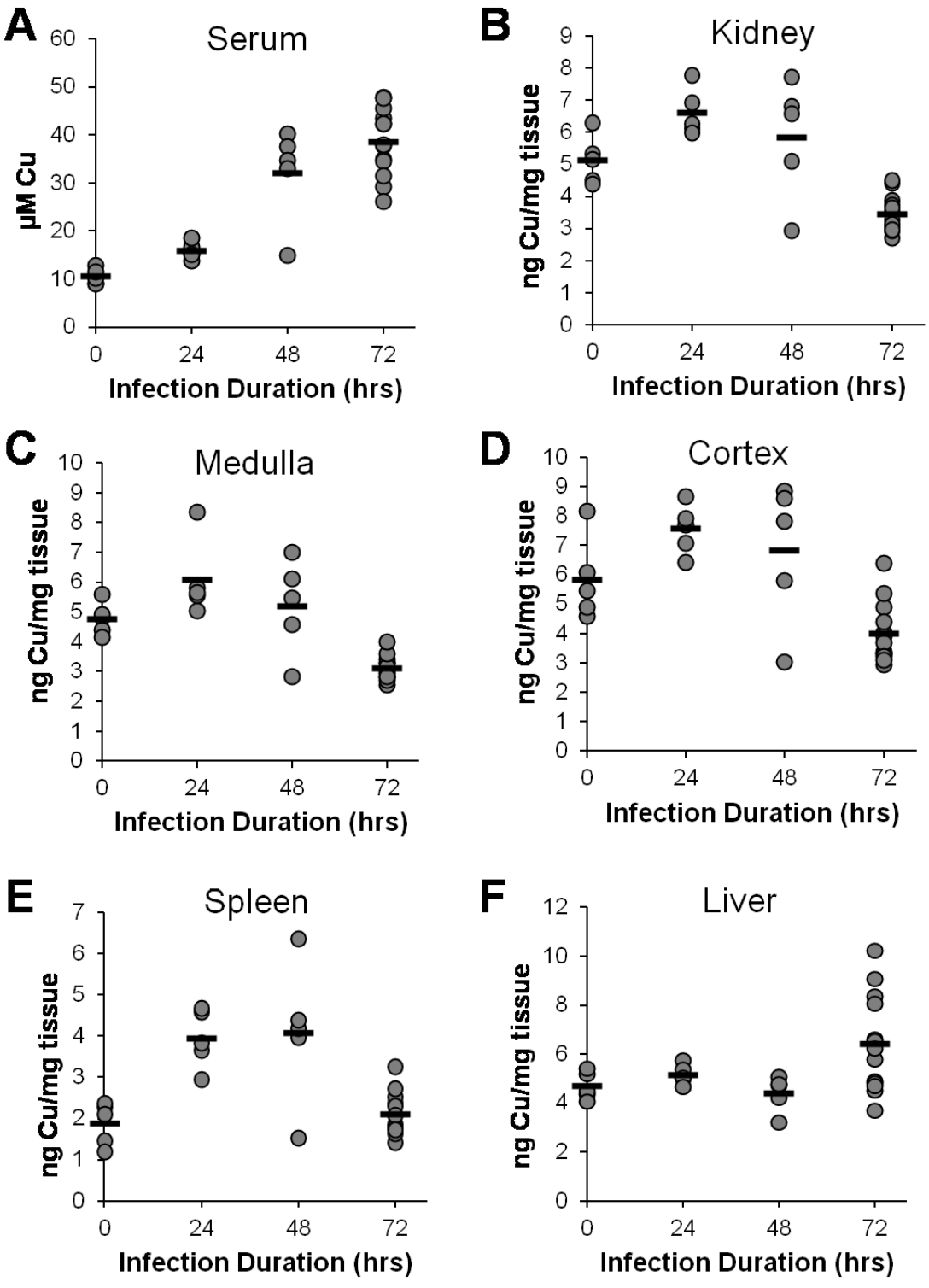
A
Serum
µM Cu
Infection Duration (hrs)
B
Kidney
ng Cu/mg tissue
Infection Duration (hrs)
C
Medulla
ng Cu/mg tissue
Infection Duration (hrs)
D
Cortex
ng Cu/mg tissue
Infection Duration (hrs)
E
Spleen
ng Cu/mg tissue
Infection Duration (hrs)
F
Liver
ng Cu/mg tissue
Infection Duration (hrs)

Figure 3-9: Fungal responses during disseminated candidiasis.

Mice were infected with *C. albicans* by lateral tail vein injection and kidneys, liver, and spleen were harvested at the specified time points, from Fig. 3-9. **(A-C)** From the kidney, *C. albicans SOD1*, *SOD3,* and *CTR1* mRNA were quantified by qRT-PCR, compared to levels of fungal *TUB2*. Results shown are averages from 5-13 individual mice at each time point; error bars represent standard error. **(D)** Colony forming units (CFUs) of *C. albicans* infected tissues demonstrates that the fungal burden in the kidney is 2-3 orders of magnitude higher than that of spleen and liver. Results are averages of 5-13 independent mice, error bars are standard error.

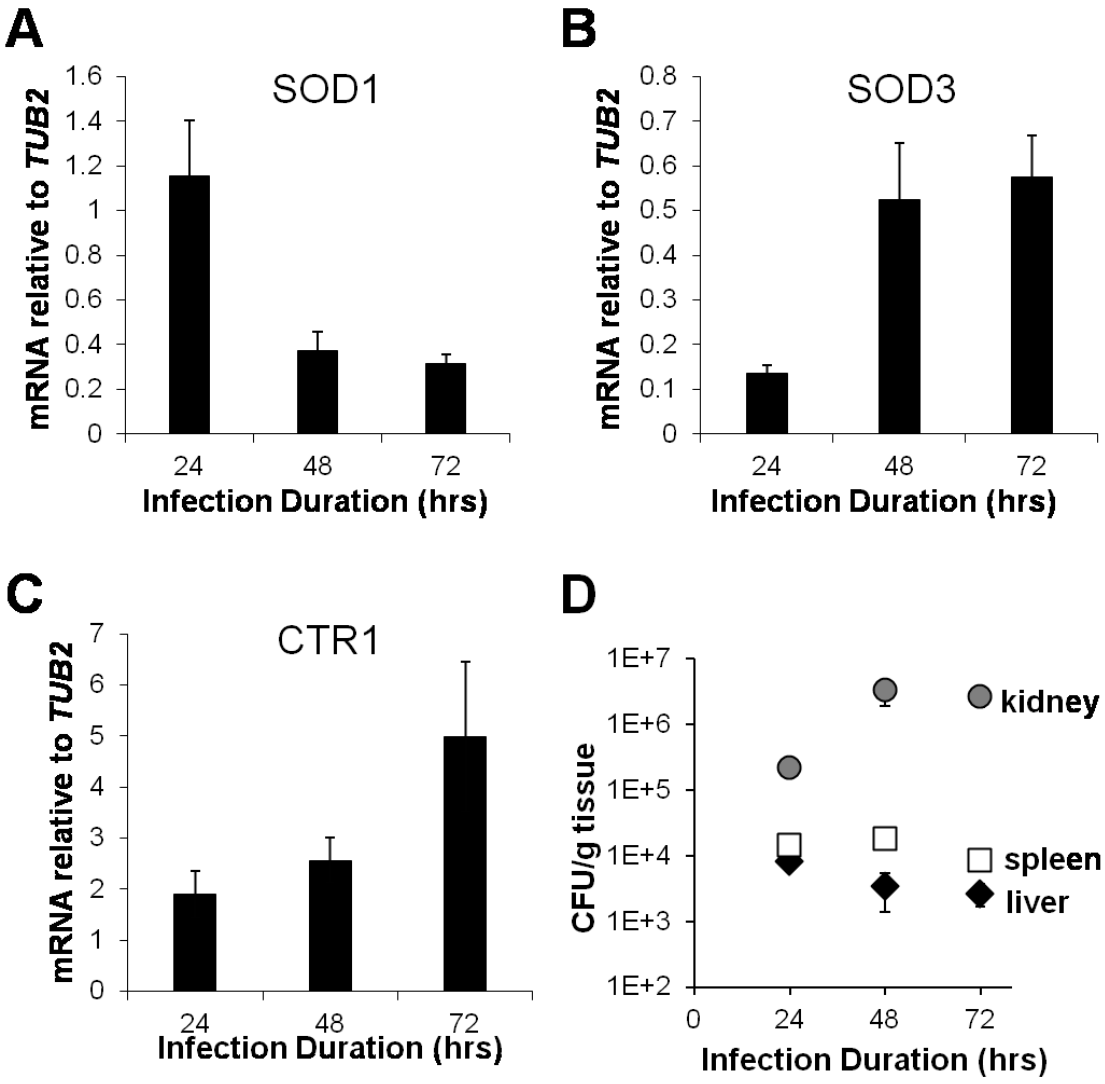
A
SOD1
mRNA relative to TUB2
1.6
1.4
1.2
1
0.8
0.6
0.4
0.2
0
24
48
72
Infection Duration (hrs)
B
SOD3
mRNA relative to TUB2
0.8
0.7
0.6
0.5
0.4
0.3
0.2
0.1
0
24
48
72
Infection Duration (hrs)
C
CTR1
mRNA relative to TUB2
7
6
5
4
3
2
1
0
24
48
72
Infection Duration (hrs)
D
CFU/g tissue
1E+7
1E+6
1E+5
1E+4
1E+3
1E+2
0
24
48
72
Infection Duration (hrs)
kidney
spleen
liver

Figure 3-10: Changes in serum versus urine copper during *C. albicans* infection. Mice were infected with *C. albicans* as in Fig. 3-9 and serum and urinary copper was measured as described in *Experimental Procedures.* Shown are values from 5-11 individual mice at each time point, bar represents average.

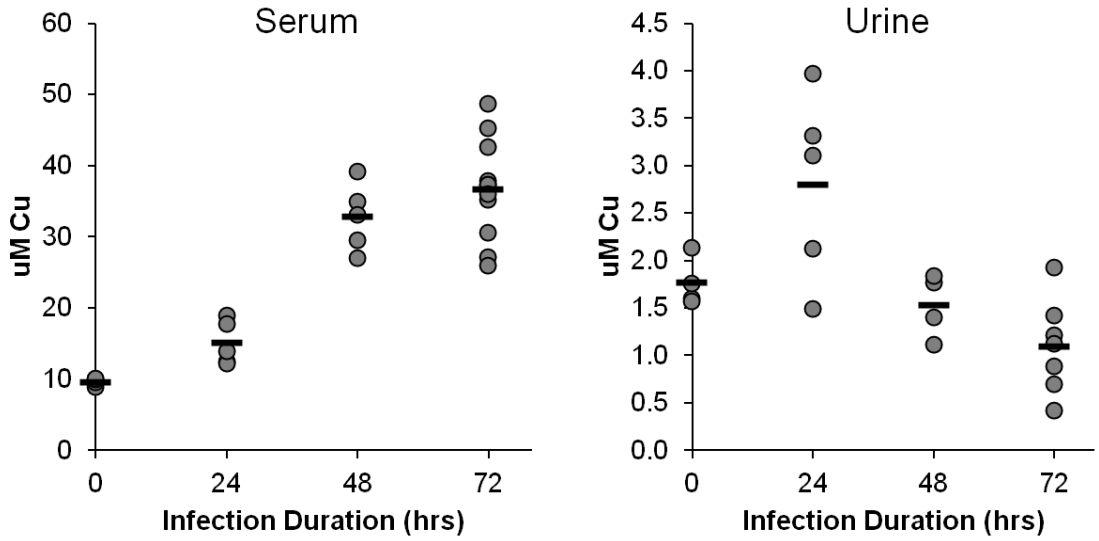

Table 3-1: Primers used in this study

Name	Sequence	Description
OCL098	CAGATATCCATCACACTGGCGGCCGCAAGTTATTGAAA TTTATGAGTTTAAAAAG	F SOD1 amplification
OCL101	ACTATAGGGCGAATTGGGCCCTTAGTTAGTTAATTACC TAAATCACCAACATGTC	R SOD1 amplification
OCL102	CAGATATCCATCACACTGGCGGCCGCATATGGAACTTG GTTAGCTGGC	F SOD3 amplification
OCL105	ACTATAGGGCGAATTGGGCCCTTAGTTAGTTAGTGTTT GCCACCACCTTTAG	R SOD3 amplification
OCL116	GACTCATCCGAATTGATCCAAATGCCTTGAGAG	F SOD1 +BplI
OCL117	GGACTCTTCGGATTTTACCTTCAATTTCCCAAGAAATTG	R SOD1 +BplI
OCL118	GACTCATCCGAATTATTGACGCACTTGAAAAAG	F SOD3 +BplI
OCL119	GGACTCTTCGGATTGCGGCATTGTACCCGTTTAC	R SOD3 +BplI
OCL120	AATTTCTAATCTTAAGATAATTGTATTCTTCCAAAAACAT G	F SOD1 Mac1-AflII
OCL121	ACTTCAATTGGTAATTTGAAATTC	R SOD1 Mac1-AflII
OCL122	AACATAGGTTCTTAAGTATATTTACATCCCAAAATGGAT AAC	F SOD3 Mac1-AflII
OCL123	TCGTACGACTCGTTATAG	R SOD3 Mac1-AflII
OCL126	AAAGCTGGCGCAACAGATATATTG	F SOD verification
OCL014	CCAGCATGACCAGTAGTTTTAGAAT	R SOD1 verification
OCL016	GATATTGCAAGTAGTACGCATGTTC	R SOD3 verification
OCL043	GAGTTGGTGATCAATTCAGTGCTAT	F TUB2 qPCR
OCL044	ATGGCGGCATCTTCTAATGGGATTT	R TUB2 qPCR
OCL013	CTACTGATGGTAATGGTGTTGCTAA	F SOD1 qPCR
OCL014	CCAGCATGACCAGTAGTTTTAGAAT	R SOD1 qPCR
OCL015	CAGTATGGGTCTGTTTCAAACCTTA	F SOD3 qPCR
OCL016	GATATTGCAAGTAGTACGCATGTTC	R SOD3 qPCR
OCL062	CAAAAGCTCGTGGAACCGGTAAATC	F CTR1 qPCR
OCL063	TCAGCAACAAATCTTCCAACACCGG	R CTR1 qPCR

APPENDIX I

Changes in kidney metals during *C. albicans* infection

Introduction

In Chapter 3 of this thesis, we found that total kidney copper levels dropped after prolonged *C. albicans* systemic infection. This was correlated with fungal repression of *SOD1* and induction of *SOD3*, which we showed to be an adaptive response to cellular copper depletion. We provided the first evidence of host copper withholding during microbial infection.

If kidney copper levels are altered during infection, other metals may be similarly affected. Brown et. al. found that iron in the kidney accumulates in the medulla during infection while iron drops in the cortex, with further iron starvation locally around fungal lesions, primarily in the cortex [256]. This is accompanied by increased fungal expression of iron acquisition genes [256]. Mammalian systemic iron homeostasis is regulated by the antimicrobial peptide hepcidin, which is expressed mostly in hepatocytes as part of the innate immune response [287,288]. The redistribution of kidney iron was correlated with an increase in kidney hepcidin [256], suggesting that hepcidin may contribute to nutritional immunity for iron during *C. albicans* infection.

Manganese and zinc are also known to be withheld from invading pathogens. This occurs with the help of calprotectin, a protein of the S100 family that can bind these two metals. Calprotectin is highly expressed in neutrophils, which infiltrate infected tissues and act as a marker of fungal lesions in the kidney [256]. Calprotection is then released in neutrophil extracellular traps (NETs) and tissue abscesses in order to sequester manganese and zinc at sites of pathogen invasion [139,151-153,253,289]. However, distribution of manganese and zinc in renal tissue during *C. albicans* infection has not been studied.

In Chapter 3, metal analysis was performed using atomic absorption spectroscopy (AAS), which limited analysis to one metal at a time. Other methods such as inductively coupled plasma mass spectrometry (ICP-MS) allow concurrent analysis of many elements [290]. Still, ICP-MS will measure total element level in the tissue, and cannot detect any local changes at sites of infection. In order to map the localization of various elements, we used synchrotron-based X-ray fluorescence microscopy (XRF). In this technique, a high power X-ray beam, generated from a third-generation synchrotron, is focused onto a specimen. The sample is scanned along the incident beam, and the fluorescence emission spectrum for many elements is detected at each pixel [291]. XRF allows high sensitivity detection of most biologically important metals with sub-micron resolution [291]. This is a powerful technique that can simultaneously measure elemental localization and concentration, and is applicable to biological samples [292]. To our knowledge, only one study has used XRF to map metals in kidneys, and it focused on selenium [293]. This method has not been applied to study kidney metals during infection.

Here, the analysis of kidney metals during *C. albicans* infection is expanded beyond copper to include iron, manganese, zinc, and calcium, using both ICP-MS and XRF. We find that whole kidney levels of manganese and iron also decline during infection, while zinc and calcium levels rise. But when looking locally at sites of fungal infection, we find that calcium is elevated while zinc is withheld from these lesions. Our work maps the elemental landscape of kidneys in fighting *C. albicans* infection.

Experimental Procedures

The murine infection model for disseminated candidiasis

The mouse infection studies were carried out as described in Chapter 3. After 48 and 72 hours of infection, 5-11 mice per time point were sacrificed, along with 5 control uninfected mice. For XRF studies, both kidneys were harvested from each control and 72 hour infected mouse and bisected, one sagittally and one transversely. One half of each kidney (cut in different orientations) were frozen in optimal cutting temperature compound, a specimen matrix for cryosectioning, and stored at -80°C until sectioning for XRF as described below. One remaining kidney half was homogenized, serially diluted, and plated onto YPD plates with 1% penicillin-streptomycin to determine colony forming units (CFUs). The last remaining half was dissolved in 1 mL of 20% Ultrex II Ultrapure nitric acid (J.T. Baker) overnight at 90°C for AAS analysis as described in Chapter 3. The frozen kidney samples from 3 control mice and the 3 mice that had highest CFUs were selected for elemental imaging analysis (XRF, below). At least one sagittal and one transverse kidney section was analyzed for each mouse.

For ICP-MS analysis, medulla and cortex samples dissolved in nitric acid for AAS in Chapter 3, Fig. 3-9B-D, were reexamined by ICP-MS at the core facility for elemental analysis at the University of Maryland School of Pharmacy using an Agilent 7700x ICP-MS. 3-5 samples per group were randomly selected for analysis, and whole kidney concentrations were calculated from medulla and cortex measurements.

X-ray fluorescence and tissue microscopy

Kidneys were sectioned to 8 μM thickness on a Microm HM550 cryostat (Thermo Scientific) at -20°C. One section was transferred to a room temperature microscope slide for hematoxylin and eosin staining; the adjacent section was mounted onto Ultralene 4 μM film. The fresh frozen tissue samples were air dried at room temperature without fixation. The samples on Ultralene film were subjected to XRF, performed using beamline 8-BM-B at the Advanced Photon Source at Argonne National Laboratory, Argonne, IL. Incident X-rays were focused to a spot size of ~25 μm. Samples were raster-scanned to measure 20 μm pixels, and fluorescence spectra were collected using pixel dwell times of 0.45 s. Quantification and image processing were done using MAPS software [294].

Results and Discussion

Using ICP-MS, we monitored various metals in whole kidney tissue during *C. albicans* infection. First, we verified the results obtained from AAS in Chapter 3, measuring an initial rise in kidney copper at 24 hours of infection, followed by a steady decline to 72 hours ($p<0.01$ for 24 hrs vs. 72 hrs) (Fig. I-1A). Manganese levels also declined slightly during infection ($p=0.05$ for control vs. 72 hrs), but did not initially rise as was the case with copper (Fig. I-1B). Iron levels remained relatively constant throughout infection ($p>0.05$ for all groups) (Fig. I-1C). Kidney zinc levels gradually increased as infection progressed ($p<0.005$ for control vs. 72 hrs) (Fig. I-1D). Finally, calcium did not significantly change during infection ($p>0.05$ for all groups) (Fig. I-1E). These results show that concentrations of specific metals in the kidney do change on a

global scale, but only slightly. However, these findings may be misleading because they do not capture any redistribution of metals within the kidney. A previous study demonstrated that iron moves from the cortex to the medulla during *C. albicans* infection [256], which would be impossible to infer from whole kidney analysis. Therefore, to see the complete picture, we turned to XRF.

Kidneys from control and infected mice were harvested and half of the tissues were prepared for XRF and the remaining was analyzed for CFUs and total copper by AAS. After validating the expected drop in kidney copper after prolonged infection, along with high CFUs (Fig. I-2A,B), three control mice and three 72 hour infected mice with the highest CFUs were selected for XRF analysis. Figs. I-3 and I-4 show results for eight elements from sagittal sections of control and 72 hour infected kidneys. The rainbow bar at the bottom shows the colors relating to element concentration, with black being the minimum and red the maximum. The apparent differences in phosphorus, sulfur, and chlorine between control and infected tissues were not reproducible across multiple tissue slices. However, there were some consistent patterns in the metals calcium, zinc, iron, manganese, and copper, which will be discussed by individual metals below.

Calcium and zinc: The most striking changes are seen with calcium and zinc localization. In infected kidneys, numerous calcium "hot spots" are seen, mostly located in the cortex (Fig. I-5B top). These hot spots are completely absent in uninfected kidneys (Fig. I-5A top), and appear to correspond to sites of fungal lesions based on preliminary hematoxylin and eosin staining (data not shown). Remarkably, the locations of these

calcium hot spots also correlate with regions of zinc depletion, what we call "zinc holes" (Fig. I-5B bottom, enlarged image in Fig. I-6).

Previous data from *S. aureus* infection in the liver have also identified calcium enrichment at sites of infection and immune cell infiltration that closely parallel clearing of zinc. This high calcium and low zinc was attributed to calcium-bound calprotectin working to remove zinc from the invading pathogen [151]. Neutrophil infiltration is also a property of fungal lesions during *C. albicans* infection of the kidney [256]. These data combined suggest that the calcium hot spots and zinc holes we observe in the kidney are the result of neutrophil infiltration, possibly NET formation, and calprotectin release at fungal lesions [139,151,153,256].

Iron: We also observed specific changes in iron localization during infection. While uninfected kidneys show iron concentrated in both the medulla and cortex (Fig. I-7 top), iron relocalized to the medulla during *C. albicans* infection (Fig. I-7 bottom), just as previously reported [256]. The mechanism of iron redistribution and sequestration is not known, but does not involve calprotectin because calprotectin does not bind iron [151,289].

Manganese: Since calprotectin is known to withhold both manganese and zinc, we expected to see manganese-deficient holes corresponding to calcium hot spots, as was observed in the aforementioned *S. aureus* infection of liver and attributed to calprotectin from infiltrating neutrophils [151]. However, the only effect observed was an overall decline in detectable manganese (Fig. I-8). We may not observe the predicted manganese withholding at sites of fungal lesions because manganese was not easily detected above background (Fig. I-8). Other techniques that may improve manganese sensitivity include

higher resolution XRF or laser capture microdissection of abscesses followed by ICP-MS.

Copper: Redistribution of copper was also not observed in infected kidneys (Fig. I-9), consistent with previous copper analysis in Chapter 3 that showed no difference between medulla and cortex (Fig. 3-9C,D). Future experiments using laser capture microdissection may uncover a local change in copper, but it is also possible that copper uniformly declines in the whole kidney. There is no published evidence that calprotectin is able to bind copper, and thus neutrophils may not clear copper at sites of infection as is the case with zinc. The uniform decline of kidney copper may occur through the mammalian copper exporter Atp7A [295], where copper may be transferred to the blood for redistribution in the body and production of serum ceruloplasmin as described in Chapter 3.

Altogether, our results show that redistribution of calcium, zinc, and iron occur in the kidney during *C. albicans* infection, consistent with the roles of these cations in nutritional immunity at sites of neutrophil infiltration [139,151,153,256] . The mechanism of whole kidney copper loss is still unknown and future work will aim to define the mechanisms behind these changes, including an analysis of mammalian copper transporter expression and localization in response to fungal invasion of the kidney (discussed in Chapter 3).

From these multi-element analyses, future experiments will focus on characterization of fungal lesions. We will first verify the localization of yeast and immune cells in infected kidney samples, using periodic acid–Schiff staining to clearly identify yeast, and IHC to identify infiltrating immune cells. Antibodies against Ly6G

and F4/80 cell surface proteins can be used to categorize neutrophils and macrophages, respectively. After identification of fungal lesions and/or immune infiltrates, we can utilize laser-capture microdissection, in collaboration with Dr. Lutsenko, to isolate these lesions and analyze either by ICP-MS to quantify various elements, or by qRT-PCR to detect gene expression. Furthermore, we seek to define the cause of the overlapping calcium hot spots and zinc holes. As discussed, we hypothesize that this is the work of calprotectin released from neutrophils. We can study this by IHC of infected kidney tissue against calprotectin to see if calprotectin accumulates in these lesions. Alternatively, we can also induce disseminated infection in calprotectin knock-out mice [296], from collaborator Dr. Thomas Kehl-Fie, and measure metal concentrations in fungal lesions as described above. We anticipate that mice lacking calprotectin will not generate the calcium hot spots and zinc holes that we see in wild type mice.

Figure I-1: Metal responses during a murine model of systemic candidiasis. Mice were infected as in Chapter 3, and kidney samples were analyzed by ICP-MS, as described in *Experimental Procedures*. Copper (A), manganese (B), iron (C), zinc (D), and calcium (E) were measured as a function of wet weight. Graphs show individual values from 3-5 mice at each time point, bar represents average.

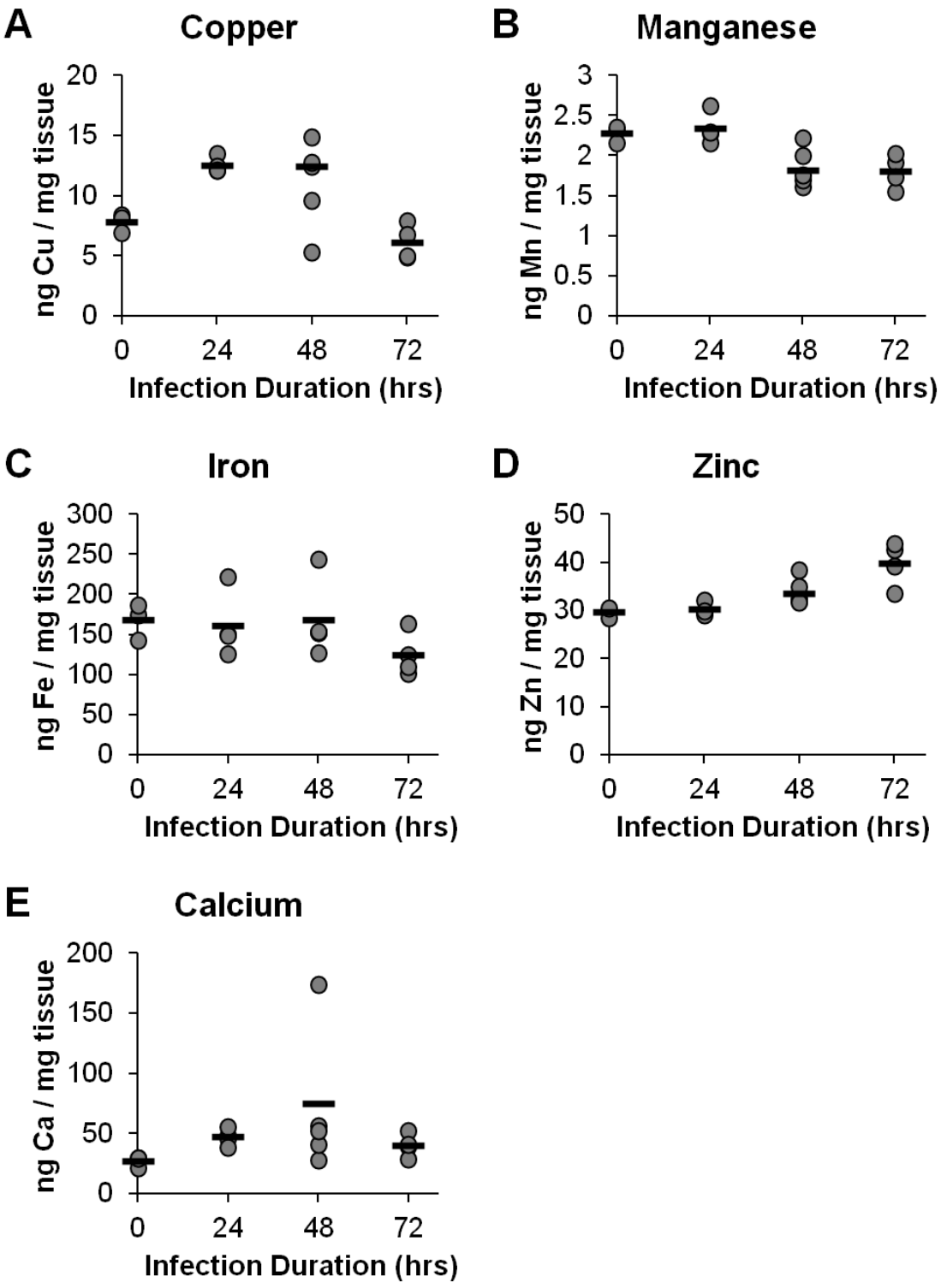
A
Copper
ng Cu / mg tissue
20
15
10
5
0
0
24
48
72
Infection Duration (hrs)
B
Manganese
ng Mn / mg tissue
3
2.5
2
1.5
1
0.5
0
0
24
48
72
Infection Duration (hrs)
C
Iron
ng Fe / mg tissue
300
250
200
150
100
50
0
0
24
48
72
Infection Duration (hrs)
D
Zinc
ng Zn / mg tissue
50
40
30
20
10
0
0
24
48
72
Infection Duration (hrs)
E
Calcium
ng Ca / mg tissue
200
150
100
50
0
0
24
48
72
Infection Duration (hrs)

Figure I-2: Kidney copper and CFUs in selecting mice for XRF metal imaging analysis.

Mice were injected with *C. albicans* in the lateral tail vein, as in described in *Experimental Procedures*. Kidneys were harvested at the specified time points and analyzed for copper by AAS and for CFU counts, all as a function of wet weight. Graphs show values from 5-11 individual mice, the bar represents average. Results were as expected, so the three mice with highest CFUs were selected for additional analysis by XRF, along with three controls.

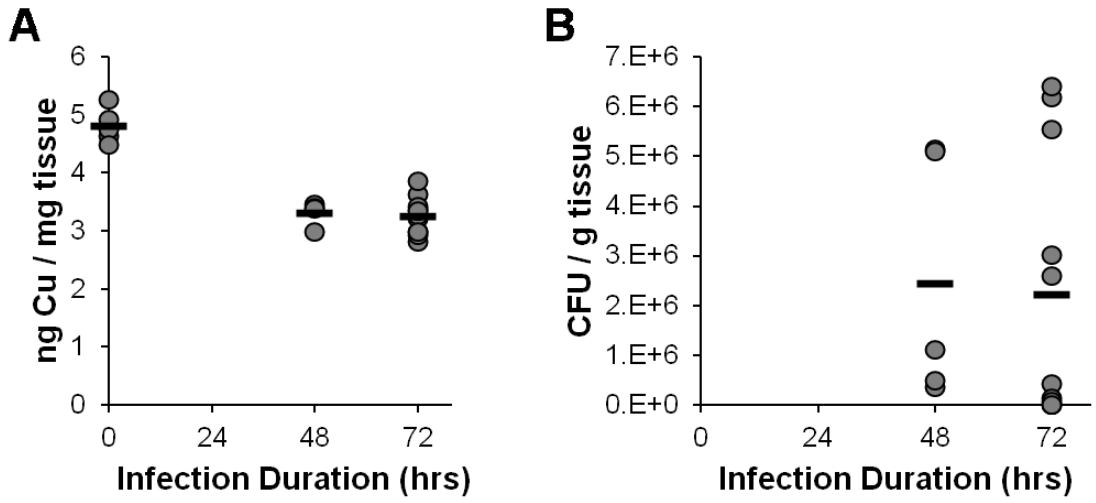

Figure I-3: Representative images of elemental distribution in uninfected kidneys. Kidneys were cryosectioned and subjected to XRF analysis as described in *Experimental Procedures*. Shown here is a representative result from a sagittal section of a control kidney. The rainbow bar at the bottom shows the colors relating to element concentration, with black being the minimum and red the maximum. The eight elements shown (left to right, top to bottom) are phosphorus (P), sulfur (S), chlorine (Cl), calcium (Ca), manganese (Mn), iron (Fe), copper (Cu), and zinc (Zn).

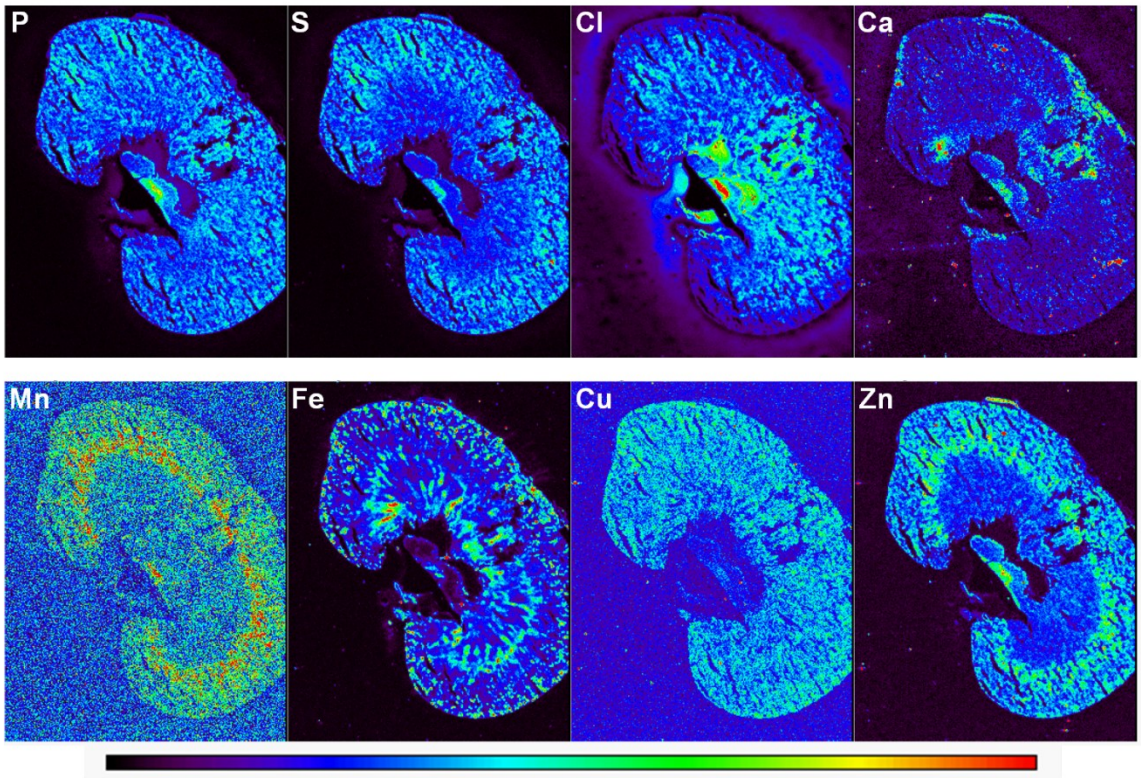

Figure I-4: Representative images of elemental distribution in infected kidneys. Data was generated by XRF as in Fig. I-3. Shown here is a representative result from a sagittal section of a 72 hour infected kidney. The rainbow bar at the bottom shows the colors relating to element concentration, with black being the minimum and red the maximum. The eight elements shown (left to right, top to bottom) are phosphorus (P), sulfur (S), chlorine (Cl), calcium (Ca), manganese (Mn), iron (Fe), copper (Cu), and zinc (Zn).

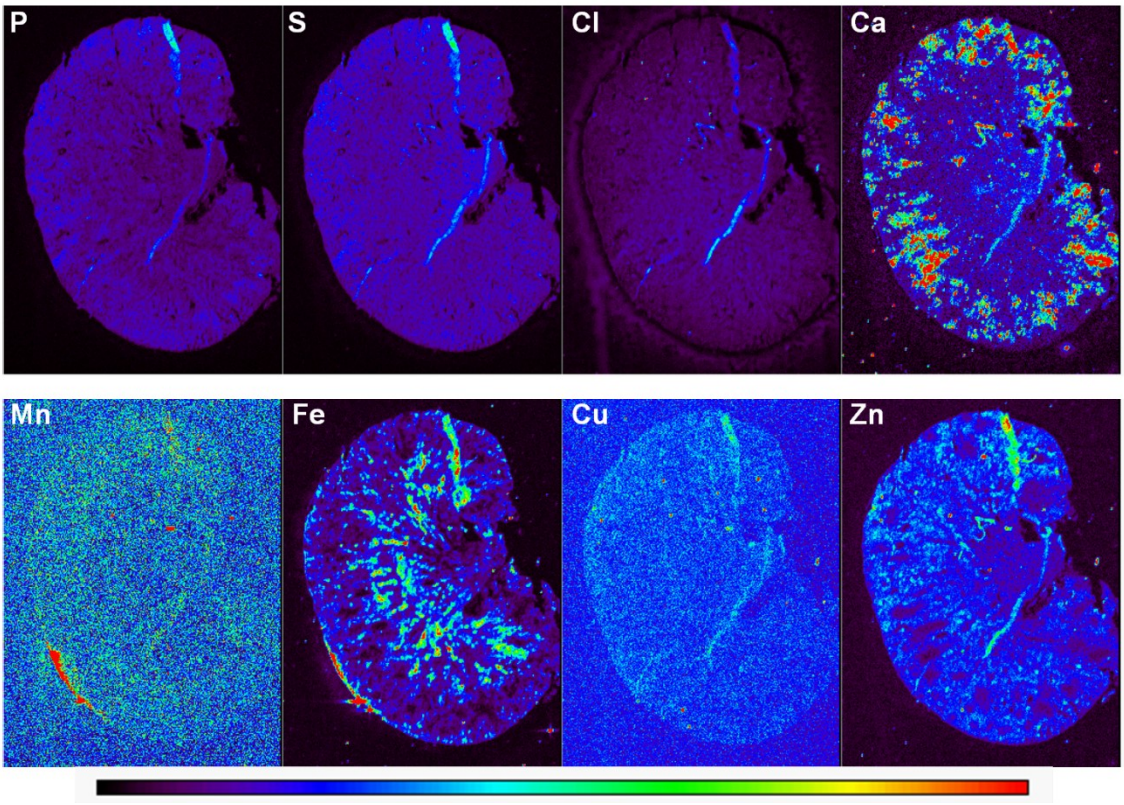

Figure I-5: Kidney localization of calcium and zinc during *C. albicans* infection. Results were generated by XRF as in Fig. I-3. Three sagittal and two transverse kidney images from control (A) and infected mice (B) are shown. Distribution of calcium (A top, B top) can be compared to that of zinc (A bottom, B bottom) within the same tissue samples.

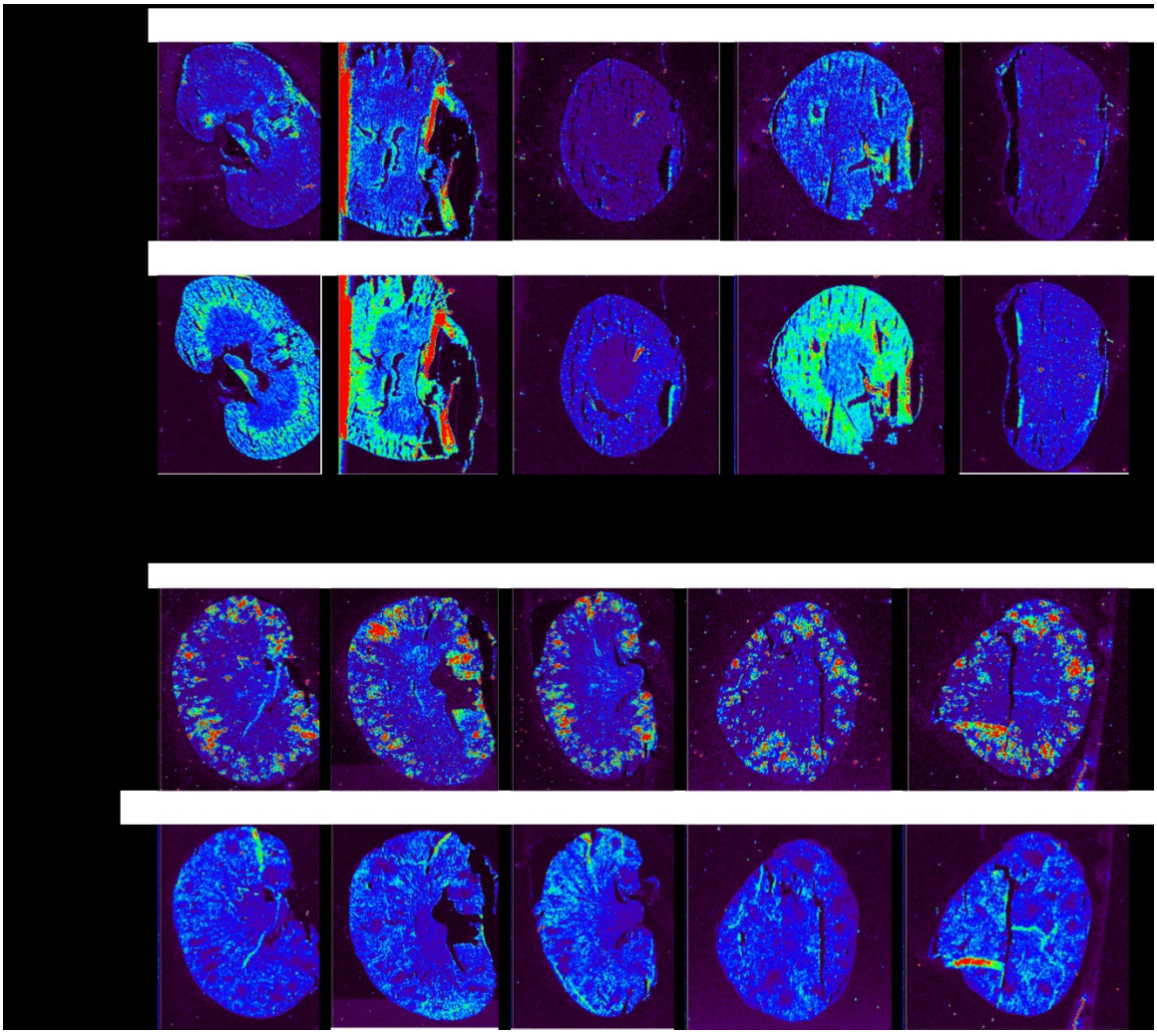

Figure I-6: Co-localization of calcium and zinc during *C. albicans* infection.

Selected images from Fig. I-5B were enlarged to show that calcium hot spots correspond to locations of zinc holes.

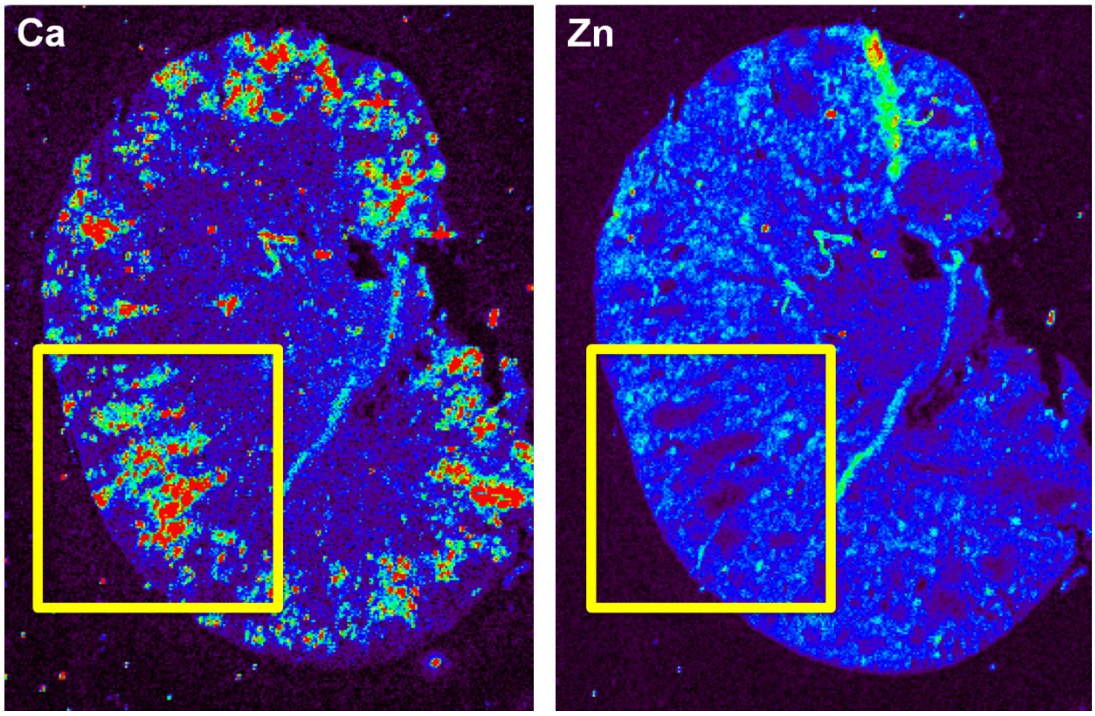

Figure I-7: Kidney localization of iron during *C. albicans* infection.

Results were generated by XRF as in Fig. I-3. Sagittal and transverse kidney images from control (top) and infected mice (bottom) are shown for iron. These tissue sections are the same samples as the first four shown in each group from Fig. I-5A,B.

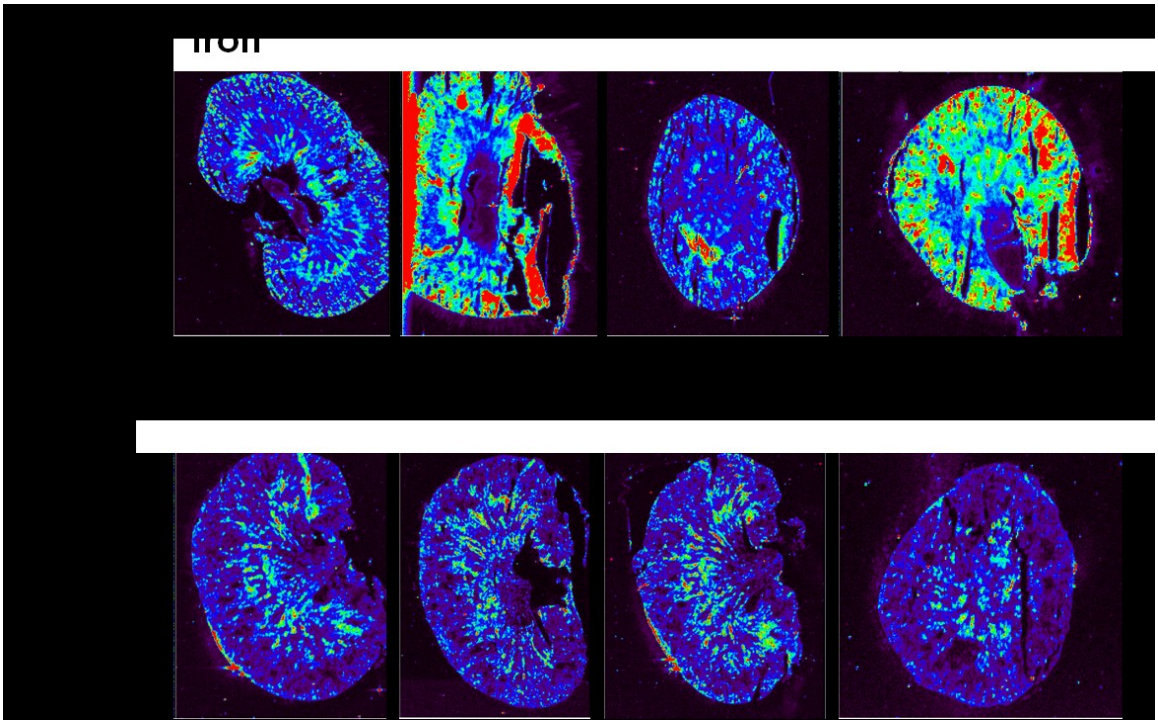

Figure I-8: Kidney localization of manganese during *C. albicans* infection.

Results were generated by XRF as in Fig. I-3. Sagittal and transverse kidney images from control (top) and infected mice (bottom) are shown for manganese. These tissue sections are the same samples as the first four shown in each group from Fig. I-5A,B.

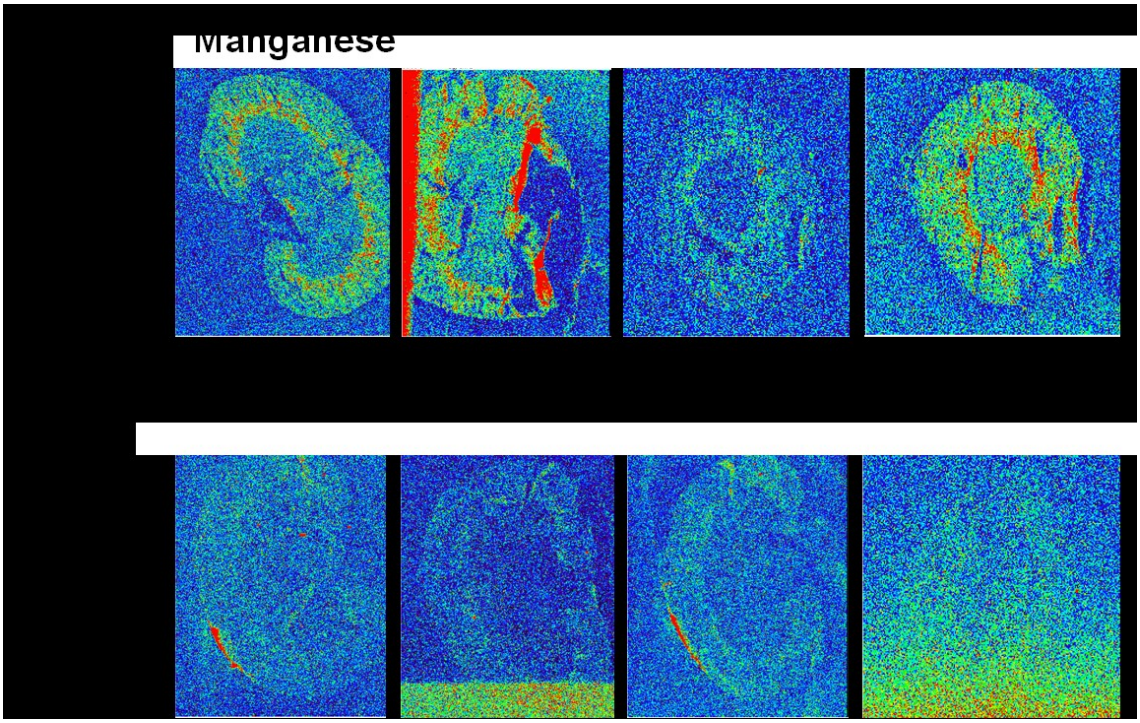

Figure I-9: Kidney localization of copper during *C. albicans* infection.

Results were generated by XRF as in Fig. I-3. Sagittal and transverse kidney images from control (top) and infected mice (bottom) are shown for copper. These tissue sections are the same samples as the first four shown in each group from Fig. I-5A,B.

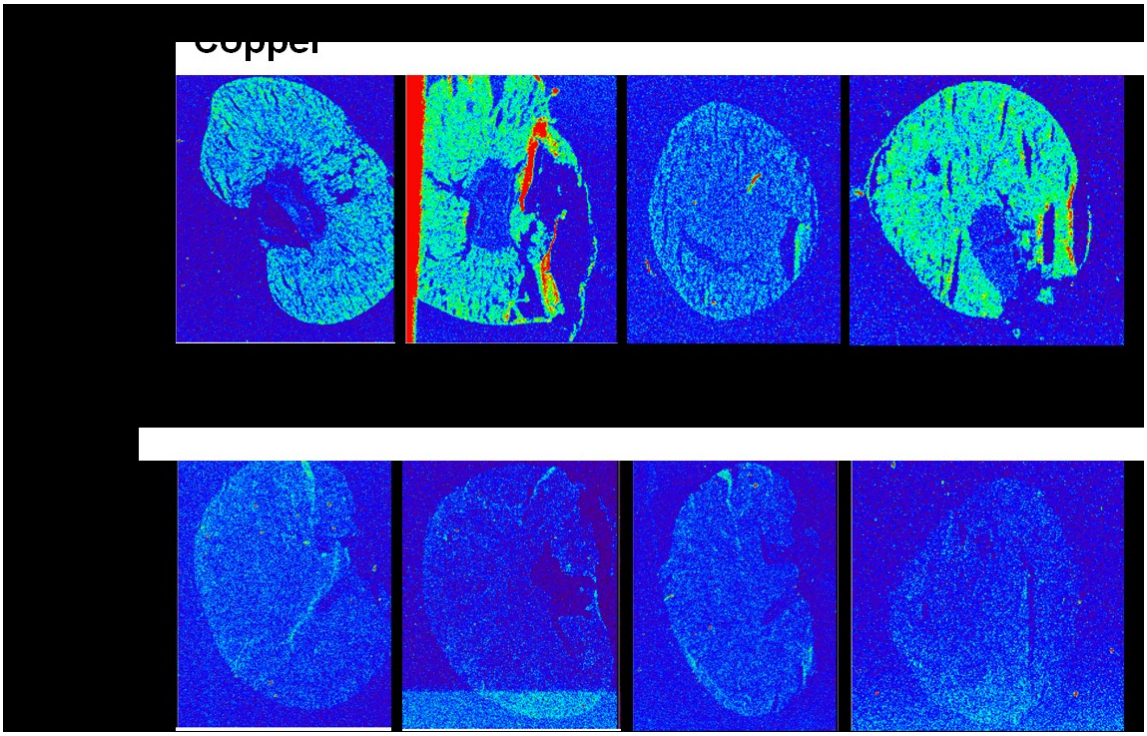

APPENDIX II

The fluorescent probe CNIR4 is an effective sensor for cellular copper in *C. albicans*

Introduction

Copper is an essential nutrient, but too much or too little can cause harm to an organism. Disruption of copper homeostasis has been implicated in a wide array of diseases [297-302]. Copper has also shown to be important in fighting off pathogens, such as during the toxic bombardment of microbes by copper in the macrophage phagolysosome [169-171]. In Chapter 3 of this thesis, we demonstrated that copper withholding may also be a method used to fight *C. albicans* infection in the kidney. Given the biological importance of copper, methods for studying copper trafficking and accumulation are surprisingly limited. Several of the currently available techniques were discussed in Appendix I, including AAS and ICP-MS which are both unable to provide spatial information within a sample. XRF is a very powerful technique that can map elemental localization at high resolution, but its use is extremely limited to a few facilities around the world. Laser ablation ICP-MS is more readily available than XRF, but many labs do not have access to such instrumentation. Thus, another technique for copper detection is needed, one that is widely available and easy to use.

To this end, Christopher Chang's lab at University of California, Berkeley, has developed a series of small molecule fluorescent probes to detect copper. Their first published probe was Coppersensor-1 (CS1), a boron dipyrromethene (BODIPY) based sensor that binds to Cu(I) at high affinity (K_d= $4x10^{-12}$ M), resulting in a 10x increase in fluorescence emission [303,304]. This probe may be used to detect localization and relative levels of copper in live cells. Various investigators have successfully used this probe to study copper in human HEK293T cells [304], bacteria [305], *S. cerevisiae* [306,307], *S. pombe* [308], and plants [309]. However, use of CS1 in other mammalian

cell lines such as M17, U87MG, SH-SY5Y, and CHO have failed; the probe fluorescence was not responsive to altered cellular copper levels, illustrating that the CS1 probe is not universally effective [310,311].

As described in Chapter 1, several studies have shown that copper is transported into the macrophage phagolysosome to kill microbes such as *E. coli*, *Salmonella*, and *M. tuberculosis* [79,169,171,258]. These studies have reported the translocation of the Atp7A copper pump to the phagosomal membrane [171], and detected high copper in macrophage compartments during infection [169,170] using XRF or CS1 labeling of macrophages. In the case of *C. albicans*, strains lacking the copper exporter Crp1 and the metallothionein Cup1 are less virulent in macrophage infection, suggesting that these cells are exposed to high copper levels in the phagolysosome [182]. However, the accumulation of high copper inside the pathogen has never been directly measured for any microbe that invades a macrophage. Is macrophage copper actually taken up by the pathogen? We would like to be able to measure copper in *C. albicans* cells during macrophage infection, and to this end we analyzed the efficacy of two distinct fluorescent probes for monitoring intracellular copper in *C. albicans*.

Experimental Procedures

Copper probe staining of C. albicans cells in yeast-only cultures

This study uses *C. albicans* wild type strain CA-IF100 and was cultured in YPD at 30°C as described in Chapter 3. *C. albicans* cells were grown to log phase, then resuspended in 500 µL of sterile PBS and transferred into a dark microcentrifuge tube. A

2 mM stock solution of CS1 or CNIR4 copper probe was prepared in DMSO. 1 µL of the stock was added to each sample, for a final concentration of 4 µM. The samples were incubated at 37°C for 30 minutes, shaking in the dark. The cells were then washed twice with sterile PBS and resuspended in 500 µL of sterile PBS. 5 µL of the stained cells was placed on a slide with 5 µL of mounting solution with DAPI (Sigma) and sealed with a coverslip. The remaining cells in the samples were used for copper quantification by atomic absorption spectroscopy as described in Chapter 3. CS1 has maximum absorption at 540 nm, and emission at 550-650 nm [304]. CNIR4 has maximum absorption at 672 nm, and emission at 651-750 nm.

Macrophage growth conditions and infection assay

J774A.1 mouse macrophage cell line (ATCC) was grown in T-25 flasks with DMEM media supplemented with 10% fetal bovine serum and 1% penicillin-streptomycin at 37°C. For the infection assay, coverslips were flame sterilized and placed in 6-well plates before $1x10^5$ macrophages were added to each well. Macrophages were grown for 1 day to ~$4x10^5$ cells per well, then treated with 1 ng/mL IFNγ for 1 day to prime cells to elicit a copper burst response through activation of Atp7A [170,171]. $4x10^5$ *C. albicans* cells grown to log phase in YPD medium and loaded with CNIR4 probe (as described above) were added to each well, at a multiplicity of infection (MOI) of 1:1. Control samples contained the same number of *C. albicans* added to cell culture media without macrophages. Cells were incubated at 37°C in the dark to prevent photobleaching. Cover slips with cells were collected and mounted onto slides for microscopy every hour up to 6 hours. Cells were visualized by microscopy on a Zeiss

Axio Observer.Z1 inverted microscope, using DIC to image cells, the Cy5 filter to detect CNIR4 fluorescence, and the GFP filter to detect CS1 fluorescence. Images were captured at 64x magnification and processed using the AxioVision Software.

Results and Discussion

Our initial studies focused on the widely published Cu(I) probe CS1 [303,304]. We sought to verify CS1 probe's sensitivity to copper levels in *C. albicans*. CS1 was taken up by the yeast and was seen to accumulate in dot-like structures (Fig. II-1A). However, CS1 did not respond to increased or decreased copper within cells, even when copper was elevated by $CuSO_4$ supplementation or depleted by BCS treatment (Fig. II-1A). We also observed that CS1 preferentially labeled a few small compartments within the cell (Fig. II-1A) that are very similar to what has previously been published as lipid droplets [312]. Knowing that CS1 is based on the BODIPY dye, which is frequently used to detect lipid droplets [313,314], we compared the staining patterns of these two dyes. We found that CS1 exhibited a similar staining pattern to BODIPY alone (Fig. II-1B). These results, from former rotation student Fengrong Wang, indicate that CS1 is unresponsive to copper levels and appears to associate with lipid droplets in *C. albicans* cells. This is not the first time that CS1 has been found to be ineffective, as this probe was unresponsive to copper levels and predominantly localized to lysosomes in mammalian cell lines M17, U87MG, SH-SY5Y, and CHO [310,311]. These findings, together with our results in *C. albicans*, emphasize that CS1 should be used with caution,

and researchers are now seeking to avoid these problems by synthesizing probes that are more water soluble [315,316].

Here, we demonstrate that a completely different copper probe by the Chang lab, CNIR4, is effective at detecting copper within yeast cells. The structure of CNIR4 is not yet published, but it is a silicon-rhodamine derivative (Fig. II-2A) with high affinity and selectivity for Cu(I) ($K_d \approx 10^{-13}$ M). Unlike results with CS1, CNIR4 fluorescence increases as copper is titrated into the growth media of the *C. albicans*, along with increased intracellular copper levels measured by atomic absorption spectroscopy (Fig. II-2B). When the copper chelator BCS was added to the media, CNIR4 fluorescence decreased, in agreement with intracellular copper levels (Fig. II-2C). This copper probe is indeed responsive to copper levels within *C. albicans*.

CNIR4 exhibits an interesting localization within *C. albicans.* The staining appears puncate and tubular, perhaps perinuclear and excluded from the vacuole (Fig. II-3 top). Previously, rhodamine-based probes have been used to identify mitochondria [317], but the staining of CNIR4 cannot be exclusively mitochondrial. As seen in Fig. 3, mitochondrial staining by mitoSOX is punctate, but does not exhibit the tubular and possible perinuclear staining of copper by CNIR4.

We used this new copper probe to examine copper within *C. albicans* cells during a macrophage infection assay. *C. albicans* cells were pre-stained with CNIR4 before co-incubation with J774A.1 macrophages or in cell culture medium alone. In growth medium alone (no macrophages), budding *C. albicans* transitioned to pseudohypae within 1-2 hours and then true hyphae within 5-6 hours (Fig. II-4A top) as would be expected by incubating these cells at 37ºC and in the presence of serum. Curiously, copper staining

by CNIR4 diminished over time with these cells. This should not reflect photobleaching because CNIR4 is resistant to photobleaching up to 12 hours or more (Chang, personal communications). Instead, the loss of fluorescence in non-engulfed *C. albicans* cells over time seems to indicate that the cells are gradually depleted of copper as they grow in the cell culture media, similar to what we see with cells grown in yeast growth medium (Chapter 3, Fig. 3-3A). The copper in DMEM cell culture medium is coming from serum, and as described in Chapter 3, 90% of this copper is tightly bound to ceruloplasmin and may not be available to the yeast.

A quite different pattern of CNIR4 staining is seen during fungal invasion of macrophages (Fig. II-4 bottom). The results show that CNIR4 fluorescence levels in the yeast remain high even after six hours of macrophage engulfment, whereas yeast incubated in the macrophage cell culture media alone lost fluorescence (Fig. II-3A). As seen in the enlarged image, only the yeast cells engulfed by macrophages retained copper probe fluorescence (Fig. II-3B), not yeast cells in the vicinity of macrophages, indicating that the engulfed cells are exposed to high copper inside the macrophage phagolysosome.

C. albicans cells engulfed by macrophages also show a gradual loss of probe fluorescence, although much less so than yeast cells alone (Fig. II-3A top). This may be due to *C. albicans* cells adapting to the high copper environment by using the cell surface ATPase Crp1 to pump copper out of the cell [182].

These results are consistent with indirect studies suggesting that macrophages pump copper into the phagolysosome [169,171], and with direct detection of copper in macrophage phagosomal compartments during infection [170]. More importantly, our results use direct measurements to provide evidence that engulfed pathogens accumulate

high copper within the phagolysosome environment, further validating the idea that the pathogens are exposed to high copper levels in macrophages.

While these studies clearly show an increase in copper accumulation within *C. albicans* during macrophage invasion, it is not fully clear where this copper is coming from. As a likely possibility, other researchers have demonstrated that the copper transporter Atp7A relocalizes to the macrophage phagolysosome during infection with *E. coli* and is presumed to account for the copper burst of the macrophage [171]. In future studies, we can use our infection assay to directly test whether the copper acquired by the fungal cells is indeed transported by Atp7a. To this end, we will use bone marrow-derived macrophages extracted from *ATP7a* macrophage-specific knock-out mice, provided by Dr. Petris. Deletion of *ATP7a* in these macrophages should deplete copper levels in the phagolysosome, and we expect that to be reflected in diminished copper accumulation by engulfed yeast cells, as monitored by CNIR4 staining.

Figure II-1: CS1 does not respond to copper levels in *C. albicans* and localizes to lipid droplets.

(A) *C. albicans* cells were grown to log phase in the presence of 500 µM BCS or 4 mM $CuSO_4$ as indicated. Cells were stained with CS1 and microscopy performed as described in *Experimental Procedures*. CS1 fluorescence levels did not fluctuate with copper treatment or depletion. **(B)** Cells were grown to log phase and stained with either CS1 or BODIPY, as indicated, then subjected to microscopy as described in *Experimental Procedures*. The two dyes stained identical lipid droplet-like structures. The chemical structures of CS1 and BODIPY are shown. Figure provided by former rotation student Fengrong Wang.

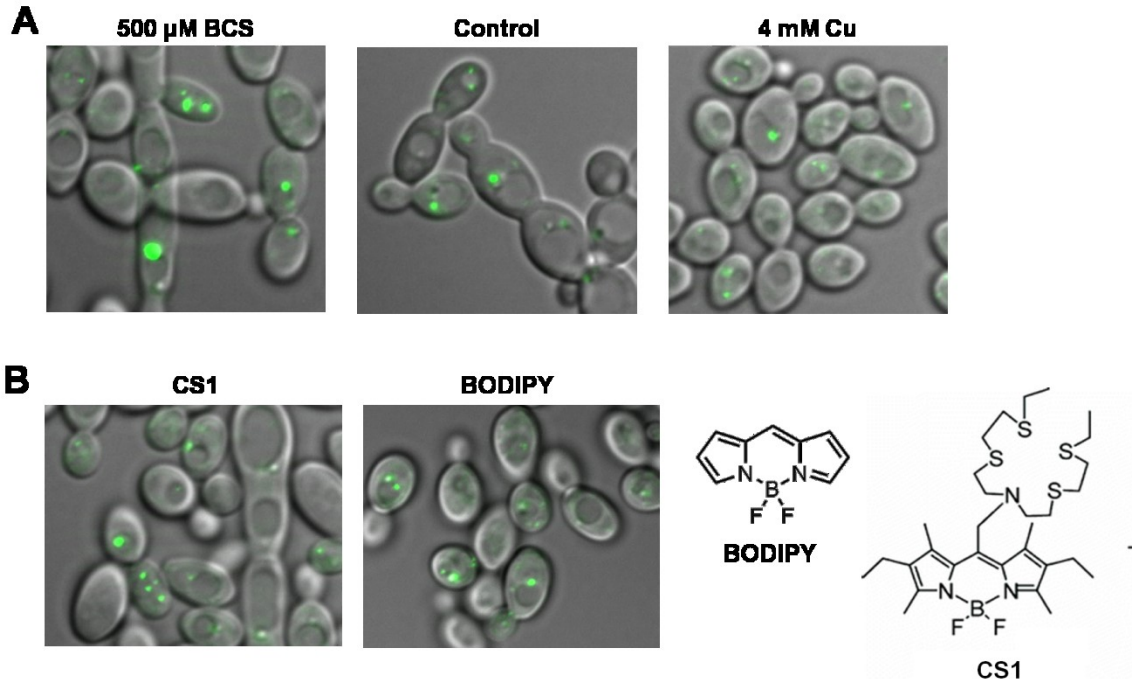

Figure II-2: The CNIR4 copper probe is responsive to changes in intracellular copper levels.

(A) The structure of CNIR4 is shown. Cells were grown to log phase in media containing the indicated amounts of $CuSO_4$ (B) or the copper chelator BCS (C). The cells were stained with CNIR4 and imaged by fluorescence microscopy as described in *Experimental Procedures*. The remaining cells were analyzed for copper content by atomic absorption spectroscopy. Results from A and B represent independent experiments.

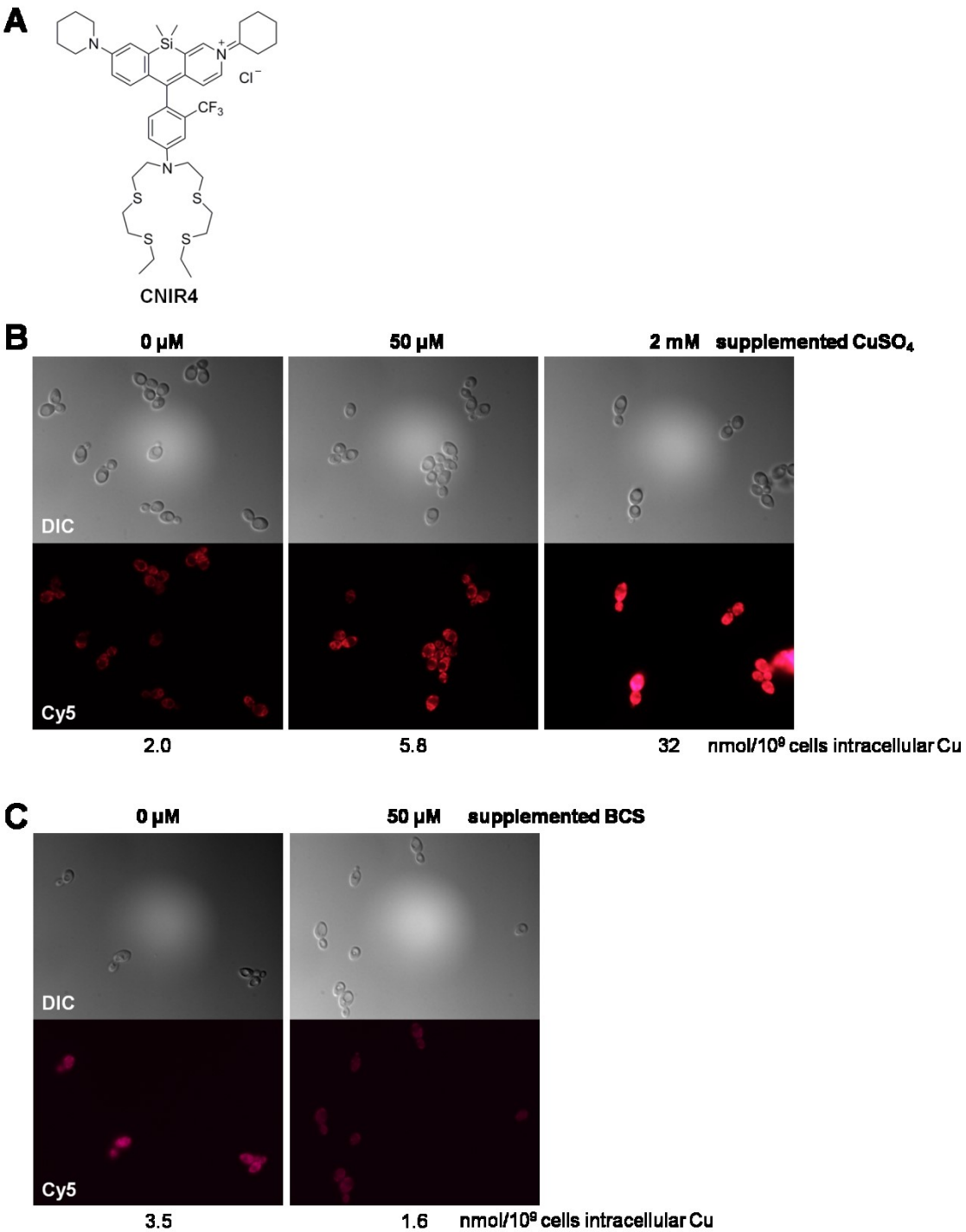
A
CNIR4
B
0 μM
50 μM
2 mM supplemented CuSO4
DIC
Cy5
2.0
5.8
32 nmol/10^9 cells intracellular Cu
C
0 μM
50 μM supplemented BCS
DIC
Cy5
3.5
1.6 nmol/10^9 cells intracellular Cu

Figure II-3: CINR4 versus mitochondrial staining.

Shown is an enlarged image of CINR4 staining from Fig. II-2B compared to mitochondrial staining of *C. albicans* cells using MitoSOX. MitoSOX image was kindly provided by Chynna Broxton.

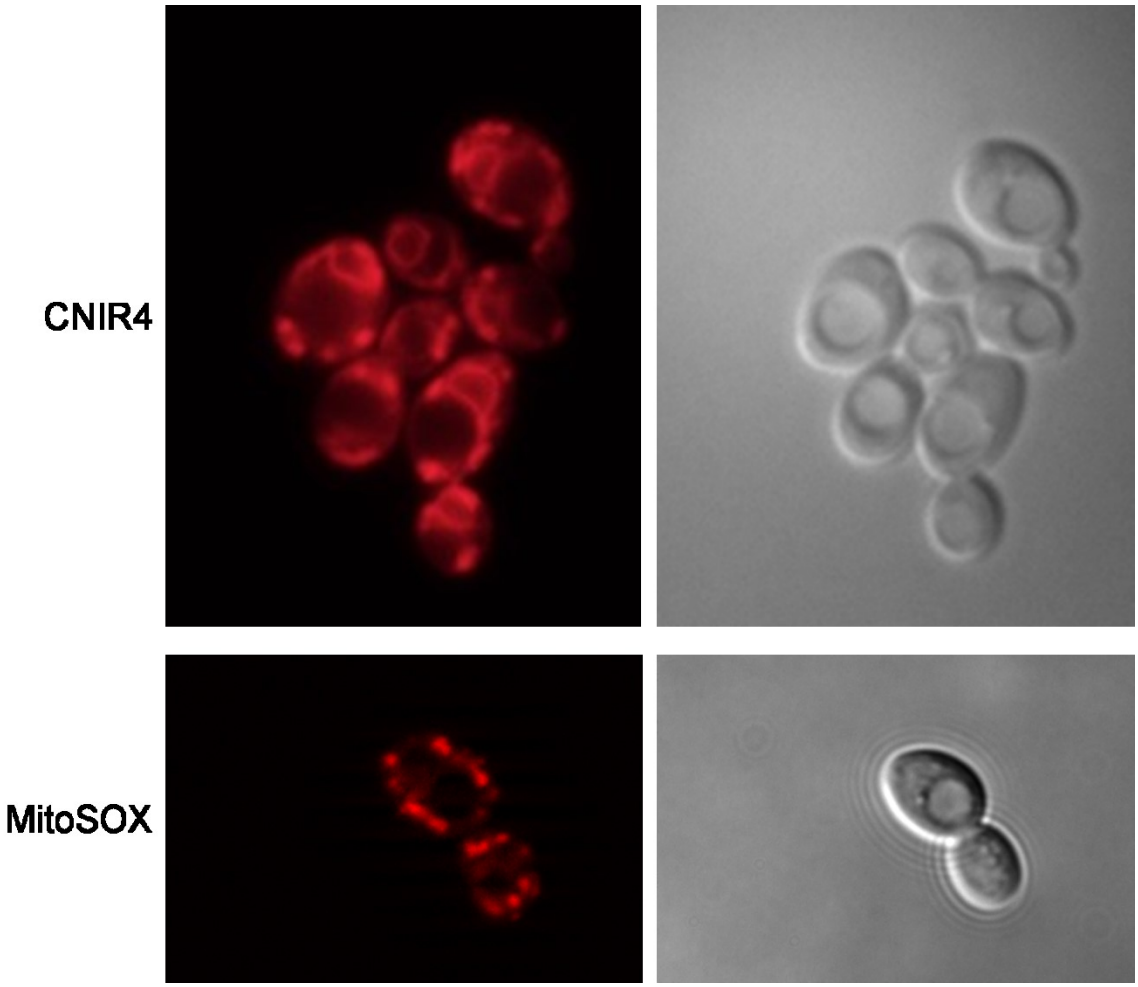

Figure II-4: Copper during macrophage infection.

C. albicans cells were grown to log phase and stained with CNIR4 as in Fig. II-2. The copper probe-loaded cells were incubated in DMEM cell culture medium alone (A top) or with J774A.1 macrophages at an MOI of 1:1 (A bottom), and visualized every hour for 6 hours. CNIR4 fluorescence levels over time are shown in (A). **(B)** DIC and Cy5 images from the 4 hour time point of macrophage infection were overlaid to show yeast cells engulfed within macrophages, yeast alone, and macrophages alone.

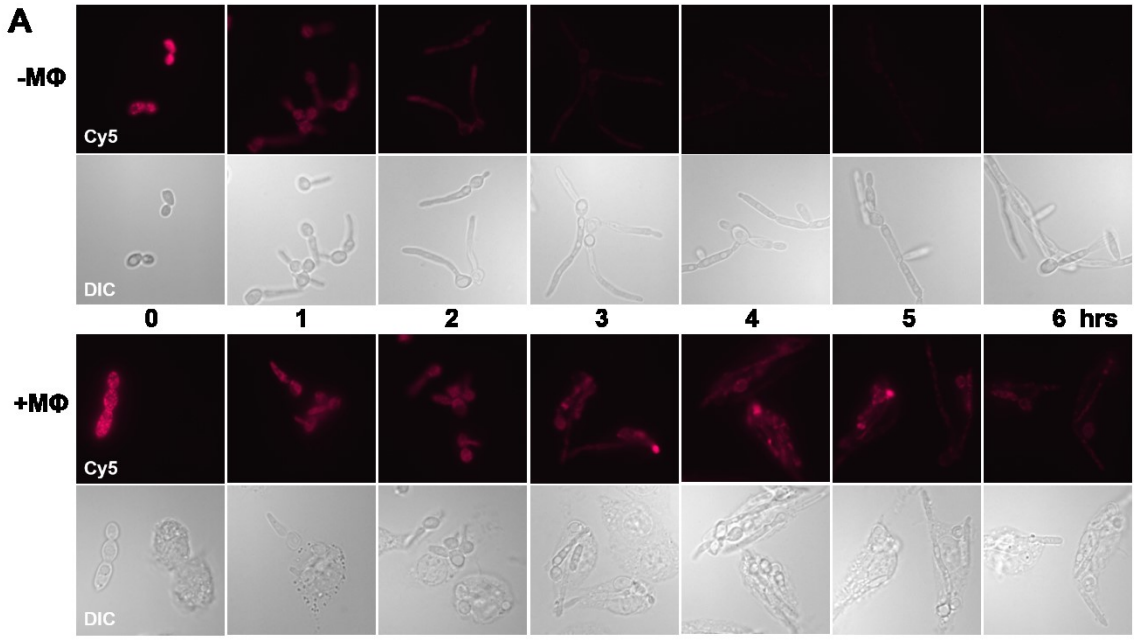

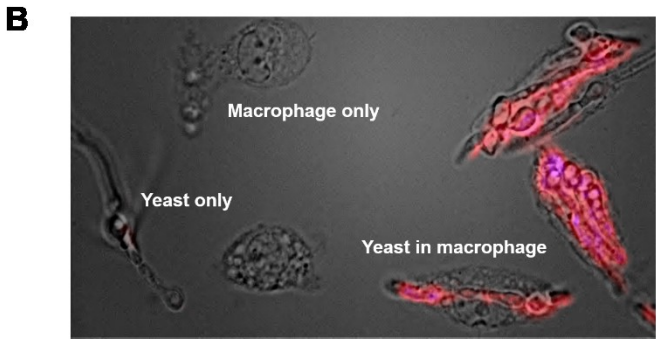

Bibliography

1. McCord JM, Fridovich I (1969) Superoxide dismutase. An enzymic function for erythrocuprein (hemocuprein). J Biol Chem 244: 6049-6055.
2. Fielden EM, Roberts PB, Bray RC, Lowe DJ, Mautner GN, et al. (1974) Mechanism of action of superoxide dismutase from pulse radiolysis and electron paramagnetic resonance. Evidence that only half the active sites function in catalysis. Biochem J 139: 49-60.
3. Forman HJ, Fridovich I (1973) Superoxide dismutase: a comparison of rate constants. Arch Biochem Biophys 158: 396-400.
4. Sheng Y, Stich TA, Barnese K, Gralla EB, Cascio D, et al. (2011) Comparison of two yeast MnSODs: mitochondrial Saccharomyces cerevisiae versus cytosolic Candida albicans. J Am Chem Soc 133: 20878-20889.
5. Miller AF (2012) Superoxide dismutases: ancient enzymes and new insights. FEBS Lett 586: 585-595.
6. Dupont CL, Butcher A, Valas RE, Bourne PE, Caetano-Anollés G (2010) History of biological metal utilization inferred through phylogenomic analysis of protein structures. Proceedings of the National Academy of Sciences 107: 10567-10572.
7. Dupont CL, Yang S, Palenik B, Bourne PE (2006) Modern proteomes contain putative imprints of ancient shifts in trace metal geochemistry. Proceedings of the National Academy of Sciences 103: 17822-17827.
8. Imlay JA (2013) The molecular mechanisms and physiological consequences of oxidative stress: lessons from a model bacterium. Nat Rev Micro 11: 443-454.

9. Imlay JA (2014) The Mismetallation of Enzymes during Oxidative Stress. Journal of Biological Chemistry 289: 28121-28128.

10. Flint DH, Tuminello JF, Emptage MH (1993) The inactivation of Fe-S cluster containing hydro-lyases by superoxide. J Biol Chem 268: 22369-22376.

11. Gardner PR, Fridovich I (1991) Superoxide sensitivity of the Escherichia coli 6-phosphogluconate dehydratase. J Biol Chem 266: 1478-1483.

12. Gardner PR, Fridovich I (1991) Superoxide sensitivity of the Escherichia coli aconitase. J Biol Chem 266: 19328-19333.

13. Liochev SI, Fridovich I (1992) Fumarase C, the stable fumarase of Escherichia coli, is controlled by the soxRS regulon. Proc Natl Acad Sci U S A 89: 5892-5896.

14. Takamatsu J, Takeshige K, Takahashi S, Yoshitake J, Minakami S (1986) NADPH-dependent superoxide-forming oxidase in phagocytic vesicles of human monocytes. J Biochem 99: 1597-1604.

15. Wallace MA, Liou LL, Martins J, Clement MH, Bailey S, et al. (2004) Superoxide inhibits 4Fe-4S cluster enzymes involved in amino acid biosynthesis. Cross-compartment protection by CuZn-superoxide dismutase. J Biol Chem 279: 32055-32062.

16. Gu M, Imlay JA (2013) Superoxide poisons mononuclear iron enzymes by causing mismetallation. Mol Microbiol 89: 123-134.

17. Poole LB, Karplus PA, Claiborne A (2004) Protein sulfenic acids in redox signaling. Annu Rev Pharmacol Toxicol 44: 325-347.

18. Winterbourn CC, Metodiewa D (1999) Reactivity of biologically important thiol compounds with superoxide and hydrogen peroxide. Free Radic Biol Med 27: 322-328.

19. Marinho HS, Real C, Cyrne L, Soares H, Antunes F (2014) Hydrogen peroxide sensing, signaling and regulation of transcription factors. Redox Biol 2: 535-562.

20. Owusu-Ansah E, Banerjee U (2009) Reactive oxygen species prime Drosophila haematopoietic progenitors for differentiation. Nature 461: 537-541.

21. Reddi AR, Culotta VC (2013) SOD1 integrates signals from oxygen and glucose to repress respiration. Cell 152: 224-235.

22. Sena LA, Chandel NS (2012) Physiological roles of mitochondrial reactive oxygen species. Mol Cell 48: 158-167.

23. Tormos KV, Anso E, Hamanaka RB, Eisenbart J, Joseph J, et al. (2011) Mitochondrial complex III ROS regulate adipocyte differentiation. Cell Metab 14: 537-544.

24. Zhang J, Khvorostov I, Hong JS, Oktay Y, Vergnes L, et al. (2011) UCP2 regulates energy metabolism and differentiation potential of human pluripotent stem cells. 4860-4873 p.

25. Repine JE, Fox RB, Berger EM (1981) Hydrogen peroxide kills Staphylococcus aureus by reacting with staphylococcal iron to form hydroxyl radical. J Biol Chem 256: 7094-7096.

26. Sandmann G, Boger P (1980) Copper-mediated Lipid Peroxidation Processes in Photosynthetic Membranes. Plant Physiol 66: 797-800.

27. Gutteridge JMC (1984) Lipid peroxidation initiated by superoxide-dependent hydroxyl radicals using complexed iron and hydrogen peroxide. FEBS Letters 172: 245-249.

28. Kim K, Kim IH, Lee KY, Rhee SG, Stadtman ER (1988) The isolation and purification of a specific "protector" protein which inhibits enzyme inactivation by a thiol/Fe(III)/O2 mixed-function oxidation system. J Biol Chem 263: 4704-4711.

29. May DW (1901) Catalase, a New Enzym of General Occurrence. Science 14: 815-816.

30. Mills GC (1957) HEMOGLOBIN CATABOLISM: I. GLUTATHIONE PEROXIDASE, AN ERYTHROCYTE ENZYME WHICH PROTECTS HEMOGLOBIN FROM OXIDATIVE BREAKDOWN. Journal of Biological Chemistry 229: 189-197.

31. Costa VM, Amorim MA, Quintanilha A, Moradas-Ferreira P (2002) Hydrogen peroxide-induced carbonylation of key metabolic enzymes in Saccharomyces cerevisiae: the involvement of the oxidative stress response regulators Yap1 and Skn7. Free Radic Biol Med 33: 1507-1515.

32. Das N, Levine RL, Orr WC, Sohal RS (2001) Selectivity of protein oxidative damage during aging in Drosophila melanogaster. Biochem J 360: 209-216.

33. Di Monte D, Bellomo G, Thor H, Nicotera P, Orrenius S (1984) Menadione-induced cytotoxicity is associated with protein thiol oxidation and alteration in intracellular Ca2+ homeostasis. Arch Biochem Biophys 235: 343-350.

34. Witkiewicz-Kucharczyk A, Bal W (2006) Damage of zinc fingers in DNA repair proteins, a novel molecular mechanism in carcinogenesis. Toxicol Lett 162: 29-42.

35. Coleman JB, Gilfor D, Farber JL (1989) Dissociation of the accumulation of single-strand breaks in DNA from the killing of cultured hepatocytes by an oxidative stress. Mol Pharmacol 36: 193-200.

36. Jovanovic SV, Simic MG (1989) The DNA guanyl radical: kinetics and mechanisms of generation and repair. Biochim Biophys Acta 1008: 39-44.

37. Mouzannar R, Miric SJ, Wiggins RC, Konat GW (2001) Hydrogen peroxide induces rapid digestion of oligodendrocyte chromatin into high molecular weight fragments. Neurochem Int 38: 9-15.

38. Sohal RS, Allen RG (1990) Oxidative stress as a causal factor in differentiation and aging: a unifying hypothesis. Exp Gerontol 25: 499-522.

39. Bragt PC, Bonta IL (1980) Oxidant stress during inflammation: anti-inflammatory effects of antioxidants. Agents Actions 10: 536-539.

40. Simic MG (1994) DNA markers of oxidative processes in vivo: relevance to carcinogenesis and anticarcinogenesis. Cancer Res 54: 1918s-1923s.

41. Trush MA, Kensler TW (1991) An overview of the relationship between oxidative stress and chemical carcinogenesis. Free Radical Biology and Medicine 10: 201-209.

42. Tsukamoto H, Rippe R, Niemela O, Lin M (1995) Roles of oxidative stress in activation of Kupffer and Ito cells in liver fibrogenesis. J Gastroenterol Hepatol 10 Suppl 1: S50-53.

43. Hybertson BM, Gao B, Bose SK, McCord JM (2011) Oxidative stress in health and disease: the therapeutic potential of Nrf2 activation. Mol Aspects Med 32: 234-246.

44. Youn HD, Kim EJ, Roe JH, Hah YC, Kang SO (1996) A novel nickel-containing superoxide dismutase from Streptomyces spp. Biochem J 318 (Pt 3): 889-896.

45. Wuerges J, Lee JW, Yim YI, Yim HS, Kang SO, et al. (2004) Crystal structure of nickel-containing superoxide dismutase reveals another type of active site. Proc Natl Acad Sci U S A 101: 8569-8574.

46. Hart PJ, Balbirnie MM, Ogihara NL, Nersissian AM, Weiss MS, et al. (1999) A structure-based mechanism for copper-zinc superoxide dismutase. Biochemistry 38: 2167-2178.

47. Borders CL, Fridovich I (1985) A comparison of the effects of cyanide, hydrogen peroxide, and phenylglyoxal on eucaryotic and procaryotic Cu,Zn superoxide dismutases. Archives of Biochemistry and Biophysics 241: 472-476.

48. Antonyuk SV, Strange RW, Marklund SL, Hasnain SS (2009) The structure of human extracellular copper-zinc superoxide dismutase at 1.7 A resolution: insights into heparin and collagen binding. J Mol Biol 388: 310-326.

49. Marklund SL (1982) Human copper-containing superoxide dismutase of high molecular weight. Proc Natl Acad Sci U S A 79: 7634-7638.

50. Sturtz LA, Diekert K, Jensen LT, Lill R, Culotta VC (2001) A fraction of yeast Cu,Zn-superoxide dismutase and its metallochaperone, CCS, localize to the intermembrane space of mitochondria. A physiological role for SOD1 in guarding against mitochondrial oxidative damage. J Biol Chem 276: 38084-38089.

51. Culotta VC, Klomp LW, Strain J, Casareno RL, Krems B, et al. (1997) The copper chaperone for superoxide dismutase. J Biol Chem 272: 23469-23472.

52. Furukawa Y, Torres AS, O'Halloran TV (2004) Oxygen-induced maturation of SOD1: a key role for disulfide formation by the copper chaperone CCS. EMBO J 23: 2872-2881.

53. Rae TD, Torres AS, Pufahl RA, O'Halloran TV (2001) Mechanism of Cu,Zn-superoxide dismutase activation by the human metallochaperone hCCS. J Biol Chem 276: 5166-5176.

54. Beckman JS, Esetvez AG, Barbeito L, Crow JP (2002) CCS knockout mice establish an alternative source of copper for SOD in ALS. Free Radic Biol Med 33: 1433-1435.

55. Carroll MC, Girouard JB, Ulloa JL, Subramaniam JR, Wong PC, et al. (2004) Mechanisms for activating Cu- and Zn-containing superoxide dismutase in the absence of the CCS Cu chaperone. Proc Natl Acad Sci U S A 101: 5964-5969.

56. Jensen LT, Culotta VC (2005) Activation of CuZn superoxide dismutases from Caenorhabditis elegans does not require the copper chaperone CCS. J Biol Chem 280: 41373-41379.

57. Leitch JM, Yick PJ, Culotta VC (2009) The right to choose: multiple pathways for activating copper,zinc superoxide dismutase. J Biol Chem 284: 24679-24683.

58. Ciriolo MR, Desideri A, Paci M, Rotilio G (1990) Reconstitution of Cu,Zn-superoxide dismutase by the Cu(I).glutathione complex. Journal of Biological Chemistry 265: 11030-11034.

59. Leitch JM, Jensen LT, Bouldin SD, Outten CE, Hart PJ, et al. (2009) Activation of Cu,Zn-superoxide dismutase in the absence of oxygen and the copper chaperone CCS. J Biol Chem 284: 21863-21871.

60. Becuwe P, Gratepanche S, Fourmaux MN, Van Beeumen J, Samyn B, et al. (1996) Characterization of iron-dependent endogenous superoxide dismutase of Plasmodium falciparum. Mol Biochem Parasitol 76: 125-134.

61. Dos Santos WG, Pacheco I, Liu MY, Teixeira M, Xavier AV, et al. (2000) Purification and characterization of an iron superoxide dismutase and a catalase from the sulfate-reducing bacterium Desulfovibrio gigas. J Bacteriol 182: 796-804.
62. Van Camp W, Bowler C, Villarroel R, Tsang EW, Van Montagu M, et al. (1990) Characterization of iron superoxide dismutase cDNAs from plants obtained by genetic complementation in Escherichia coli. Proc Natl Acad Sci U S A 87: 9903-9907.
63. del Rio LA, Sandalio LM, Altomare DA, Zilinskas BA (2003) Mitochondrial and peroxisomal manganese superoxide dismutase: differential expression during leaf senescence. J Exp Bot 54: 923-933.
64. Narasipura SD, Chaturvedi V, Chaturvedi S (2005) Characterization of Cryptococcus neoformans variety gattii SOD2 reveals distinct roles of the two superoxide dismutases in fungal biology and virulence. Mol Microbiol 55: 1782-1800.
65. Weisiger RA, Fridovich I (1973) Superoxide dismutase. Organelle specificity. J Biol Chem 248: 3582-3592.
66. Weser U, Fretzdorff A, Prinz R (1972) Superoxide dismutase in baker's yeast. FEBS Lett 27: 267-269.
67. Allen MD, Kropat J, Tottey S, Del Campo JA, Merchant SS (2007) Manganese deficiency in Chlamydomonas results in loss of photosystem II and MnSOD function, sensitivity to peroxides, and secondary phosphorus and iron deficiency. Plant Physiol 143: 263-277.
68. Brouwer M, Hoexum Brouwer T, Grater W, Brown-Peterson N (2003) Replacement of a cytosolic copper/zinc superoxide dismutase by a novel cytosolic manganese

superoxide dismutase in crustaceans that use copper (haemocyanin) for oxygen transport. Biochem J 374: 219-228.

69. Kitayama K, Kitayama M, Osafune T, Togasaki RK (1999) SUBCELLULAR LOCALIZATION OF IRON AND MANGANESE SUPEROXIDE DISMUTASE IN CHLAMYDOMONAS REINHARDTII (CHLOROPHYCEAE). Journal of Phycology 35: 136-142.
70. Hsieh SI, Castruita M, Malasarn D, Urzica E, Erde J, et al. (2013) The Proteome of Copper, Iron, Zinc, and Manganese Micronutrient Deficiency in Chlamydomonas reinhardtii. Molecular & Cellular Proteomics 12: 65-86.
71. Beyer WF, Fridovich I (1991) In vivo competition between iron and manganese for occupancy of the active site region of the manganese-superoxide dismutase of Escherichia coli. Journal of Biological Chemistry 266: 303-308.
72. Mizuno K, Whittaker MM, Bachinger HP, Whittaker JW (2004) Calorimetric studies on the tight binding metal interactions of Escherichia coli manganese superoxide dismutase. J Biol Chem 279: 27339-27344.
73. Luk E, Carroll M, Baker M, Culotta VC (2003) Manganese activation of superoxide dismutase 2 in Saccharomyces cerevisiae requires MTM1, a member of the mitochondrial carrier family. Proc Natl Acad Sci U S A 100: 10353-10357.
74. Yang M, Cobine PA, Molik S, Naranuntarat A, Lill R, et al. (2006) The effects of mitochondrial iron homeostasis on cofactor specificity of superoxide dismutase 2. EMBO J 25: 1775-1783.
75. Aguirre JD, Clark HM, McIlvin M, Vazquez C, Palmere SL, et al. (2013) A Manganese-rich Environment Supports Superoxide Dismutase Activity in a Lyme

Disease Pathogen, Borrelia burgdorferi. Journal of Biological Chemistry 288: 8468-8478.

76. Eide D, Clark S, Nair TM, Gehl M, Gribskov M, et al. (2005) Characterization of the yeast ionome: a genome-wide analysis of nutrient mineral and trace element homeostasis in Saccharomyces cerevisiae. Genome Biology 6: R77.
77. Outten CE, O'Halloran, V. T (2001) Femtomolar Sensitivity of Metalloregulatory Proteins Controlling Zinc Homeostasis. Science 292: 2488-2492.
78. Rosenfeld L, Reddi A, Leung E, Aranda K, Jensen L, et al. (2010) The effect of phosphate accumulation on metal ion homeostasis in Saccharomyces cerevisiae. JBIC Journal of Biological Inorganic Chemistry 15: 1051-1062.
79. Fu Y, Chang FM, Giedroc DP (2014) Copper transport and trafficking at the host-bacterial pathogen interface. Acc Chem Res 47: 3605-3613.
80. Hodgkinson V, Petris MJ (2012) Copper homeostasis at the host-pathogen interface. J Biol Chem 287: 13549-13555.
81. Pontel LB, Soncini FC (2009) Alternative periplasmic copper-resistance mechanisms in Gram negative bacteria. Mol Microbiol 73: 212-225.
82. Samanovic MI, Ding C, Thiele DJ, Darwin KH (2012) Copper in microbial pathogenesis: meddling with the metal. Cell Host Microbe 11: 106-115.
83. Ward SK, Abomoelak B, Hoye EA, Steinberg H, Talaat AM (2010) CtpV: a putative copper exporter required for full virulence of Mycobacterium tuberculosis. Mol Microbiol 77: 1096-1110.
84. Aguirre JD, Culotta VC (2012) Battles with Iron: Manganese in Oxidative Stress Protection. Journal of Biological Chemistry 287: 13541-13548.

85. Naranuntarat A, Jensen LT, Pazicni S, Penner-Hahn JE, Culotta VC (2009) The interaction of mitochondrial iron with manganese superoxide dismutase. J Biol Chem 284: 22633-22640.

86. Lamarre C, LeMay JD, Deslauriers N, Bourbonnais Y (2001) Candida albicans expresses an unusual cytoplasmic manganese-containing superoxide dismutase (SOD3 gene product) upon the entry and during the stationary phase. J Biol Chem 276: 43784-43791.

87. Barja G, Herrero A (1998) Localization at complex I and mechanism of the higher free radical production of brain nonsynaptic mitochondria in the short-lived rat than in the longevous pigeon. J Bioenerg Biomembr 30: 235-243.

88. Bleier L, Drose S (2013) Superoxide generation by complex III: from mechanistic rationales to functional consequences. Biochim Biophys Acta 1827: 1320-1331.

89. Turrens JF (2003) Mitochondrial formation of reactive oxygen species. J Physiol 552: 335-344.

90. Turrens JF, Boveris A (1980) Generation of superoxide anion by the NADH dehydrogenase of bovine heart mitochondria. Biochem J 191: 421-427.

91. Han D, Antunes F, Canali R, Rettori D, Cadenas E (2003) Voltage-dependent anion channels control the release of the superoxide anion from mitochondria to cytosol. J Biol Chem 278: 5557-5563.

92. Beckman JS, Koppenol WH (1996) Nitric oxide, superoxide, and peroxynitrite: the good, the bad, and ugly. Am J Physiol 271: C1424-1437.

93. Imlay JA, Fridovich I (1991) Assay of metabolic superoxide production in Escherichia coli. J Biol Chem 266: 6957-6965.

94. Duttaroy A, Paul A, Kundu M, Belton A (2003) A Sod2 null mutation confers severely reduced adult life span in Drosophila. Genetics 165: 2295-2299.

95. Lebovitz RM, Zhang H, Vogel H, Cartwright J, Jr., Dionne L, et al. (1996) Neurodegeneration, myocardial injury, and perinatal death in mitochondrial superoxide dismutase-deficient mice. Proc Natl Acad Sci U S A 93: 9782-9787.

96. Li Y, Huang TT, Carlson EJ, Melov S, Ursell PC, et al. (1995) Dilated cardiomyopathy and neonatal lethality in mutant mice lacking manganese superoxide dismutase. Nat Genet 11: 376-381.

97. Melov S, Coskun P, Patel M, Tuinstra R, Cottrell B, et al. (1999) Mitochondrial disease in superoxide dismutase 2 mutant mice. Proc Natl Acad Sci U S A 96: 846-851.

98. Strassburger M, Bloch W, Sulyok S, Schuller J, Keist AF, et al. (2005) Heterozygous deficiency of manganese superoxide dismutase results in severe lipid peroxidation and spontaneous apoptosis in murine myocardium in vivo. Free Radic Biol Med 38: 1458-1470.

99. Huang R, Yamamoto K, Zhang M, Popovych N, Hung I, et al. (2014) Probing the Transmembrane Structure and Dynamics of Microsomal NADPH-cytochrome P450 oxidoreductase by Solid-State NMR. Biophysical Journal 106: 2126-2133.

100. Lyakhovich V, Mishin V, Pokrovsky A (1977) Relationship between the reduction of oxygen, artificial acceptors and cytochrome P-450 by NADPH--cytochrome c reductase. Biochem J 168: 133-139.

101. Bösterling B, Trudell JR (1981) Spin trap evidence for production of superoxide radical anions by purified NADPH-cytochrome P-450 reductase. Biochemical and Biophysical Research Communications 98: 569-575.

102. Li Y, Zhu H, Kuppusamy P, Roubaud V, Zweier JL, et al. (1998) Validation of Lucigenin (Bis-N-methylacridinium) as a Chemilumigenic Probe for Detecting Superoxide Anion Radical Production by Enzymatic and Cellular Systems. Journal of Biological Chemistry 273: 2015-2023.

103. McCord JM, Fridovich I (1968) The Reduction of Cytochrome c by Milk Xanthine Oxidase. Journal of Biological Chemistry 243: 5753-5760.

104. Amaya Y, Yamazaki K, Sato M, Noda K, Nishino T, et al. (1990) Proteolytic conversion of xanthine dehydrogenase from the NAD-dependent type to the O2-dependent type. Amino acid sequence of rat liver xanthine dehydrogenase and identification of the cleavage sites of the enzyme protein during irreversible conversion by trypsin. J Biol Chem 265: 14170-14175.

105. Kuwabara Y, Nishino T, Okamoto K, Matsumura T, Eger BT, et al. (2003) Unique amino acids cluster for switching from the dehydrogenase to oxidase form of xanthine oxidoreductase. Proceedings of the National Academy of Sciences of the United States of America 100: 8170-8175.

106. Bedard K, Lardy B, Krause KH (2007) NOX family NADPH oxidases: not just in mammals. Biochimie 89: 1107-1112.

107. Takemoto D, Tanaka A, Scott B (2007) NADPH oxidases in fungi: diverse roles of reactive oxygen species in fungal cellular differentiation. Fungal Genet Biol 44: 1065-1076.

108. Brandes RP, Weissmann N, Schroder K (2014) Nox family NADPH oxidases: Molecular mechanisms of activation. Free Radic Biol Med 76: 208-226.

109. Ambasta RK, Kumar P, Griendling KK, Schmidt HH, Busse R, et al. (2004) Direct interaction of the novel Nox proteins with p22phox is required for the formation of a functionally active NADPH oxidase. J Biol Chem 279: 45935-45941.

110. Rinnerthaler M, Buttner S, Laun P, Heeren G, Felder TK, et al. (2012) Yno1p/Aim14p, a NADPH-oxidase ortholog, controls extramitochondrial reactive oxygen species generation, apoptosis, and actin cable formation in yeast. Proc Natl Acad Sci U S A 109: 8658-8663.

111. Bedard K, Krause K-H (2007) The NOX Family of ROS-Generating NADPH Oxidases: Physiology and Pathophysiology. 245-313 p.

112. Hohn DC, Lehrer RI (1975) NADPH oxidase deficiency in X-linked chronic granulomatous disease. J Clin Invest 55: 707-713.

113. Iyer GY, Questel JH (1963) NADPH and NADH oxidation by guinea pig polymorphonuclear leucocytes. Can J Biochem Physiol 41: 427-434.

114. Rossi F, Zatti M (1964) CHANGES IN THE METABOLIC PATTERN OF POLYMORPHO-NUCLEAR LEUCOCYTES DURING PHAGOCYTOSIS. Br J Exp Pathol 45: 548-559.

115. Briggs RT, Drath DB, Karnovsky ML, Karnovsky MJ (1975) Localization of NADH oxidase on the surface of human polymorphonuclear leukocytes by a new cytochemical method. J Cell Biol 67: 566-586.

116. Nunes P, Demaurex N, Dinauer MC (2013) Regulation of the NADPH oxidase and associated ion fluxes during phagocytosis. Traffic 14: 1118-1131.

117. De Groote MA, Ochsner UA, Shiloh MU, Nathan C, McCord JM, et al. (1997) Periplasmic superoxide dismutase protects Salmonella from products of phagocyte NADPH-oxidase and nitric oxide synthase. Proceedings of the National Academy of Sciences 94: 13997-14001.

118. Fang FC, DeGroote MA, Foster JW, Bäumler AJ, Ochsner U, et al. (1999) Virulent Salmonella typhimurium has two periplasmic Cu, Zn-superoxide dismutases. Proceedings of the National Academy of Sciences 96: 7502-7507.

119. Farrant JL, Sansone A, Canvin JR, Pallen MJ, Langford PR, et al. (1997) Bacterial copper- and zinc-cofactored superoxide dismutase contributes to the pathogenesis of systemic salmonellosis. Molecular Microbiology 25: 785-796.

120. Pacello F, Ceci P, Ammendola S, Pasquali P, Chiancone E, et al. (2008) Periplasmic Cu,Zn superoxide dismutase and cytoplasmic Dps concur in protecting Salmonella enterica serovar Typhimurium from extracellular reactive oxygen species. Biochim Biophys Acta 1780: 226-232.

121. Wilks KE, Dunn KLR, Farrant JL, Reddin KM, Gorringe AR, et al. (1998) Periplasmic Superoxide Dismutase in Meningococcal Pathogenicity. Infection and Immunity 66: 213-217.

122. Piddington DL, Fang FC, Laessig T, Cooper AM, Orme IM, et al. (2001) Cu,Zn Superoxide Dismutase of Mycobacterium tuberculosis Contributes to Survival in Activated Macrophages That Are Generating an Oxidative Burst. Infection and Immunity 69: 4980-4987.

123. Sansone A, Watson PR, Wallis TS, Langford PR, Kroll JS (2002) The role of two periplasmic copper- and zinc-cofactored superoxide dismutases in the virulence of Salmonella choleraesuis. Microbiology 148: 719-726.

124. Gee JM, Valderas MW, Kovach ME, Grippe VK, Robertson GT, et al. (2005) The Brucella abortus Cu,Zn Superoxide Dismutase Is Required for Optimal Resistance to Oxidative Killing by Murine Macrophages and Wild-Type Virulence in Experimentally Infected Mice. Infection and Immunity 73: 2873-2880.

125. San Mateo LR, Toffer KL, Orndorff PE, Kawula TH (1999) Neutropenia Restores Virulence to an Attenuated Cu,Zn Superoxide Dismutase-Deficient Haemophilus ducreyi Strain in the Swine Model of Chancroid. Infection and Immunity 67: 5345-5351.

126. Hwang CS, Rhie G, Kim ST, Kim YR, Huh WK, et al. (1999) Copper- and zinc-containing superoxide dismutase and its gene from Candida albicans. Biochim Biophys Acta 1427: 245-255.

127. Rhie GE, Hwang CS, Brady MJ, Kim ST, Kim YR, et al. (1999) Manganese-containing superoxide dismutase and its gene from Candida albicans. Biochim Biophys Acta 1426: 409-419.

128. Martchenko M, Alarco AM, Harcus D, Whiteway M (2004) Superoxide dismutases in Candida albicans: transcriptional regulation and functional characterization of the hyphal-induced SOD5 gene. Mol Biol Cell 15: 456-467.

129. Gleason JE, Galaleldeen A, Peterson RL, Taylor AB, Holloway SP, et al. (2014) Candida albicans SOD5 represents the prototype of an unprecedented class of Cu-

only superoxide dismutases required for pathogen defense. Proc Natl Acad Sci U S A 111: 5866-5871.

130. Fradin C, De Groot P, MacCallum D, Schaller M, Klis F, et al. (2005) Granulocytes govern the transcriptional response, morphology and proliferation of Candida albicans in human blood. Mol Microbiol 56: 397-415.

131. Frohner IE, Bourgeois C, Yatsyk K, Majer O, Kuchler K (2009) Candida albicans cell surface superoxide dismutases degrade host-derived reactive oxygen species to escape innate immune surveillance. Mol Microbiol 71: 240-252.

132. Perlroth J, Choi B, Spellberg B (2007) Nosocomial fungal infections: epidemiology, diagnosis, and treatment. Med Mycol 45: 321-346.

133. Wisplinghoff H, Bischoff T, Tallent SM, Seifert H, Wenzel RP, et al. (2004) Nosocomial bloodstream infections in US hospitals: analysis of 24,179 cases from a prospective nationwide surveillance study. Clin Infect Dis 39: 309-317.

134. Nobile CJ, Fox EP, Nett JE, Sorrells TR, Mitrovich QM, et al. (2012) A recently evolved transcriptional network controls biofilm development in Candida albicans. Cell 148: 126-138.

135. Kumamoto CA, Vinces MD (2005) Contributions of hyphae and hypha-co-regulated genes to Candida albicans virulence. Cell Microbiol 7: 1546-1554.

136. Sudbery PE (2011) Growth of Candida albicans hyphae. Nat Rev Microbiol 9: 737-748.

137. Gow NA, van de Veerdonk FL, Brown AJ, Netea MG (2012) Candida albicans morphogenesis and host defence: discriminating invasion from colonization. Nat Rev Microbiol 10: 112-122.

138. McKenzie CG, Koser U, Lewis LE, Bain JM, Mora-Montes HM, et al. (2010) Contribution of Candida albicans cell wall components to recognition by and escape from murine macrophages. Infect Immun 78: 1650-1658.

139. Urban CF, Ermert D, Schmid M, Abu-Abed U, Goosmann C, et al. (2009) Neutrophil extracellular traps contain calprotectin, a cytosolic protein complex involved in host defense against Candida albicans. PLoS Pathog 5: e1000639.

140. Cassone A (2015) Vulvovaginal Candida albicans infections: pathogenesis, immunity and vaccine prospects. BJOG 122: 785-794.

141. Gouba N, Drancourt M (2015) Digestive tract mycobiota: a source of infection. Med Mal Infect 45: 9-16.

142. Singh A, Verma R, Murari A, Agrawal A (2014) Oral candidiasis: An overview. J Oral Maxillofac Pathol 18: S81-85.

143. Clancy CJ, Cheng S, Nguyen MH (2009) Animal models of candidiasis. Methods Mol Biol 499: 65-76.

144. Hood MI, Skaar EP (2012) Nutritional immunity: transition metals at the pathogen–host interface. Nat Rev Micro 10: 525-537.

145. Andreini C, Bertini I, Cavallaro G, Holliday GL, Thornton JM (2008) Metal ions in biological catalysis: from enzyme databases to general principles. J Biol Inorg Chem 13: 1205-1218.

146. Kurnick JE (1972) Mechanism of the Anemia of Chronic Disorders. Archives of Internal Medicine 130: 323.

147. Weinberg ED (2009) Iron availability and infection. Biochim Biophys Acta 1790: 600-605.

148. Forbes JR, Gros P (2003) Iron, manganese, and cobalt transport by Nramp1 (Slc11a1) and Nramp2 (Slc11a2) expressed at the plasma membrane. Blood 102: 1884-1892.

149. Jabado N (2000) Natural resistance to intracellular infections: natural resistance-associated macrophage protein 1 (NRAMP1) functions as a pH-dependent manganese transporter at the phagosomal membrane. Journal of Experimental Medicine 192: 1237-1248.

150. Zaharik ML, Cullen VL, Fung AM, Libby SJ, Kujat Choy SL, et al. (2004) The Salmonella enterica serovar typhimurium divalent cation transport systems MntH and SitABCD are essential for virulence in an Nramp1G169 murine typhoid model. Infect Immun 72: 5522-5525.

151. Corbin BD, Seeley EH, Raab A, Feldmann J, Miller MR, et al. (2008) Metal chelation and inhibition of bacterial growth in tissue abscesses. Science 319: 962-965.

152. Kehl-Fie TE, Chitayat S, Hood MI, Damo S, Restrepo N, et al. (2011) Nutrient metal sequestration by calprotectin inhibits bacterial superoxide defense, enhancing neutrophil killing of Staphylococcus aureus. Cell Host Microbe 10: 158-164.

153. McCormick A, Heesemann L, Wagener J, Marcos V, Hartl D, et al. (2010) NETs formed by human neutrophils inhibit growth of the pathogenic mold Aspergillus fumigatus. Microbes Infect 12: 928-936.

154. Noble SM (2013) Candida albicans specializations for iron homeostasis: from commensalism to virulence. Curr Opin Microbiol 16: 708-715.

155. Beasley FC, Marolda CL, Cheung J, Buac S, Heinrichs DE (2011) Staphylococcus aureus transporters Hts, Sir, and Sst capture iron liberated from human transferrin by

Staphyloferrin A, Staphyloferrin B, and catecholamine stress hormones, respectively, and contribute to virulence. Infect Immun 79: 2345-2355.

156. Knight SA, Vilaire G, Lesuisse E, Dancis A (2005) Iron acquisition from transferrin by Candida albicans depends on the reductive pathway. Infect Immun 73: 5482-5492.

157. Heymann P, Gerads M, Schaller M, Dromer F, Winkelmann G, et al. (2002) The Siderophore Iron Transporter of Candida albicans (Sit1p/Arn1p) Mediates Uptake of Ferrichrome-Type Siderophores and Is Required for Epithelial Invasion. Infection and Immunity 70: 5246-5255.

158. Miethke M (2013) Molecular strategies of microbial iron assimilation: from high-affinity complexes to cofactor assembly systems. Metallomics 5: 15-28.

159. Cassat JE, Skaar EP (2013) Iron in infection and immunity. Cell Host Microbe 13: 509-519.

160. Weissman Z, Kornitzer D (2004) A family of Candida cell surface haem-binding proteins involved in haemin and haemoglobin-iron utilization. Mol Microbiol 53: 1209-1220.

161. Anderson ES, Paulley JT, Gaines JM, Valderas MW, Martin DW, et al. (2009) The manganese transporter MntH is a critical virulence determinant for Brucella abortus 2308 in experimentally infected mice. Infect Immun 77: 3466-3474.

162. Bearden SW, Perry RD (1999) The Yfe system of Yersinia pestis transports iron and manganese and is required for full virulence of plague. Molecular Microbiology 32: 403-414.

163. Champion OL, Karlyshev A, Cooper IA, Ford DC, Wren BW, et al. (2011) Yersinia pseudotuberculosis mntH functions in intracellular manganese accumulation, which is

essential for virulence and survival in cells expressing functional Nramp1. Microbiology 157: 1115-1122.

164. Corbett D, Wang J, Schuler S, Lopez-Castejon G, Glenn S, et al. (2012) Two zinc uptake systems contribute to the full virulence of Listeria monocytogenes during growth in vitro and in vivo. Infect Immun 80: 14-21.

165. Kehres DG, Janakiraman A, Slauch JM, Maguire ME (2002) SitABCD Is the Alkaline Mn2+ Transporter of Salmonella enterica Serovar Typhimurium. Journal of Bacteriology 184: 3159-3166.

166. Osman D, Cavet JS (2008) Chapter 8 - Copper Homeostasis in Bacteria. In: Allen I. Laskin SS, Geoffrey MG, editors. Advances in Applied Microbiology: Academic Press. pp. 217-247.

167. Casey AL, Adams D, Karpanen TJ, Lambert PA, Cookson BD, et al. (2010) Role of copper in reducing hospital environment contamination. J Hosp Infect 74: 72-77.

168. Noyce JO, Michels H, Keevil CW (2006) Potential use of copper surfaces to reduce survival of epidemic meticillin-resistant Staphylococcus aureus in the healthcare environment. J Hosp Infect 63: 289-297.

169. Achard ME, Stafford SL, Bokil NJ, Chartres J, Bernhardt PV, et al. (2012) Copper redistribution in murine macrophages in response to Salmonella infection. Biochem J 444: 51-57.

170. Wagner D, Maser J, Lai B, Cai Z, Barry CE, 3rd, et al. (2005) Elemental analysis of Mycobacterium avium-, Mycobacterium tuberculosis-, and Mycobacterium smegmatis-containing phagosomes indicates pathogen-induced microenvironments within the host cell's endosomal system. J Immunol 174: 1491-1500.

171. White C, Lee J, Kambe T, Fritsche K, Petris MJ (2009) A role for the ATP7A copper-transporting ATPase in macrophage bactericidal activity. J Biol Chem 284: 33949-33956.

172. Ding C, Festa RA, Chen YL, Espart A, Palacios O, et al. (2013) Cryptococcus neoformans copper detoxification machinery is critical for fungal virulence. Cell Host Microbe 13: 265-276.

173. Humann-Ziehank E, Menzel A, Roehrig P, Schwert B, Ganter M, et al. (2014) Acute and subacute response of iron, zinc, copper and selenium in pigs experimentally infected with Actinobacillus pleuropneumoniae. Metallomics 6: 1869-1879.

174. Mirastschijski U, Martin A, Jorgensen LN, Sampson B, Agren MS (2013) Zinc, copper, and selenium tissue levels and their relation to subcutaneous abscess, minor surgery, and wound healing in humans. Biol Trace Elem Res 153: 76-83.

175. Arguello JM, Gonzalez-Guerrero M, Raimunda D (2011) Bacterial transition metal P(1B)-ATPases: transport mechanism and roles in virulence. Biochemistry 50: 9940-9949.

176. Wolschendorf F, Ackart D, Shrestha TB, Hascall-Dove L, Nolan S, et al. (2011) Copper resistance is essential for virulence of Mycobacterium tuberculosis. Proc Natl Acad Sci U S A 108: 1621-1626.

177. Osman D, Waldron KJ, Denton H, Taylor CM, Grant AJ, et al. (2010) Copper homeostasis in Salmonella is atypical and copper-CueP is a major periplasmic metal complex. J Biol Chem 285: 25259-25268.

178. Gold B, Deng H, Bryk R, Vargas D, Eliezer D, et al. (2008) Identification of a copper-binding metallothionein in pathogenic mycobacteria. Nat Chem Biol 4: 609-616.

179. Oh KB, Watanabe T, Matsuoka H (1999) A novel copper-binding protein with characteristics of a metallothionein from a clinical isolate of Candida albicans. Microbiology 145 (Pt 9): 2423-2429.

180. Riggle PJ, Kumamoto CA (2000) Role of a Candida albicans P1-type ATPase in resistance to copper and silver ion toxicity. J Bacteriol 182: 4899-4905.

181. Weissman Z, Berdicevsky I, Cavari BZ, Kornitzer D (2000) The high copper tolerance of Candida albicans is mediated by a P-type ATPase. Proc Natl Acad Sci U S A 97: 3520-3525.

182. Douglas LM, Wang HX, Keppler-Ross S, Dean N, Konopka JB (2012) Sur7 promotes plasma membrane organization and is needed for resistance to stressful conditions and to the invasive growth and virulence of Candida albicans. MBio 3.

183. Xiao Z, Loughlin F, George GN, Howlett GJ, Wedd AG (2004) C-terminal domain of the membrane copper transporter Ctr1 from Saccharomyces cerevisiae binds four Cu(I) ions as a cuprous-thiolate polynuclear cluster: sub-femtomolar Cu(I) affinity of three proteins involved in copper trafficking. J Am Chem Soc 126: 3081-3090.

184. Labbe S, Thiele DJ (1999) Pipes and wiring: the regulation of copper uptake and distribution in yeast. Trends Microbiol 7: 500-505.

185. Nevitt T, Ohrvik H, Thiele DJ (2012) Charting the travels of copper in eukaryotes from yeast to mammals. Biochim Biophys Acta 1823: 1580-1593.

186. Georgatsou E, Mavrogiannis LA, Fragiadakis GS, Alexandraki D (1997) The yeast Fre1p/Fre2p cupric reductases facilitate copper uptake and are regulated by the copper-modulated Mac1p activator. J Biol Chem 272: 13786-13792.

187. Hassett R, Kosman DJ (1995) Evidence for Cu(II) Reduction as a Component of Copper Uptake by Saccharomyces cerevisiae. Journal of Biological Chemistry 270: 128-134.

188. Jeeves RE, Mason RP, Woodacre A, Cashmore AM (2011) Ferric reductase genes involved in high-affinity iron uptake are differentially regulated in yeast and hyphae of Candida albicans. Yeast 28: 629-644.

189. Martins LJ, Jensen LT, Simon JR, Keller GL, Winge DR (1998) Metalloregulation of FRE1 and FRE2Homologs in Saccharomyces cerevisiae. Journal of Biological Chemistry 273: 23716-23721.

190. Dancis A, Yuan DS, Haile D, Askwith C, Eide D, et al. (1994) Molecular characterization of a copper transport protein in S. cerevisiae: an unexpected role for copper in iron transport. Cell 76: 393-402.

191. Knight SA, Labbe S, Kwon LF, Kosman DJ, Thiele DJ (1996) A widespread transposable element masks expression of a yeast copper transport gene. Genes Dev 10: 1917-1929.

192. Marvin ME, Williams PH, Cashmore AM (2003) The Candida albicans CTR1 gene encodes a functional copper transporter. Microbiology 149: 1461-1474.

193. Lin SJ, Pufahl RA, Dancis A, O'Halloran TV, Culotta VC (1997) A role for the Saccharomyces cerevisiae ATX1 gene in copper trafficking and iron transport. J Biol Chem 272: 9215-9220.

194. Pufahl RA, Singer CP, Peariso KL, Lin SJ, Schmidt PJ, et al. (1997) Metal ion chaperone function of the soluble Cu(I) receptor Atx1. Science 278: 853-856.

195. Weissman Z, Shemer R, Kornitzer D (2002) Deletion of the copper transporter CaCCC2 reveals two distinct pathways for iron acquisition in Candida albicans. Mol Microbiol 44: 1551-1560.

196. Beers J, Glerum DM, Tzagoloff A (1997) Purification, characterization, and localization of yeast Cox17p, a mitochondrial copper shuttle. J Biol Chem 272: 33191-33196.

197. Carr HS, George GN, Winge DR (2002) Yeast Cox11, a protein essential for cytochrome c oxidase assembly, is a Cu(I)-binding protein. J Biol Chem 277: 31237-31242.

198. Glerum DM, Shtanko A, Tzagoloff A (1996) Characterization of COX17, a yeast gene involved in copper metabolism and assembly of cytochrome oxidase. J Biol Chem 271: 14504-14509.

199. Glerum DM, Shtanko A, Tzagoloff A (1996) SCO1 and SCO2 Act as High Copy Suppressors of a Mitochondrial Copper Recruitment Defect in Saccharomyces cerevisiae. Journal of Biological Chemistry 271: 20531-20535.

200. Inglis DO, Arnaud MB, Binkley J, Shah P, Skrzypek MS, et al. (2012) The Candida genome database incorporates multiple Candida species: multispecies search and analysis tools with curated gene and protein information for Candida albicans and Candida glabrata. Nucleic Acids Res 40: D667-674.

201. Maxfield AB, Heaton DN, Winge DR (2004) Cox17 is functional when tethered to the mitochondrial inner membrane. J Biol Chem 279: 5072-5080.

202. Schulze M, Rodel G (1988) SCO1, a yeast nuclear gene essential for accumulation of mitochondrial cytochrome c oxidase subunit II. Mol Gen Genet 211: 492-498.

203. Jungmann J, Reins H, Lee J, Romeo A, Hassett R, et al. (1993) MAC1, a nuclear regulatory protein related to Cu-dependent transcription factors is involved in Cu/Fe utilization and stress resistance in yeast. EMBO J 13: 5051-5056.

204. Keller G, Bird A, Winge DR (2005) Independent metalloregulation of Ace1 and Mac1 in Saccharomyces cerevisiae. Eukaryot Cell 4: 1863-1871.

205. Schwartz JA, Olarte KT, Michalek JL, Jandu GS, Michel SL, et al. (2013) Regulation of copper toxicity by Candida albicans GPA2. Eukaryot Cell 12: 954-961.

206. Thiele DJ (1988) ACE1 regulates expression of the Saccharomyces cerevisiae metallothionein gene. Mol Cell Biol 8: 2745-2752.

207. Dameron CT, Winge DR, George GN, Sansone M, Hu S, et al. (1991) A copper-thiolate polynuclear cluster in the ACE1 transcription factor. Proc Natl Acad Sci U S A 88: 6127-6131.

208. Gralla EB, Thiele DJ, Silar P, Valentine JS (1991) ACE1, a copper-dependent transcription factor, activates expression of the yeast copper, zinc superoxide dismutase gene. Proc Natl Acad Sci U S A 88: 8558-8562.

209. Jensen LT, Posewitz MC, Srinivasan C, Winge DR (1998) Mapping of the DNA binding domain of the copper-responsive transcription factor Mac1 from Saccharomyces cerevisiae. J Biol Chem 273: 23805-23811.

210. Jensen LT, Winge DR (1998) Identification of a copper-induced intramolecular interaction in the transcription factor Mac1 from Saccharomyces cerevisiae. EMBO J 17: 5400-5408.

211. Serpe M, Joshi A, Kosman DJ (1999) Structure-function analysis of the protein-binding domains of Mac1p, a copper-dependent transcriptional activator of copper uptake in Saccharomyces cerevisiae. J Biol Chem 274: 29211-29219.

212. Jamison McDaniels CP, Jensen LT, Srinivasan C, Winge DR, Tullius TD (1999) The yeast transcription factor Mac1 binds to DNA in a modular fashion. J Biol Chem 274: 26962-26967.

213. Borghouts C, Scheckhuber CQ, Stephan O, Osiewacz HD (2002) Copper homeostasis and aging in the fungal model system Podospora anserina: differential expression of PaCtr3 encoding a copper transporter. Int J Biochem Cell Biol 34: 1355-1371.

214. Marvin ME, Mason RP, Cashmore AM (2004) The CaCTR1 gene is required for high-affinity iron uptake and is transcriptionally controlled by a copper-sensing transactivator encoded by CaMAC1. Microbiology 150: 2197-2208.

215. Woodacre A, Mason RP, Jeeves RE, Cashmore AM (2008) Copper-dependent transcriptional regulation by Candida albicans Mac1p. Microbiology 154: 1502-1512.

216. Nichols TL, Whitehouse CA, Austin FE (2000) Transcriptional analysis of a superoxide dismutase gene of Borrelia burgdorferi. FEMS Microbiol Lett 183: 37-42.

217. Benov L, Chang LY, Day B, Fridovich I (1995) Copper, zinc superoxide dismutase in *Escherichia coli:* periplasmic localization. Arch Biochem Biophys 319: 508-511.

218. Barnese K, Sheng Y, Stich TA, Gralla EB, Britt RD, et al. (2010) Investigation of the highly active manganese superoxide dismutase from Saccharomyces cerevisiae. J Am Chem Soc 132: 12525-12527.

219. Furukawa Y, O'Halloran TV (2006) Posttranslational modifications in Cu,Zn-superoxide dismutase and mutations associated with amyotrophic lateral sclerosis. Antioxid Redox Signal 8: 847-867.

220. Schmidt P, Rae TD, Pufahl RA, Hamma T, Strain J, et al. (1999) Multiple protein domains contribute to the action of the copper chaperone for superoxide dismutase. J Biol Chem 274: 23719-23725.

221. Lyons TJ, Nerissian A, Goto JJ, Zhu H, Gralla EB, et al. (1998) Metal ion reconstitution studies of yeast copper-zinc superoxide dismutase: the "phantom" subunit and the possible role of Lys7p. J Biol Inorg Chem 3: 650-662.

222. Banci L, Cantini F, Kozyreva T, Rubino JT (2013) Mechanistic Aspects of hSOD1 Maturation from the Solution Structure of Cu -Loaded hCCS Domain 1 and Analysis of Disulfide-Free hSOD1 Mutants. Chembiochem.

223. Banci L, Bertini I, Cantini F, Kozyreva T, Massagni C, et al. (2012) Human superoxide dismutase 1 (hSOD1) maturation through interaction with human copper chaperone for SOD1 (hCCS). Proc Natl Acad Sci U S A 109: 13555-13560.

224. Lamb AL, Torres AS, O'Halloran TV, Rosenzweig AC (2001) Heterodimeric structure of supeoxide dismutase in complex with its metallochaperone. Nature Struc Biol 8: 751-755.

225. Lamb AL, Wernimont AK, Pufahl RA, O'Halloran TV, Rosenzweig AC (2000) Crystal structure of the second domain of the human copper chaperone for superoxide dismutase. Biochemistry 39: 1589-1595.

226. Lamb AL, Wernimont AK, Pufahl RA, Culotta VC, O'Halloran TV, et al. (1999) Crystal structure of the copper chaperone for superoxide dismutase. Nat Struct Biol 6: 724-729.

227. Hall LT, Sanchez RJ, Holloway SP, Zhu H, Stine JE, et al. (2000) X-ray Crystallographic and Analytical Ultracentrifugation Analyses of Truncated and Full-Length Yeast Copper Chaperones for SOD (LYS7): A Dimer-Dimer Model of LYS7-SOD Association and Copper Delivery(,). Biochemistry 39: 3611-3623.

228. Eisses JF, Stasser jP, Ralle M, Kaplan JH, Blackburn NJ (2000) Domains I and III of the human copper chaperone for superoxide dismutase interact via a cysteine-bridged dicopper(I) center. Biochemistry 39: 7337-7342.

229. Stasser JP, Siluvai GS, Barry AN, Blackburn NJ (2007) A multinuclear copper(I) cluster forms the dimerization interface in copper-loaded human copper chaperone for superoxide dismutase. Biochemistry 46: 11845-11856.

230. Proescher JB, Son M, Elliott JL, Culotta VC (2008) Biological effects of CCS in the absence of SOD1 enzyme activation: implications for disease in a mouse model for ALS. Hum Mol Genet 17: 1728-1737.

231. Kirby K, Jensen LT, Binnington J, Hilliker AJ, Ulloa J, et al. (2008) Instability of superoxide dismutase 1 of Drosophila in mutants deficient for its cognate copper chaperone. J Biol Chem 283: 35393-35401.

232. Laliberte J, Whitson LJ, Beaudoin J, Holloway SP, Hart PJ, et al. (2004) The Schizosaccharomyces pombe Pccs protein functions in both copper trafficking and metal detoxification pathways. J Biol Chem 279: 28744-28755.

233. Corson LB, Strain J, Culotta VC, Cleveland DW (1998) Chaperone-facilitated copper binding is a property common to several classes of familial amyotrophic lateral sclerosis-linked superoxide dismutase mutants. Proc Natl Acad Sci USA 95: 6361-6366.

234. Huang CH, Kuo WY, Weiss C, Jinn TL (2012) Copper chaperone-dependent and -independent activation of three copper-zinc superoxide dismutase homologs localized in different cellular compartments in Arabidopsis. Plant Physiol 158: 737-746.

235. Abdel-Ghany SE, Burkhead JL, Gogolin KA, Andres-Colas N, Bodecker JR, et al. (2005) AtCCS is a functional homolog of the yeast copper chaperone Ccs1/Lys7. FEBS Lett 579: 2307-2312.

236. Leitch JM, Li CX, Baron JA, Matthews LM, Cao X, et al. (2012) Post-translational modification of Cu/Zn superoxide dismutase under anaerobic conditions. Biochemistry 51: 677-685.

237. Arnesano F, Banci L, Bertini I, Martinelli M, Furukawa Y, et al. (2004) The unusually stable quaternary structure of human SOD1 is controlled by both metal occupancy and disulfide status. J Biol Chem 279: 47998-48003.

238. Luk E, Yang M, Jensen LT, Bourbonnais Y, Culotta VC (2005) Manganese activation of superoxide dismutase 2 in the mitochondria of *Saccharomyces cerevisiae*. J Biol Chem 280: 22715-22720.

239. Hwang CS, Rhie GE, Oh JH, Huh WK, Yim HS, et al. (2002) Copper- and zinc-containing superoxide dismutase (Cu/ZnSOD) is required for the protection of Candida albicans against oxidative stresses and the expression of its full virulence. Microbiology 148: 3705-3713.

240. Sherman F (1991) Getting started with yeast. Meths Enzymol 194: 3-21.

241. Noble SM, Johnson AD (2005) Strains and Strategies for Large-Scale Gene Deletion Studies of the Diploid Human Fungal Pathogen Candida albicans. Eukaryotic Cell 4: 298-309.

242. Gleason JE, Li CX, Odeh HM, Culotta VC (2014) Species-specific activation of Cu/Zn SOD by its CCS copper chaperone in the pathogenic yeast Candida albicans. J Biol Inorg Chem 19: 595-603.

243. Carroll MC, Outten CE, Proescher JB, Rosenfeld L, Watson WH, et al. (2006) The effects of glutaredoxin and copper activation pathways on the disulfide and stability of Cu,Zn superoxide dismutase. J Biol Chem 281: 28648-28656.

244. Gleason JE, Corrigan DJ, Cox JE, Reddi AR, McGinnis LA, et al. (2011) Analysis of hypoxia and hypoxia-like states through metabolite profiling. PLoS One 6: e24741.

245. Flohe L, Otting F (1984) Superoxide dismutase assays. In: Packer L, editor. Methods in enzymology: oxygen radicals in biological systems. New York: Academic press. pp. 93-104.

246. Bilinski T, Krawiec Z, Liczmanski L, Litwinska. J (1985) Is hydroxyl radical generated by the fenton reaction in vivo? Biochem Biophys Res Comm 130: 533-539.

247. Chu CC, Lee WC, Guo WY, Pan SM, Chen LJ, et al. (2005) A copper chaperone for superoxide dismutase that confers three types of copper/zinc superoxide dismutase activity in Arabidopsis. Plant Physiol 139: 425-436.

248. Bystrom R, Andersen PM, Grobner G, Oliveberg M (2010) SOD1 mutations targeting surface hydrogen bonds promote amyotrophic lateral sclerosis without reducing apo-state stability. J Biol Chem 285: 19544-19552.

249. Pramatarova A, Figlewicz DA, Krizus A, Han FY, Ceballos-Picot I, et al. (1995) Identification of new mutations in the Cu/Zn superoxide dismutase gene of patients with familial amyotrophic lateral sclerosis. Am J Hum Genet 56: 592-596.

250. Bannister J, Bannister W, Wood E (1971) Bovine erythrocyte cupro-zinc protein. 1. Isolation and general characterization. Eur J Biochem 18: 178-186.

251. Seeliger HP (1976) Opportunistic fungal infections with particular reference of Candida albicans. Mykosen 19: 87-97.

252. Drakesmith H, Prentice AM (2012) Hepcidin and the iron-infection axis. Science 338: 768-772.

253. Kehl-Fie TE, Skaar EP (2010) Nutritional immunity beyond iron: a role for manganese and zinc. Curr Opin Chem Biol 14: 218-224.

254. Chen C, Pande K, French SD, Tuch BB, Noble SM (2011) An iron homeostasis regulatory circuit with reciprocal roles in Candida albicans commensalism and pathogenesis. Cell Host Microbe 10: 118-135.

255. Kuznets G, Vigonsky E, Weissman Z, Lalli D, Gildor T, et al. (2014) A relay network of extracellular heme-binding proteins drives C. albicans iron acquisition from hemoglobin. PLoS Pathog 10: e1004407.

256. Potrykus J, Stead D, Maccallum DM, Urgast DS, Raab A, et al. (2013) Fungal iron availability during deep seated candidiasis is defined by a complex interplay involving systemic and local events. PLoS Pathog 9: e1003676.

257. Xu W, Solis NV, Ehrlich RL, Woolford CA, Filler SG, et al. (2015) Activation and alliance of regulatory pathways in C. albicans during mammalian infection. PLoS Biol 13: e1002076.

258. Rowland JL, Niederweis M (2012) Resistance mechanisms of Mycobacterium tuberculosis against phagosomal copper overload. Tuberculosis (Edinb) 92: 202-210.

259. Festa RA, Helsel ME, Franz KJ, Thiele DJ (2014) Exploiting innate immune cell activation of a copper-dependent antimicrobial agent during infection. Chem Biol 21: 977-987.

260. Garcia-Santamarina S, Thiele DJ (2015) Copper at the Fungal Pathogen-Host Axis. J Biol Chem.

261. Sun TS, Ju X, Gao HL, Wang T, Thiele DJ, et al. (2014) Reciprocal functions of Cryptococcus neoformans copper homeostasis machinery during pulmonary infection and meningoencephalitis. Nat Commun 5: 5550.

262. Waterman SR, Park YD, Raja M, Qiu J, Hammoud DA, et al. (2012) Role of CTR4 in the Virulence of Cryptococcus neoformans. MBio 3.

263. Cheng X, Xu N, Yu Q, Ding X, Qian K, et al. (2013) Novel insight into the expression and function of the multicopper oxidases in Candida albicans. Microbiology 159: 1044-1055.

264. Helmerhorst EJ, Stan M, Murphy MP, Sherman F, Oppenheim FG (2005) The concomitant expression and availability of conventional and alternative, cyanide-insensitive, respiratory pathways in Candida albicans. Mitochondrion 5: 200-211.

265. Sheng Y, Abreu IA, Cabelli DE, Maroney MJ, Miller AF, et al. (2014) Superoxide dismutases and superoxide reductases. Chem Rev 114: 3854-3918.

266. Juarez JC, Manuia M, Burnett ME, Betancourt O, Boivin B, et al. (2008) Superoxide dismutase 1 (SOD1) is essential for H2O2-mediated oxidation and inactivation of phosphatases in growth factor signaling. Proc Natl Acad Sci U S A 105: 7147-7152.

267. Tsang CK, Liu Y, Thomas J, Zhang Y, Zheng XF (2014) Superoxide dismutase 1 acts as a nuclear transcription factor to regulate oxidative stress resistance. Nat Commun 5: 3446.

268. Hwang CS, Baek YU, Yim HS, Kang SO (2003) Protective roles of mitochondrial manganese-containing superoxide dismutase against various stresses in Candida albicans. Yeast 20: 929-941.

269. Fonzi WA, Irwin MY (1993) Isogenic strain construction and gene mapping in Candida albicans. Genetics 134: 717-728.

270. McCluskey K, Wiest A, Plamann M (2010) The Fungal Genetics Stock Center: a repository for 50 years of fungal genetics research. J Biosci 35: 119-126.

271. Noble SM, French S, Kohn LA, Chen V, Johnson AD (2010) Systematic screens of a Candida albicans homozygous deletion library decouple morphogenetic switching and pathogenicity. Nat Genet 42: 590-598.

272. Symington LS (2002) Role of RAD52 epistasis group genes in homologous recombination and double-strand break repair. Microbiol Mol Biol Rev 66: 630-670, table of contents.

273. Beese-Sims SE, Pan SJ, Lee J, Hwang-Wong E, Cormack BP, et al. (2012) Mutants in the Candida glabrata glycerol channels are sensitized to cell wall stress. Eukaryot Cell 11: 1512-1519.

274. Uppuluri P, Chaffin WL (2007) Defining Candida albicans stationary phase by cellular and DNA replication, gene expression and regulation. Mol Microbiol 64: 1572-1586.

275. Whittaker JW (2010) Metal uptake by manganese superoxide dismutase. Biochim Biophys Acta 1804: 298-307.

276. Whittaker MM, Whittaker JW (2012) Metallation state of human manganese superoxide dismutase expressed in Saccharomyces cerevisiae. Arch Biochem Biophys 523: 191-197.

277. Labbe S, Zhu Z, Thiele DJ (1997) Copper-specific transcriptional repression of yeast genes encoding critical components in the copper transport pathway. J Biol Chem 272: 15951-15958.

278. Yamaguchi-Iwai Y, Serpe M, Haile D, Yang W, Kosman DJ, et al. (1997) Homeostatic regulation of copper uptake in yeast via direct binding of MAC1 protein to upstream regulatory sequences of FRE1 and CTR1. J Biol Chem 272: 17711-17718.

279. Chaturvedi KS, Henderson JP (2014) Pathogenic adaptations to host-derived antibacterial copper. Front Cell Infect Microbiol 4: 3.

280. Festa RA, Thiele DJ (2012) Copper at the front line of the host-pathogen battle. PLoS Pathog 8: e1002887.

281. Puig S, Andres-Colas N, Garcia-Molina A, Penarrubia L (2007) Copper and iron homeostasis in Arabidopsis: responses to metal deficiencies, interactions and biotechnological applications. Plant Cell Environ 30: 271-290.

282. Harris ZL, Takahashi Y, Miyajima H, Serizawa M, MacGillivray RTA, et al. (1995) Aceruloplasminemia: Molecular characterization of this disorder of iron metabolism. Proc Natl Acad Sci USA 92: 2539-2543.

283. Hellman NE, Gitlin JD (2002) Ceruloplasmin metabolism and function. Annu Rev Nutr 22: 439-458.

284. Linz R, Barnes NL, Zimnicka AM, Kaplan JH, Eipper B, et al. (2008) Intracellular targeting of copper-transporting ATPase ATP7A in a normal and Atp7b−/− kidney. F53-F61 p.

285. Harris ZL, Durley AP, Man TK, Gitlin JD (1999) Targeted gene disruption reveals an essential role for ceruloplasmin in cellular iron efflux. Proc Natl Acad Sci U S A 96: 10812-10817.

286. Kong EF, Kucharikova S, Van Dijck P, Peters BM, Shirtliff ME, et al. (2015) Clinical implications of oral candidiasis: host tissue damage and disseminated bacterial disease. Infect Immun 83: 604-613.

287. Armitage AE, Eddowes LA, Gileadi U, Cole S, Spottiswoode N, et al. (2011) Hepcidin regulation by innate immune and infectious stimuli. 4129-4139 p.

288. Park CH, Valore EV, Waring AJ, Ganz T (2001) Hepcidin, a Urinary Antimicrobial Peptide Synthesized in the Liver. Journal of Biological Chemistry 276: 7806-7810.

289. Damo SM, Kehl-Fie TE, Sugitani N, Holt ME, Rathi S, et al. (2013) Molecular basis for manganese sequestration by calprotectin and roles in the innate immune response to invading bacterial pathogens. Proc Natl Acad Sci U S A 110: 3841-3846.

290. Skipor AK, Jacobs JJ, Yu L, Black J (1999) Comparison of Zeeman Background Corrected Atomic Absorption Spectrometric and Inductively Coupled Plasma Mass Spectrometric detection of trace elements in electrothermally vaporized serum. J Biomed Mater Res 48: 90-93.

291. Paunesku T, Vogt S, Maser J, Lai B, Woloschak G (2006) X-ray fluorescence microprobe imaging in biology and medicine. Journal of Cellular Biochemistry 99: 1489-1502.

292. Vogt S (2007) X-Ray Microscopy and Imaging: X-ray Fluorescence Mapping. Argonne National Laboratory.

293. Malinouski M, Kehr S, Finney L, Vogt S, Carlson BA, et al. (2011) High-Resolution Imaging of Selenium in Kidneys: A Localized Selenium Pool Associated with Glutathione Peroxidase 3. Antioxidants & Redox Signaling 16: 185-192.

294. Vogt S (2003) MAPS : A set of software tools for analysis and visualization of 3D X-ray fluorescence data sets. J Phys IV France 104: 635-638.

295. Gupta A, Lutsenko S (2009) Human copper transporters: mechanism, role in human diseases and therapeutic potential. Future Med Chem 1: 1125-1142.

296. Gaddy JA, Radin JN, Loh JT, Piazuelo MB, Kehl-Fie TE, et al. (2014) The Host Protein Calprotectin Modulates the <italic>Helicobacter pylori cag</italic> Type IV Secretion System via Zinc Sequestration. PLoS Pathog 10: e1004450.

297. Bellingham SA, Ciccotosto GD, Needham BE, Fodero LR, White AR, et al. (2004) Gene knockout of amyloid precursor protein and amyloid precursor-like protein-2 increases cellular copper levels in primary mouse cortical neurons and embryonic fibroblasts. J Neurochem 91: 423-428.

298. Brewer GJ (2005) Anticopper therapy against cancer and diseases of inflammation and fibrosis. Drug Discov Today 10: 1103-1109.

299. Brown DR, Kozlowski H (2004) Biological inorganic and bioinorganic chemistry of neurodegeneration based on prion and Alzheimer diseases. Dalton Trans: 1907-1917.

300. Bull PC, Thomas GR, Rommens JM, Forbes JR, Cox DW (1993) The Wilson disease gene is a putative copper transporting P-type ATPase similar to the Menkes gene. Nat Genet 5: 327-337.

301. Sparks DL, Schreurs BG (2003) Trace amounts of copper in water induce beta-amyloid plaques and learning deficits in a rabbit model of Alzheimer's disease. Proc Natl Acad Sci U S A 100: 11065-11069.

302. Vulpe C, Levinson B, Whitney S, Packman S, Gitschier J (1993) Isolation of a candidate gene for Menkes disease and evidence that it encodes a copper-transporting ATPase. Nat Genet 3: 7-13.

303. Miller EW, Zeng L, Domaille DW, Chang CJ (2006) Preparation and use of Coppersensor-1, a synthetic fluorophore for live-cell copper imaging. Nat Protoc 1: 824-827.

304. Zeng L, Miller EW, Pralle A, Isacoff EY, Chang CJ (2006) A selective turn-on fluorescent sensor for imaging copper in living cells. J Am Chem Soc 128: 10-11.

305. Espirito Santo C, Lam EW, Elowsky CG, Quaranta D, Domaille DW, et al. (2011) Bacterial killing by dry metallic copper surfaces. Appl Environ Microbiol 77: 794-802.

306. Cusick KD, Minkin SC, Dodani SC, Chang CJ, Wilhelm SW, et al. (2012) Inhibition of copper uptake in yeast reveals the copper transporter Ctr1p as a potential molecular target of saxitoxin. Environ Sci Technol 46: 2959-2966.

307. Quaranta D, Krans T, Espirito Santo C, Elowsky CG, Domaille DW, et al. (2011) Mechanisms of contact-mediated killing of yeast cells on dry metallic copper surfaces. Appl Environ Microbiol 77: 416-426.

308. Beaudoin J, Ioannoni R, Lopez-Maury L, Bahler J, Ait-Mohand S, et al. (2011) Mfc1 is a novel forespore membrane copper transporter in meiotic and sporulating cells. J Biol Chem 286: 34356-34372.

309. Bernal M, Casero D, Singh V, Wilson GT, Grande A, et al. (2012) Transcriptome sequencing identifies SPL7-regulated copper acquisition genes FRO4/FRO5 and the copper dependence of iron homeostasis in Arabidopsis. Plant Cell 24: 738-761.

310. Cotruvo JA, Jr., Aron AT, Ramos-Torres KM, Chang CJ (2015) Synthetic fluorescent probes for studying copper in biological systems. Chem Soc Rev 44: 4400-4414.

311. Price KA, Hickey JL, Xiao Z, Wedd AG, James SA, et al. (2012) The challenges of using a copper fluorescent sensor (CS1) to track intracellular distributions of copper in neuronal and glial cells. Chemical Science 3: 2748-2759.

312. Wolinski H, Kolb D, Hermann S, Koning RI, Kohlwein SD (2011) A role for seipin in lipid droplet dynamics and inheritance in yeast. J Cell Sci 124: 3894-3904.

313. Gocze PM, Freeman DA (1994) Factors underlying the variability of lipid droplet fluorescence in MA-10 leydig tumor cells. Cytometry 17: 151-158.

314. Ohsaki Y, Shinohara Y, Suzuki M, Fujimoto T (2010) A pitfall in using BODIPY dyes to label lipid droplets for fluorescence microscopy. Histochem Cell Biol 133: 477-480.

315. Fahrni CJ (2013) Synthetic fluorescent probes for monovalent copper. Current Opinion in Chemical Biology 17: 656-662.

316. Giuffrida ML, Rizzarelli E, Tomaselli GA, Satriano C, Trusso Sfrazzetto G (2014) A novel fully water-soluble Cu(i) probe for fluorescence live cell imaging. Chemical Communications 50: 9835-9838.

317. Johnson LV, Walsh ML, Chen LB (1980) Localization of mitochondria in living cells with rhodamine 123. Proceedings of the National Academy of Sciences of the United States of America 77: 990-994.

Curriculum Vitae

Cissy Xiyou Li

Work Address	615 N Wolfe Street W8104 Baltimore, MD 21205 cli42@jhu.edu 410-955-9643	**Home Address**	1 E Chase Street Apt 1010 Baltimore, MD 21202 li.cissyx@gmail.com 651-815-7979

Education

Ph.D. candidate in Molecular and Translational Toxicology; Dept. of Environmental Health Sciences; Johns Hopkins Bloomberg School of Public Health, Baltimore, MD; 2015

Risk Sciences and Public Policy certificate program; Johns Hopkins Bloomberg School of Public Health, Baltimore, MD; 2014

B.S. in Chemistry (magna cum laude); Furman University, Greenville, SC; 2010

Research

PhD Thesis Research, Advisor Dr. Valeria Culotta
(2010-2015)
Johns Hopkins School of Public Health, Baltimore, MD

- Utilize biochemical, analytical, cellular, and genetic tools to study the regulation of antioxidant enzymes in the pathogenic yeast Candida *albicans*
- Utilize a mouse model of infection to assess impacts of disease
- Present posters at conferences and symposiums
- Present orally to technical researchers and broader environmental health audience

Research Assistant, Center for a Livable Future
(2014-2015)
Johns Hopkins Bloomberg School of Public Health, Baltimore, MD

- Conduct literature review on risks and benefits of raw vs. pasteurized milk
- Write report detailing methods, findings, and recommendations
- Present report in a briefing to subcommittee delegates at the Maryland General Assembly, to inform their decision on a proposed bill to legalize raw milk

Undergraduate Research, Chemistry Department
(2008-2010)
Furman University, Greenville, SC

- Analyzed kinetics of DNA-peptide interactions
- Presented posters and oral presentations at conferences and to peers

Intern, Bioinformatics and Bioengineering Summer Institute
(2008)
Clemson University, Clemson, SC

- Explored topics in bioengineering through workshops and seminars
- Conducted research using neurons and microfluidics

Technical Aide, Fuel Cell Division
(2007)
3M Company, St. Paul, MN

- Conducted experiments on fuel cell durability
- Engineered water-cooling apparatus for test station

Publications

Gleason JE, Li CX, Odeh HM, Culotta VC. Species-specific activation of Cu/Zn SOD by its CCS copper chaperone in the pathogenic yeast Candida albicans. *J Biol Inorg Chem*. 2013 Sep 17.

Leitch JM, Li CX, Baron JA, Matthews LM, Cao X, Hart PJ, Culotta VC. Post-translational modification of Cu/Zn superoxide dismutase under anaerobic conditions. *Biochemistry*. 2012 Jan 17.

Awards & Honors

- Overall winner at the Delta Omega Poster Competition, Johns Hopkins Bloomberg School of Public Health, 2015
- Phi Beta Kappa Honor Society, Furman University Chapter, inducted 2010
- WCACS Outstanding Senior Award, Western Carolinas Chapter of the American Chemical Society, 2010
- 1st place in Undergraduate Oral Presentations at the Southeast Regional Meeting of the American Chemical Society, 2009
- Phi Eta Sigma Honor Society, Furman University Chapter, inducted 2006

Leadership

Doctor of Philosophy Board (University-wide board)
Student Representative (2013-2014)

- Present the student perspective in the formulation and implementation of University-wide policies to improve PhD education and experience
- Communicate board proceedings to the student government heads at the Schools of Medicine, Public Health, and Nursing

Student Grievance Board
Presiding Officer (2014)

- Hear cases and provide recommendations to resolve disputes between students and faculty/staff at the School of Public Health

Environmental Health Sciences Student Organization
Faculty/Student Representative (2012-2013, 2014-2015)

- Maintained communication between students and faculty in EHS department
- Attended faculty meetings and EHSSO board meetings
- Planned educational, service, and social events in conjunction with the board

Teaching

Teaching Assistant, Johns Hopkins Bloomberg School of Public Health:

Public Health Toxicology (2012-2013)
Hosted review sessions, graded quizzes and exams, maintained course website, assisted students; 3 terms. Dr. James Yager and Dr. Michael Trush

Methods in Quantitative Risk Assessment (2014)
Graded homework, maintained course website, assisted students; 1 term. Dr. Mary Fox